

Quantum Black Holes in the Sky

by

Qingwen Wang

A thesis
presented to the University of Waterloo
in fulfillment of the
thesis requirement for the degree of
Doctor of Philosophy
in
Physics

Waterloo, Ontario, Canada, 2020

© Qingwen Wang 2020

Examining Committee Membership

The following served on the Examining Committee for this thesis. The decision of the Examining Committee is by majority vote.

External Examiner: Kostas Kokkotas
Professor (Chair), Theoretical Astrophysics
Eberhard Karls University Tübingen, Germany.

Supervisor: Niayesh Afshordi
Associate Professor, Dept. of Physics and Astronomy,
University of Waterloo
Associate Faculty, Perimeter Institute for Theoretical Physics.

Internal Member: Avery Broderick
Associate Professor, Dept. of Physics and Astronomy,
University of Waterloo
Associate Faculty, Perimeter Institute for Theoretical Physics.

Huan Yang
Assistant Professor, Dept. of Physics and Astronomy,
University of Guelph
Associate Faculty, Perimeter Institute for Theoretical Physics.

Internal-External Member: Francis Poulin
Professor, Dept. of Applied Mathematics, University of Waterloo

Author's Declaration

This thesis consists of material all of which I authored or co-authored: see Statement of Contributions included in the thesis. This is a true copy of the thesis, including any required final revisions, as accepted by my examiners.

I understand that my thesis may be made electronically available to the public.

Statement of Contribution

The chapters of this thesis contain material produced in different collaborations, and (with the exception of of Chapter VI) they have been independently published in peer-reviewed journals: Chapter I, II, and VII were in collaboration with Jahed Abedi, Niayesh Afshordi, Naritaka Oshita, published in [24]. Chapter III was in collaboration with Niayesh Afshordi, published in [280]. Chapter IV, V and Appendix A were in collaboration with Niayesh Afshordi and Naritaka Oshita, and were published in [211, 281]. Chapter VI is based on an ongoing collaboration with Baoyi Chen and Yanbei Chen at Caltech, and is not yet submitted for publication. The specific parts that I was responsible for: Chapter I, Chapter II Section 2.5-2.7, Chapter III, Chapter V, main calculations of Chapter VI, Chapter VII Section 7.2 and 7.6.

Abstract

Black Holes are possibly the most enigmatic objects in our Universe. From their detection in gravitational waves upon their mergers, to their snapshot eating at the centres of galaxies, black hole astrophysics has undergone an observational renaissance in the past 4 years. Nevertheless, they remain active playgrounds for strong gravity and quantum effects, where novel aspects of the elusive theory of quantum gravity may be hard at work. In this thesis, we provide an overview of the strong motivations for why “Quantum Black Holes” may be radically different from their classical counterparts in Einstein’s General Relativity. We then discuss the observational signatures of quantum black holes, focusing on gravitational wave echoes as smoking guns for quantum horizons (or exotic compact objects), which have led to significant recent excitement and activity. We review the theoretical underpinning of gravitational wave echoes and build up realistic templates for further data analysis. Finally, we discuss the future theoretical and observational landscape for unraveling the “Quantum Black Holes in the Sky”.

Acknowledgements

I would like to thank all the little people who made this thesis possible. In particular I would like to thank my supervisor Niayesh Afshordi from whom I learned much and get lots of support. I would like to thank myself, for overcoming unprecedented loneliness, bad health condition and stress and even become a much better person with this thesis now. I would like to thank my parents and friends who are always by my side, support me even if some of them don't know what I am actually pursuing. I really enjoy the intricate and elegant physics world as well as the simple and elegant love we share.

I would like to thank Connor Adair, Michael Balogh, Ofek Birnholtz, Avery Broderick, Yanbei Chen, Baoyi Chen, Vitor Cardoso, Ramit Dey, Hannah Dykaar, Will East, Steve Giddings, Bob Holdom, Badri Krishnan, Lam Hui, Luis Lehner, Luis Longo, Elisa Maggio, Emil Motolla, Samir Mathur, Emil Mottola, Shinji Mukohyama, Rob Myers, Ramesh Narayan, Alex Nielsen, Naritaka Oshita, Paolo Pani, Joe Polchinski (RIP), Chanda Prescod-Weinstein, Jing Ren, Krishan Saraswat, Rafael Sorkin, Sergey Sibiryakov, Daichi Tsuna, Yasaman Yazdi, Yuki Yokokura, Huan Yang, Aaron Zimmerman, and many others for discussions and/or collaborations about Quantum Black Holes. I also thank all the participants in our weekly group meetings for their patience during our discussions. This work was supported by the University of Waterloo, Natural Sciences and Engineering Research Council of Canada (NSERC), and the Perimeter Institute for Theoretical Physics, and the JSPS Overseas Research Fellowships (N. O.). Research at the Perimeter Institute is supported by the Government of Canada through Industry Canada, and by the Province of Ontario through the Ministry of Research and Innovation.

This research has made use of data, software and/or web tools obtained from the Gravitational Wave Open Science Center (<https://www.gw-openscience.org>), a service of LIGO Laboratory, the LIGO Scientific Collaboration and the Virgo Collaboration. LIGO is funded by the U.S. National Science Foundation. Virgo is funded by the French Centre National de Recherche Scientifique (CNRS), the Italian Istituto Nazionale della Fisica Nucleare (INFN) and the Dutch Nikhef, with contributions by Polish and Hungarian institutes.

Dedication

This is dedicated to the one I love, to the elegant science, and to the charming and fascinating world.

Table of Contents

List of Tables	xi
List of Figures	xii
1 Introduction	1
1.1 Classical BHs	3
1.1.1 Schwarzschild spacetime	4
1.1.2 Kerr spacetime	5
1.1.3 Blue-shift near horizon	6
1.1.4 Thermodynamics of Semi-classical BH	6
1.2 Membrane Paradigm	7
1.3 Dawn of Gravitational Wave Astronomy	9
1.4 Quantum Gravity and Equivalence Principle	10
2 Quantum Black Holes	12
2.1 Evaporation of BHs and the Information Paradox	12
2.2 BH complementarity	15
2.3 Firewalls	15
2.4 Gravastars	17
2.5 Fuzzballs	18
2.6 Aether Holes and Dark Energy	19

2.7	2-2 holes	21
2.8	Non-violent Unitarization	21
3	Black Hole Echology	23
3.1	Introduction	23
3.2	Propagation and Boundary Conditions in Kerr spacetime	25
3.3	Making Echoes	27
3.4	Superradiance	31
3.5	Minimal Echo templates	34
3.6	Beyond the minimal model	38
	3.6.1 Nonlinear Mergers Effects	38
	3.6.2 Soft Wall	42
3.7	Ergoregion Instability	49
3.8	Conclusions	53
4	Boltzmann Reflectivity	54
4.1	Boltzmann reflectivity from Detailed Balance	54
4.2	Boltzmann reflection and CP-symmetry.	55
4.3	Boltzmann reflectivity and Fluctuation-Dissipation theorem	57
4.4	GW Echoes and absence of ergoregion instability.	60
4.5	Conclusions.	61
5	Echoes from Boltzmann Reflectivity	65
5.1	Introduction	65
5.2	Quasinormal modes	66
5.3	Real time Echoes	68
	5.3.1 Numerical Echoes from geometric optics approximation	68
	5.3.2 On the accuracy of the geometric optics approximation	70

5.3.3	On the γ -dependence of echo spectrum	71
5.3.4	Analytic Echoes from QNMs	71
5.3.5	On detectability of Boltzmann echoes	73
5.4	Ergoregion Instability?	74
5.5	Conclusion	75
6	Hybrid Method	84
6.1	Dividing the Binary BH collision spacetime into two regions	84
6.2	Kerr Spacetime	85
6.2.1	Solution in Region I and Continuation to Region II	85
6.2.2	Data on Boundary Σ_{SF} between Region I and Region II	87
6.3	Taking the Schwarzschild Special Case	88
6.4	Outlook	90
7	Future Prospects and Conclusion	91
7.1	Towards Synergistic Statistical Methodologies	91
7.2	Echoes in Numerical Relativity	91
7.3	Quantum Gravity, Holography, and Echoes	92
7.4	Einstein Telescope, Cosmic Explorer	93
7.5	LISA	95
7.6	Pulsar Timing Arrays	97
7.7	Final Word	97
	References	100
	APPENDICES	122
A	Derivation of $e^{- \tilde{\omega} /T}$ from the modified dispersion relation	123

List of Tables

3.1	Corresponding field ψ for different spin weight s in Master equation	25
3.2	Physical quantities of a single echo from the gaussian echo template.	36
3.3	Best fit gaussian echo template quantities	36
3.4	Same as Table 3.3, but with redshifted initial conditions.	42
3.5	Same as Table 3.3, but contrasting perfect and soft wall.	46
3.6	Integrals of superradiance profiles in Fig.3.15.	49

List of Figures

2.1	The Penrose diagram describing an evaporating BH.	14
3.1	BHs and QBHs with an ingoing wavepacket.	28
3.2	Echoes with different wall positions.	29
3.3	Predicted echoes for LIGO event GW150914 in the time domain.	32
3.4	Predicted echoes for LIGO event GW150914 in the frequency domain.	33
3.5	Superradiance in frequency domain for BHs and QBHs.	35
3.6	Best fit gaussians to echoes	37
3.7	Best fit gaussian template parameters in our minimal model.	39
3.8	SNR_{temp} compared to $\text{SNR}_{\text{model}}$	40
3.9	Echoes predicted for GW150914 with redshifted (blueshifted) condition	41
3.10	Signal-to-noise ratios and energy for blueshifted echoes.	43
3.11	Same is Fig. (3.7), but using the different blueshift factors.	44
3.12	Comparison of reflectivity used, with that of the Kerr angular momentum barrier.	46
3.13	Echoes for GW15014, for soft vs. perfect walls.	47
3.14	Same is Fig. 3.7, comparing walls with different energy reflectivity	48
3.15	Superradiance by a spinning ECO/BH assuming different wall reflectivity R_{wall}	50
3.16	Same as Fig. 3.15, but with $a = 0$	51
3.17	Same as Fig. 3.15, but with different wall positions.	51

3.18	Occurrence of ergoregion instability in later echoes with near extremal QBHs	52
4.1	Spontaneous and stimulated emission for QBHs	56
4.2	The mode function $\psi_\omega(x)$ with and without the dissipation term.	59
4.3	The ringdown signals followed by the echoes with $\sigma = 2r_g$.	63
4.4	The frequency dependence of the Boltzmann reflectivity.	64
5.1	Real time echoes from the geometric optics approximation.	69
5.2	The expected ratio of outgoing GW amplitude to that of the main event.	76
5.3	Amplitude spectral densities of ringdown + echo GWs	77
5.4	The real-time echoes from the geometric optics approximation.	78
5.5	The single real time echoes from the numerical and analytic model.	79
5.6	The real time echoes from the Lorentzian model for different spins.	80
5.7	The echoes in the frequency domain compared to LIGO Hanford and Livingston noise.	81
5.8	SNR of echoes over main event with the shifted mass.	82
5.9	Comparison between reflectivity of angular momentum barrier for Kerr BHs and Boltzmann reflectivity	83
6.1	Penrose paragraph of hybrid method	86
6.2	Plot of $\mathcal{M}(t)$ for a Schwarzschild black hole.	89
7.1	Spectra of ringdown and echo phases with different reflectivity.	95
7.2	Spectra of ringdown and echo phases in the Boltzmann reflectivity model with $\bar{a} = 0.1$.	96
7.3	Spectra of GW echoes in the Boltzmann reflectivity model with $\bar{a} = 0.6$	98
A.1	Plot of $\tilde{F}(r = r_+, \theta)$ for various values of spin.	126

Chapter 1

Introduction

Black holes (BHs) are very interesting “stars” in the Universe where both strong gravity and macroscopic quantum behavior are expected to coexist. Classical BHs in General Relativity (GR) have been thought to have only three hairs, i.e., mass, angular momentum, and charge, making observational predictions for BHs relatively easy [155, 88] (compared to other astrophysical compact objects). For astrophysical BHs, due to the effect of ambient plasma, this charge is vanishingly small, leaving us with effectively two hairs for isolated black holes, with small accretion rates. In other words, finding conclusive deviations from standard predictions of these 2-parameter models, may be interpreted as fingerprints of a quantum theory of gravity or other possible deviations from GR. For example, the quasinormal modes (QNMs) of spinning BHs, which have been widely-studied over the past few decades (a subject often referred to as BH spectroscopy), only depend on the mass and spin of the Kerr BH (e.g., [164]). The ringdown of the perturbations of the BH is regarded as a superposition of these QNMs, and thus can be used to test the accuracy of GR predictions and no-hair theorem (e.g., see [154]). As a result, precise detection of QNMs from the ringdown phase (from BH mergers or formation) in gravitational wave (GW) observations may enable us to test the classical and quantum modifications to GR (e.g., [276, 277, 64]).

A concrete path towards this goal is paved through the study of “GW echoes”, a smoking gun for near-horizon modifications of GR which are motivated from the resolutions of the proposed resolutions to the BH information paradox and dark energy problems [39, 232]. The list of these models include wormholes [81], gravastars [195], fuzzballs [174], 2-2 holes [152], Aether Holes [232], Firewalls [39] and the Planckian correction in the dispersion relation of gravitational field [209, 211].

The possibility of observing GW echoes was first proposed shortly after the first de-

tection of GWs by LIGO [81, 82, 85], which has led to several observational searches [28, 268, 99, 282, 203, 22, 244, 150, 45, 30, 31]. Tentative evidence for and/or detection of these echoes can be seen in the results reported by different groups [28, 99, 282, 203, 22, 244, 268, 150] from O1 and O2 LIGO observations of binary BH and neutron star mergers, but the origin and the statistical significance of these signals remain controversial [282, 45, 30, 31, 244], motivating further investigation.

Given their uncertain theoretical and observational status, GW echoes are gathering much attention from those who are interested in the observational signatures of quantum gravity, and the field remains full of excitement, controversy and confusion. In the thesis, I summarize our contribution to this area, from its motivation to its models, and into its future outlook.

The thesis is organized as follows: In this chapter, we provide basis feature of BHs, setting stage for the motivation to investigate the quantum signatures from BHs. In Chapter 2, we discuss theoretical models of quantum BHs to motivate our echoes analysis. In Chapter 3, we discuss how to predict the GW echoes from spinning Quantum BHs with any reflectivity. Chapter 4 and 5 study a specific physical model – the Boltzmann reflectivity [211, 281] for quantum BHs and its echoes. In Chapter 6, we provide a novel Hybrid method for studying echoes with more realistic nonlinear initial condition, while Chapter 7 we discuss the future prospects for advancement in theoretical and observational studies of quantum BHs.

Throughout the thesis, we use the following notations:

Symbol	Description
a	spin parameter
\bar{a}	non-dimensional spin parameter ($a/(GM)$)
c	speed of light
\hbar	Planck constant
k_B	Boltzmann constant
G	gravitational constant
M_{Pl}	Planck mass
E_{Pl}	Planck energy
l_{Pl}	Planck length
M	mass of a BH or QBH
M_{\odot}	solar mass (1.988×10^{30} kg)
r_g	Schwarzschild radius
T_{H}	Hawking temperature

Furthermore, unless noted otherwise, we use the natural Planck units with $\hbar = c = 1 = G = 1$.

1.1 Classical BHs

Schwarzschild and Kerr spacetimes are solutions of general relativity giving the spacetime configurations of BHs, which are the most dense objects in our universe. In some regions, matter accumulates and attracts more matter with its gravity which is classically always attractive. At the end, the force is so strong that even the light cannot escape from those regions, where then BHs form.

The first and most important feature (the definition of BHs) is the formation of horizon. Inside the (event) horizon, all the light cones are directed into the singularity, and nothing can escape, unless it could travel faster than the speed of light. Therefore, horizons stand as the causal boundaries of BHs in Einstein’s theory of Relativity.

Realistic BHs in the sky have different hairs (mass, spin and charge), and their dynamics share more complicated structure, thus, have different kinds of horizons. To list some of them, event horizons are defined as the boundaries where no light can escape to the infinite future. However, for a dynamically evolving BH, event horizons are teleological, i.e. we cannot predict them until we have the entire history of the spacetime. Apparent horizons, however, are predictable at a specific time without knowing the future. Any surface has two null normal vectors and if expansion of both of them are negative, the surface is called “trapped”. Apparent horizons are the outermost of all the trapped surfaces, which is why they are also known as the “marginally outer trapped surface”.

Here is a simple example to distinguish these two horizons — we start with a Schwarzschild BH at time t_1 , now the event and apparent horizons coincide at the Schwarzschild radius. We throw a spherical null shell into the BH and let it cool down at t_2 . This process is perfectly described by Vaidya metric [228]. The apparent horizon changes immediately when the shell falls into the BH but the event horizon starts to expand earlier, even before the shell reaches it. It is because that after throwing the shell, the gravity of BH increases. Thus it is harder for light to escape from the BH to infinity. In other words, particles might be doomed to fall into a singularity, even before they had a chance to meet the infalling gravitating matter that is responsible for their fate. Therefore, the event horizon is modified earlier than the apparent horizon. While this result is counter-intuitive, it is a result of the formal definition of the event horizons, which requires the information about the entire history of spacetime, in particular, the future!

Beyond the horizons, another intriguing trait of BHs is the curvature singularity, which sits at the centre of the BHs. Horizons can also be singular, but usually only coordinate singularities and (in classical General Relativity) removable by changing to a proper coordinate system. However, the singularities inside the BHs are where the general relativity breaks down and so far we do not have any good physics to describe them. We cannot chase the information lost into these singularities (using standard physics), which leads to the information paradox (more on this later).

Back in November 1784, John Michell, an English clergyman, advanced the idea that light might not be able to escape from a very massive object (at a fixed density). For example, light cannot escape from the surface of a star with the density of the sun, if it was 500 times bigger than the sun. Albert Einstein, later in 1915, developed general relativity. Soon after this, Karl Schwarzschild solved the Einstein vacuum field equation under spherical symmetry with a singular mass at the center, which was the first solution for BHs, the Schwarzschild metric.

While 20th century saw a golden age of general relativity with blooming of dozens of different BH solutions, the existence of BHs was not directly confirmed until one century later in 2015. LIGO-Virgo collaboration reported unprecedented detection of GWs from the binary BH merger events [13, 12, 15, 14, 21, 18, 19, 17]. Numerical relativity is consistent with LIGO data at least up to quite near the horizon range. But the detection has not confirmed the existence of the horizons. We will discuss in this thesis how the detection opens a window for searching for quantum nature of the BHs beyond the general relativity.

1.1.1 Schwarzschild spacetime

The Schwarzschild spacetime was the first exact solution in the Einstein theory of general relativity. It models a static gravitational field outside a mass which has spherical symmetry, zero charge and rotation. Karl Schwarzschild[252] found this solution in 1915, and four months later, Johannes Droste[112] published a more concrete study on this independently. The metric in the Schwarzschild coordinate is:

$$ds^2 = - \left(1 - \frac{2M}{r}\right) dt^2 + \left(1 - \frac{2M}{r}\right)^{-1} dr^2 + r^2 d\Omega^2, \quad (1.1)$$

where M is the mass of the centre object, $2M$ is Schwarzschild radius and $d\Omega^2 = d\theta^2 + \sin^2\theta d\phi^2$ is the metric on a 2-sphere. The metric describes gravitational field outside any spherical object without charges. If the radius of the central object is smaller than the

Schwarzschild radius, the object is then too dense to be stable, and will go through a gravitational collapse and form a Schwarzschild BH.

Later in 1923, G.D.Birkhoff[65] proved that any spherically symmetric solution of the vacuum Einstein field equation must be static and asymptotically flat. Hence, Schwarzschild metric is the only solution in the case. For any static solution, the event horizon always coincides with the apparent horizon. In general relativity, Schwarzschild coordinate is singular at the horizon. However, as stated above, this is only a coordinate artifact. That is to say, a free falling observer feels no drama going through the horizon. It takes the observer a finite amount of proper time but infinite coordinate time. Particularly, we can remove the singularity by a proper coordinate transformation.

In contrast, origin $r = 0$ is intrinsic curvature singularity. Scalar curvature is infinite and general relativity is no longer valid at this point.

1.1.2 Kerr spacetime

The Kerr spacetime [160], discovered by Roy Kerr, is a realistic generalization of the Schwarzschild spacetime. It describes the gravitational field of an empty spacetime outside a rotating object. The spacetime is stationary and has axial symmetry. The metric in the Boyer-Lindquist coordinate is:

$$ds^2 = - \left(1 - \frac{2Mr}{\rho^2} \right) dt^2 + \frac{\rho^2}{\Delta} dr^2 + \rho^2 d\theta^2 \quad (1.2)$$

$$+ \left(r^2 + a^2 + \frac{2Mra^2}{\rho^2} \sin^2 \theta \right) \sin^2 \theta d\phi^2 - \frac{4Mra \sin^2 \theta}{\rho^2} dt d\phi, \quad (1.3)$$

$$= - \frac{\rho^2 \Delta}{\Sigma} dt^2 + \frac{\Sigma}{\rho^2} \sin^2 \theta (d\phi - \omega dt)^2 + \frac{\rho^2}{\Delta} dr^2 + \rho^2 d\theta^2, \quad (1.4)$$

where $a = J/M$, $\rho^2 = r^2 + a^2 \cos^2 \theta$, $\Delta = r^2 - 2Mr + a^2$, $\Sigma = (r^2 + a^2)^2 - a^2 \Delta \sin^2 \theta$ and $\omega = -g_{t\phi}/g_{\phi\phi} = 2Mar/\Sigma$. The Cartesian coordinates can be defined as

$$x = \sqrt{r^2 + a^2} \sin \theta \cos \phi, \quad y = \sqrt{r^2 + a^2} \sin \theta \sin \phi, \quad z = r \cos \theta. \quad (1.5)$$

There are two singularities easily reading from the coordinate where the g^{rr} and g_{tt} vanish. The first one gives $r_{\pm} = M \pm \sqrt{M^2 - a^2}$ corresponding to the horizon analog to the Schwarzschild metric. The larger root $r_+ = M + \sqrt{M^2 - a^2}$ is the event horizon, while the other root is inner apparent horizon.

The second singularity is related to an interesting effect in the Kerr spacetime called frame-dragging effect: When reaching close to the Kerr BHs, the observers even with zero angular momentum (ZAMOs) will co-rotate with the BHs because of the swirling of spacetime from the rotating body. We assume that u^α is the four-velocity of ZAMOs, and from the conservation of angular momentum $g_{\phi t}\dot{t} + g_{\phi\phi}\dot{\phi} = 0$, where an overdot is differentiation with respect to the proper time of the observers τ . Thus, $d\phi/dt = -g_{t\phi}/g_{\phi\phi}$. Because of this frame-dragging effect, there is a region of spacetime where static observers cannot exist, no matter how much external force is applied. This region is known as the “ergosphere” $r \leq M + \sqrt{M^2 - a^2 \cos^2 \theta}$. The rotation also leads to another interesting feature, called “superradiance”. That is, we can extract energy from scattering waves off the Kerr BHs.

Finally, the Kerr spacetime also possesses a curvature singularity at the origin $\rho^2 = r^2 + a^2 \cos^2 \theta$. However, in contrast to Schwarzschild case, this singularity can be avoided since it is a ring at $r = 0$ and $\theta = \pi/2$, where $z = 0$ and $x^2 + y^2 = a^2$. In principle, observers can go through the ring without hitting the singularity. However, it is widely believed that the inner horizon, r_- in Kerr spacetime is subject to an instability which would make the analytic extension of Kerr metric beyond r_- unphysical [229].

1.1.3 Blue-shift near horizon

As shown in the metric, different observers have different proper time. Hence, in the general relativity, the clocks at a gravitational field tick in a different speed in a different spacetime point. This is the blue(red)-shift effect, and it is extremely strong close to the dense object, especially near horizon.

Assuming static clocks in the Schwarzschild spacetime $ds^2 = -d\tau^2 = -(1 - 2M/r_o)dt^2$, where τ is the proper (clock) time of an observer at distance r_o . Hence, t is the proper time of an observer at infinity. The shifted wavelength λ_o measured by observers at r_o compared to observers at infinite is

$$\frac{\lambda_o}{\lambda_\infty} = \frac{d\tau}{dt} = \left(1 - \frac{2M}{r_o}\right)^{1/2}. \quad (1.6)$$

1.1.4 Thermodynamics of Semi-classical BH

Jacob Bekenstein and Stephen Hawking first proposed that the entropy of BHs is related to the area of their event horizons divided by the Planck area [56, 58, 59, 124, 144]. Further-

more, in 1974, Stephen Hawking showed that rather than being totally black, BHs emit thermal radiation at the Hawking temperature, $T_H = \kappa/2\pi$, where κ is the surface gravity at the horizon [141, 142, 140]. This then led to the celebrated Bekenstein-Hawking entropy formula $S_{\text{BH}} = A/4$ [124, 144], where A is the area of the event horizon. However, the nature of microstates of BHs that are enumerated by this entropy remains so far unknown. String theory associates it with higher dimensional fuzzball solutions, as discussed later in Sec. 2.5. Loop quantum gravity relates the quantum geometries of the horizon to the microstates [240]. Both these approaches can give the right Bekenstein-Hawking entropy, given specific assumptions and idealizations.

Interestingly, not only the entropy exists for the BHs, but also Brandon Carter, Stephen Hawking and James Bardeen [54] discovered the four laws of BH thermality analogous to the four laws of thermodynamics. The latter is presented in the parentheses.

- **The zeroth law:** A stationary BH has constant surface gravity κ . (A thermal equilibrium system has a constant temperature T_H .)
- **The first law:** A small change of mass for a stationary BH is related to the changes in the horizon area A , the angular momentum J , and the electric charge Q : $dM = \frac{\kappa}{8\pi}dA + \Omega dJ + \Phi dQ$, where Ω is the angular velocity and Φ is the electrostatic potential (Energy conservation: $dE = TdS - PdV - \mu dN$).
- **The second law:** The area of event horizon A never decreases in general relativity (The entropy of isolated systems never decreases).
- **The third law:** BHs with a zero surface gravity cannot be achieved (Matter in a zero temperature cannot be reached).

1.2 Membrane Paradigm

As mentioned above, in classical general relativity, freely falling observers experience no drama as they cross the event BH horizons, at least not until they reach the singularity inside the BH. However, to a distant and static observer outside a BH, any infalling objects are frozen at the horizons due to the blue-shift effect. Hence, the BH interior can be regarded as an irrelevant region for the static observers. Based on this complementary picture near horizon, in 1986, Kip S. Thorne, Richard H. Price and Douglas A. Macdonald published the idea of *membrane paradigm* [264]. They use a classically radiating membrane

to model the BHs, which is motivated as a useful tool to study physics outside BHs without involving any obscure behavior within BH interior.

Here we provide a simple calculation motivated by membrane paradigm for relating viscosity and reflectivity. We introduce a spherical membrane located infinitesimally outside the Schwarzschild radius, or the would-be horizon of QBHs. When the membrane is sufficiently thin, one can use the Israel junction condition to nicely embed the membrane in the Schwarzschild spacetime. The condition is

$$(K^{(+)}f_{ab} - K_{ab}^{(+)}) - (K^{(-)}f_{ab} - K_{ab}^{(-)}) = 8\pi T_{ab}, \quad (1.7)$$

where f_{ab} is the induced metric of the membrane, $K_{ab}^{(\pm)}$ is the extrinsic curvatures on its two sides, and T_{ab} is its stress tensor. The infalling observer will cross the horizon and enter the BH interior without possibility of seeing the membrane. However the static observer outside the BH can remove irrelevant interior region from the remaining spacetime inside the membrane. Assuming reflection symmetry $K_{ab}^+ = -K_{ab}^-$, the Israel junction condition on the membrane becomes

$$K^{(+)}f_{ab} - K_{ab}^{(+)} = 4\pi T_{ab}, \quad (1.8)$$

where the stress tensor T_{ab} is no longer zero but has contribution from the extrinsic curvature on the membrane.

Modifying Einstein gravity which revises the structure of BHs can provide a modified structure of the thin-shell membrane. We start by perturbing the Schwarzschild spacetime, whose metric is $g_{\mu\nu}^{\text{Sch}}$. Within Regge-Wheeler formalism [237], the axial axisymmetric perturbation $g_{\mu\nu} = g_{\mu\nu}^{\text{Sch}}(r) + \delta g_{\mu\nu}(r, \theta, t)$ take the form:

$$\delta g_{t\phi} = \epsilon e^{-i\omega t} h_0(r) y(\theta), \quad (1.9)$$

$$\delta g_{r\phi} = \epsilon e^{-i\omega t} h_1(r) y(\theta), \quad (1.10)$$

where other $\delta g_{\mu\nu}$ components vanish, and $\epsilon \ll 1$ controls the order of perturbation. The membrane stands at $r = r_0 + \epsilon R(t, \theta)$, where r_0 is its unperturbed position. We apply the Israel junction conditions $K_{ab} - K f_{ab} = -4\pi T_{ab}$ to Brown-York stress tensor as defined in [156]. The indexes μ, ν run over (t, r, θ, ϕ) in the 4d spacetime, while a, b run over (t, θ, ϕ) on the 3d membrane. We further assume that T_{ab} is the energy stress tensor of a viscous fluid:

$$T_{ab} = [\rho_0 + \epsilon \rho_1(t, \theta)] u_a u_b + [p_0 + \epsilon p_1(t, \theta) - \zeta \Theta] \gamma_{ab} - 2\eta \sigma_{ab}, \quad (1.11)$$

$$\sigma_{ab} = \frac{1}{2} (u_{a;c} \gamma_b^c + u_{b;c} \gamma_a^c - \Theta \gamma_{ab}), \quad (1.12)$$

$$\gamma_{ab} \equiv h_{ab} + u_a u_b, \quad \Theta \equiv u_{;a}^a, \quad (1.13)$$

where ρ_0 and p_0 (ρ_1 and p_1) are background (perturbation on) membrane density and pressure, and u_a , η and ζ are fluid velocity, shear viscosity, and bulk viscosity, respectively. Plugging Eqs. (1.9-1.13) into the the Israel junction condition, we find in the zeroth order in ϵ :

$$\rho_0(r_0) = -\frac{\sqrt{f(r_0)}}{4\pi r_0}, \quad (1.14)$$

$$p_0(r_0) = \frac{\sqrt{f(r_0)}(g(r_0) + r_0 g'(r_0))}{8\pi r_0 g(r_0)}, \quad (1.15)$$

where $g(r_0) = (1 - 2M/r_0)^{1/2}$ and $f(r_0) = 1 - 2M/r_0$. Assuming $u_\phi = 0$, $\theta\phi$ component of Israel junction condition gives in next order of ϵ :

$$\omega h_1(r) = -8i\pi\eta[h_1(r) + (r - r_g)h_1'(r)]. \quad (1.16)$$

We can further use $\psi_\omega = 1/r(1 - 2M/r)h_1(r)$ and the tortoise coordinate $x = r + 2M \log[r/(2M) - 1]$ to rewrite Eq. (1.16) as

$$\omega\psi_\omega = 16i\pi\eta\frac{\partial\psi_\omega}{\partial x}. \quad (1.17)$$

For the classical BHs with a purely ingoing boundary condition $\psi_\omega \propto e^{-i\omega x}$ at the horizon, Eq. (1.17) gives $\eta = 1/16\pi$, which is consistent with the standard membrane paradigm. If instead we assume there is no longer horizon but a reflective surface with $\psi_\omega = A_{out}e^{i\omega x} + A_{in}e^{-i\omega x}$, Eq. (1.17) gives:

$$\frac{A_{out}}{A_{in}} = \frac{1 - 16\pi\eta}{1 + 16\pi\eta}e^{-2i\omega x}. \quad (1.18)$$

Which relates the reflectivity of the membrane to the viscosity of the surface fluid.

1.3 Dawn of Gravitational Wave Astronomy

From 2015 onwards, the LIGO/Virgo collaboration reported unprecedented GW observations from binary BH merger events [13, 12, 15, 14, 21, 18, 19, 17]. It is the first time that humankind can detect GWs after one century of the Einstein's general theory of gravity. In

2017, Rainer Weiss, Kip Thorne and Barry C. Barish won the Nobel Prize in Physics “for decisive contributions to the LIGO detector and the observation of Gravitational Waves”.

Gravitational wave detectors are designed and improved for detecting any distorted spacetime by accelerated mass since 1960. LIGO/Virgo collaboration has the most sensitive detections based on laser interferometry. Gravitational wave will affect the distance between two free mass, which is then caught by the interferometry. By template from numerical relativity, they can reconstruct the waveform. Along this thesis, we will introduce modified theory of gravity which gives a different theoretical template for waveform, to be search in the data.

The first and most prominent binary BH merger signal seen by LIGO, GW150914, matches well with predictions of numerical relativity simulations that settle into Kerr metric, but contrary to original claims, it could not confirm the existence of the event horizons [81]. However, it opened a new front to test general relativity in strong gravity regime and Kerr-like spacetimes (e.g., Quantum BHs) from modified gravity, which is the main topic of this thesis.

This is the dawn of GW astronomy, and we stand at the threshold of a new age. We are detecting even more compact binary merger events with a better sensitivity from the O3 run of LIGO/Virgo. Future experiments such as Einstein Telescope, Cosmic Explorer, and LISA are expected to improve this by orders of magnitude. More studies on the echo-emission mechanism as well as observational strategies will be crucial for taking advantage of these new observations, to shed light on the nature of quantum BHs. It is our point of view that the best bet is on a sustained synergy between theory and observation, relying on well-motivated theoretical models (such as the Boltzmann reflectivity, aether holes, 2-2 holes, or fuzzballs, discussed in this review) to provide concrete templates for data analysis, which in turn could be used to pin down the correct theory underlying quantum BHs. With some luck, this has the potential to revolutionize our understanding of fundamental physics and quantum gravity.

1.4 Quantum Gravity and Equivalence Principle

The Einstein’s general theory of relativity is classical. However, in the Einstein field equation $G_{\mu\nu} = 8\pi GT_{\mu\nu}$, the classical spacetime geometry is related to stress energy tensor of quantum matter. For decades, scientist have tried to reconcile this inconsistency by embedding general relativity (or its generalizations) within some quantum mechanical framework, i.e. quantum gravity.

Conventional approach to quantizing Einstein gravity fails because it is not renormalizable. This implies that making predictions for observables, such as scattering cross-sections, requires knowledge of infinitely many parameters at high energies, leading to loss of *predictivity*. In the modern language, general relativity could at best be an effective field theory, and requires UV-completion beyond a cutoff near (or below) Planck energy (e.g., [111]).

Most proposals for this UV-completion involve replacing spacetime geometry with a more fundamental degree of freedom, such as strings (string theory) [230], discrete spins (loop quantum gravity) [44], spacetime atoms (causal sets) [68], or tetra-hydra (causal dynamical triangulation) [41]. More exotic possibilities include Asymptotic Safety [202], Quadratic Gravity [151], and Fakeon approach [42] that introduce a non-perturbative or non-traditional quantization schemes for 4d geometry. Yet another possibility is to modify the symmetry structure of General Relativity in the UV, as is proposed in Lorentz-violating (or Horava-Lifshitz) quantum gravity [153].

While proponents of these various proposals (with varying degrees of popularity) have claimed limited success in empirical explanations of some natural phenomena, it should be fair to say that none can objectively pass muster of *predictivity*. As such, for now, the greatest successes of these proposals remain in the realm of Mathematics.

Due to this lack of concrete predictivity, the EFT estimates (discussed above) are instead commonly used to argue that the quantum gravitational effects should only show up at Planck scale $\sim 10^{-35}$ m or 10^{28} eV, which is far from anything accessible by current experiments. However, such arguments miss the possibilities of non-perturbative effects (such as phase transitions) which depend on a more comprehensive understanding of the full phase space of the specific quantum gravity proposal.

For example, it has been shown that the non-perturbative quantum gravitational effects may lead to Planck-scale modifications of the classical BH horizons [186]. Proposed models like gravastars [195], fuzzballs [174, 175, 187, 188, 193], aether BHs [232], and firewalls [70, 40] amongst others [51, 159, 127, 89] all drastically alter the standard structure of the BH stretched horizons with a non-classical surface. Soon after the first reported detection of gravitational waves, [81] discerned that Planck-length structure modification around horizons leads to a similar waveform as in classical GR, but followed by later repeating signal — *echoes* — in the ringdown from the reflective surface that replaces the classical horizon. This discovery equals a new road leading to Rome — quantum nature of gravity — and has sparked off a novel area of modeling and searching for signatures from Quantum BHs. The next chapter will discuss the quantum theories of BH models and possible road maps to probe them, inspired by the detection of binary BH merger events in gravitational waves.

Chapter 2

Quantum Black Holes

2.1 Evaporation of BHs and the Information Paradox

It was already recognized by Stephen Hawking in the 1970s that the evaporation of a BH leads to an apparent breakdown of the unitarity of quantum mechanics. Here, we will briefly review this problem, which is known as the BH information loss paradox [143]. In the context of quantum field theory in curved spacetime, the energy flux out of a BH horizon is obtained by specifying a proper vacuum state and fixing the (classical) background spacetime. However, a radiating BH must lose its mass in time, and so fixing the background is valid only for a much shorter timescale than the evaporation timescale. One can roughly estimate the lifetime of a BH as follows: The energy expectation value of a Hawking particle is of the order of the Hawking temperature $T_H \equiv (8\pi M)^{-1}$, which would be emitted over the timescale of $t \sim M$. Then we can estimate the luminosity of the BH as

$$\frac{dM}{dt} \sim \frac{-T_H}{M} \sim -(M^2)^{-1}, \quad (2.1)$$

and this gives its lifetime t_{life}

$$t_{\text{life}} \sim M^3. \quad (2.2)$$

To be consistent with the result of a more rigorous calculation (see e.g. [117]), we need a factor of about 10^5 in (2.2)

$$t_{\text{life}} \simeq 10^5 M^3 \sim 10^{75} \left(\frac{M}{M_\odot} \right)^3 [\text{sec}], \quad (2.3)$$

which is much much longer than the cosmic age of $\sim 4 \times 10^{17}$ [sec] for astrophysical BHs whose mass are $\gtrsim M_\odot$. It may be true that BHs evaporate due to the Hawking radiation, at least, until reaching the Planck mass. However, the gravitational curvature near the horizon eventually reaches the Planckian scale and the classical picture of background gravitational field would break down. As such, the possibility of leaving a “remnant” after the evaporation has been discussed (see e.g. [38, 48, 125, 33]), but the most natural possibility would be that only Hawking radiation is left after the completion of the BH evaporation.

If the Hawking evaporation just leaves the “thermal” radiation afterwards, one can immediately understand why the evaporation process is paradoxical. Let us suppose that a pure quantum state collapses into a BH and it radiates Hawking quanta until the BH evaporates. If the final state is a thermal mixed state, the evaporation is a process which transforms a pure to mixed state. Therefore, if the final state of any BH is a completely thermal state, one can say that the evaporation process is a non-unitary process. The information loss paradox can be also explained from the geometric aspect using the Penrose diagram. In quantum mechanics, the time-evolution of a quantum state is described by a unitary operator, \hat{U} , that maps an initial quantum state $|\text{in}\rangle$ on a past Cauchy surface Σ_i into a final quantum state $|\text{f}\rangle$ on a future Cauchy surface Σ_f . Since the unitary operator gives a reversible process, one can also obtain the initial state from the final state as

$$|\text{in}\rangle = \hat{U}^\dagger |\text{f}\rangle. \quad (2.4)$$

Although this is true in a flat space, the argument is very controversial in the existence of an evaporating BH. Assuming a gravitational collapse forms a horizon and singularity, then it eventually evaporates, leaving behind a thermal radiation, the Penrose diagram describing the whole process is given by Fig. 2.1. Let us consider three quantum states: an initial quantum state $|\text{in}\rangle$ on Σ_i , an intermediate quantum state $|\text{mid}\rangle$ on Σ_m , and a final state $|\text{f}\rangle$ on Σ_f , where Σ_i , Σ_m , and Σ_f are the Cauchy surfaces and Σ_m intersects the future horizon H^+ and so one can split it into the exterior and interior regions as $\Sigma_m \equiv \Sigma_{\text{ext}} \cup \Sigma_{\text{int}}$ (see Fig. 2.1).

The final quantum state $|\text{f}\rangle$ is determined by information on the exterior part of the intermediate Cauchy surface Σ_{ext} rather than that on the whole intermediate Cauchy surface Σ_m , which leads to the information loss paradox. To see this in more detail, let us consider an initial pure quantum state

$$|\text{in}\rangle = \sum_i c_i^{\text{in}} |\psi_i\rangle, \quad (2.5)$$

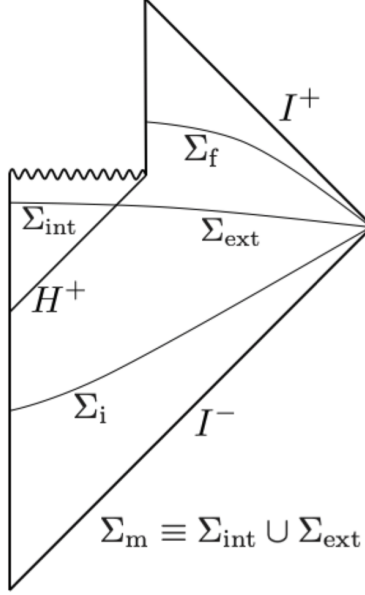


Figure 2.1: The Penrose diagram describing an evaporating BH.

where $\{c_i^{\text{in}}\}$ is an initial vector in the Hilbert space. The intermediate state is still a pure state due to the unitary evolution of $|\text{in}\rangle$

$$|\text{mid}\rangle = \hat{U} |\text{in}\rangle = \sum_{i,j} c_{i,j} |\psi_i\rangle_{\text{int}} \otimes |\psi_j\rangle_{\text{ext}}, \quad (2.6)$$

the time-evolution from Σ_m to Σ_f is non-unitary, provided that the final state on Σ_f is obtained by the unitary evolution of the exterior intermediate state. The density matrix of the exterior intermediate state, denoted by $\hat{\rho}_{\text{ext}}$, is obtained by tracing over all the internal basis states:

$$\hat{\rho}_{\text{ext}} = \sum_k \langle \psi_k |_{\text{int}} |\text{mid}\rangle \langle \text{mid} | \psi_k \rangle_{\text{int}} = \sum_{k,j,j'} c_{k,j} c_{k,j'}^* |\psi_j\rangle_{\text{ext}} \langle \psi_{j'} |_{\text{ext}}. \quad (2.7)$$

The resulting density matrix, (2.7), is independent of the interior orthogonal basis $\{|\psi_j\rangle_{\text{int}}\}$ due to the tracing operation. Therefore, the loss of the interior information results in a non-unitary evolution and an initial quantum state evolves to a mixed state after the BH evaporation.

2.2 BH complementarity

The BH complementarity has been one of the leading proposals for the retrieval of BH information, which was first put forth by Susskind, Thorlacius, and Uglum [260]. According to a distant observer, due to the infinite redshift at a BH horizon, the Hawking radiation involves modes of transplanckian frequency whose energy can be arbitrarily large in the vicinity of the horizon. In the BH complementarity proposal, the energetic modes form the membrane, which can absorb, thermalize, and reemit information, on the BH horizon. They argue that such a picture regarding the retrieval of BH information by the stretched horizon is consistent with the following three plausible postulates:

Postulate 1 (unitarity)— According to a distant observer, the formation of a BH and the evaporation process can be described by the standard quantum theory. There exists a unitary S-matrix which describes a process from infalling matter to outgoing non-thermal radiation.

Postulate 2 (semi-classical equations)— Outside the stretched horizon of a massive BH, physics can be approximately described by a set of semi-classical field equations.

Postulate 3 (degrees of freedom)— For a distant observer, the number of microscopic states of a BH can be estimated by $\exp S(M)$, where the exponent $S(M)$ is the Bekenstein-Hawking entropy.

On the other hand, it has been presumed that a freely infalling observer would not observe anything special when passing through the horizon due to the equivalence principle. In this sense, there are two totally different and seemingly inconsistent scenarios that co-exist in the BH complementarity. However, the contradiction arises only when attempting to compare the experiments performed inside and outside horizon, which might be impossible due to a backreaction of the high-energy modes near the stretched horizon [259].

2.3 Firewalls

In 2012, Almheiri, Marolf, Polchinski and Sully (AMPS) argued [40] that the Postulates 1-3 in the BH complementarity and the Equivalence principle of GR are mutually inconsistent for an *old BH* [218, 219, 220], provided that the monogamy of entanglement is satisfied. Then they argued that the “most conservative” resolution is a violation of the equivalence principle near the BH and its horizon should be replaced by high-energetic quanta, so called “firewall”, to avoid the inconsistency. Before introducing the original firewall argument in

more detail, let us review a theorem in quantum information theory, the monogamy of entanglement. Let us consider three independent quantum systems, A, B, and C. The strong subadditivity relation of entropy is given by

$$S_{AB} + S_{BC} \geq S_B + S_{ABC}. \quad (2.8)$$

If A and B is fully entangled, we have

$$S_{AB} = 0 \quad \text{and} \quad S_{ABC} = S_C. \quad (2.9)$$

Then the strong subadditivity relation reduces to

$$S_B + S_C - S_{BC} \leq 0. \quad (2.10)$$

Since the left hand side in (2.10) is the mutual information of B and C, denoted by I_{BC} , and it is a non-negative quantity, (2.10) reduces to

$$I_{BC} = S_B + S_C - S_{BC} = 0, \quad (2.11)$$

which means that the quantum system B cannot fully correlate with C when B and A are fully entangled mutually. Therefore, any quantum system cannot fully entangle with other two quantum systems simultaneously. This is the monogamy of entanglement that is an essential theorem in the firewall argument.

Let us consider an old BH, whose origin is a gravitational collapse of a pure state, with early Hawking particles A, late Hawking particle B, and infalling particle inside the horizon C. In order for the final state of the BH to be pure state, A and B should be fully entangled mutually, that is a necessary condition for the Postulate 1. On the other hand, created pair particles, B and C, are also fully entangled according to the quantum field theory in classical background (Postulate 2). That is, imposing the Postulate 1 and 2 inevitably results in that B is fully and simultaneously entangled with both A and C, which obviously contradicts with the monogamy of entanglement. In order to avoid this contradiction, AMPS argued that there is no interior of BHs and the horizons should be replaced by energetic boundaries that the entanglement of Hawking pairs are broken. They called these boundaries “firewalls”. According to this proposal, any object falling into a BH would burn up at the firewall, which contradicts the equivalence principle (in vacuum) and replaces the BH complementarity proposal. Although there are some updates of this proposal, based on ER=EPR conjecture [39, 222, 180, 258, 69], backreaction due to gravitational shockwaves [286], and quantum decoherence of Hawking pair due to the interior tidal force [208]), they do remain speculative, and at the level of toy models. However, on general grounds, if quantum effects lead to such an energetic wall at the stretched horizon, it could contribute to the reflectivity of BH which may be observable by merger events leading to the formation of BHs.

2.4 Gravastars

The gravitational vacuum condensate star (gravastar) was proposed as a final state of gravitational collapse by Mazur and Mottola [195]. According to the proposal, the resulting state of gravitational collapse is a cold compact object whose interior is a de Sitter condensate, which is separated from the outside black hole spacetime by a null surface. In this state, there is no singularity (with the exception of the null boundary) and no event horizon, which avoids the BH information loss paradox. Such gravitational condensation could be caused by quantum backreaction at the Schwarzschild horizon $r = r_g$ even for an arbitrarily large-mass collapsing object. One might wonder why the backreaction can lead to such a drastic effect for any mass since the tidal force which acts on an infalling test body can be arbitrarily weak for an arbitrarily large mass at the Schwarzschild radius. The argument is that considering a photon with asymptotic frequency ω near the Schwarzschild radius, the (infinite) blue-shift effect by which the local energy is enhanced as $\hbar\omega/\sqrt{1 - r_g/r}$, could lead to a drastic effect at the Schwarzschild radius. This is unavoidable since any object is immersed in quantum vacuum fluctuations and virtual particles always exist around them. From this argument, the gravitational condensation has been expected to take place at the final stage of gravitational collapse. The authors in [195] also estimate the entropy on the surface of gravastar by starting with a simplified vacuum condensate model which consists of three different equations of state

$$0 \leq r < r_1, \quad \rho = -p, \quad (2.12)$$

$$r_1 < r < r_1 + \delta r, \quad \rho = p, \quad (2.13)$$

$$r_1 + \delta r < r, \quad \rho = p = 0, \quad (2.14)$$

where r_1 is the radius of interior region and δr is the thickness of the thin-shell of the gravastar. Then the obtained entropy of the shell was found out to be $S \sim 10^{57} g k_B (M/M_\odot)^{3/2}$, where g is a dimensionless constant. Recently, the derivation of gravastar-like configuration was performed by Carballo-Rubio [79]. He derived the semi-classical Tolman-Oppenheimer-Volkoff (TOV) equation by taking into account the polarization of quantum vacuum and solved it to obtain the exact solution of an equilibrium stellar configuration. It also has its de Sitter interior and thin-shell near the Schwarzschild radius, which is consistent with the original gravastar proposal [195].

From the observational point of view, the shadows of a gravastar was investigated in [243] where they argue the shadows of a BH and gravastar could be distinguishable. In addition, tests of gravastar with GW observations have been discussed in e.g. [221, 82, 99].

2.5 Fuzzballs

Samir D. Mathur has proposed fuzzballs [187] as description of true microstates of the quantum BHs from string theory. A fuzzball state has the BH mass inside a horizon-sized region and a smooth (but higher-dimensional) geometry. Here are some crucial features of the conjecture:

1. Different fuzzball geometries represent different microstates of the quantum BH — fuzzball. Application the AdS/CFT duality [181] suggests that the counting of the microstates is consistent with the Bekenstein-Hawking entropy.
2. Fuzzballs do not possess horizons. Instead, they end with smooth "caps" near where the horizons would have been. Every microstate has almost the same geometry outside the would-be horizon matching the classical BH picture for the outside observers. But the microstates differ from each other near the would-be horizons.
3. Fuzzball solves the information paradox by removing the horizon and singularity. The horizon is replaced by fuzzy matter and no longer vacuum. The particles created near the would-be horizon now have access to the information of fuzzball interior. Moreover, the higher-dimensional spacetime ends smoothly around the would-be horizon and is singularity-free. The infalling particles at the low frequencies interact with the "fuzz" for a relatively long time scale, while high frequency ones excite the microstates and lose their energy the same as in the classical BHs case. Hence, the traditional horizons only show up effectively from the point of view of an outside observers, over relatively short time scale $\lesssim M \log(M)$.

How do these higher dimensional "microstates" with the smooth and horizonless geometries looks like? Applying Kaluza-Klein reduction of non-supersymmetric microstates

of the D1-D5-KK system [132]. the metric in 4D is

$$ds_4^2 = -\frac{f^2}{\sqrt{AD}}(dt + c_1 c_5 \omega)^2 + \sqrt{AD} \left[\frac{dr^2}{\Delta} + d\theta^2 + \frac{\Delta}{f^2} \sin^2 \theta d\varphi^2 \right] \quad (2.15)$$

$$\Delta = r^2 - r_0^2, \quad (2.16)$$

$$f^2 = \Delta + r_0^2 n^2 \sin^2 \theta, \quad (2.17)$$

$$A = f^2 + 2p[(r - r_0) + n^2 r_0(1 + \cos \theta)], \quad (2.18)$$

$$B = f^2 + 2\frac{r_0(r-r_0)(n^2-1)}{p-r_0(1+n^2)}[(r - r_0) + n^2 r_0(1 - \cos \theta)], \quad (2.19)$$

$$C = 2\frac{r_0\sqrt{r_0(r+r_0)n(n^2-1)}}{p-r_0(1+n^2)}[(r - r_0) + (p + r_0)(1 - \cos \theta)], \quad (2.20)$$

$$G = \frac{Af^2 - C^2}{B^2}, \quad (2.21)$$

$$D = Bc_1^2 c_5^2 - f^2(c_1^2 s_5^2 + s_1^2 c_5^2) + \frac{Gf^2}{A} s_1^2 s_5^2, \quad (2.22)$$

$$J^2 = \frac{r_0^3 p(r+r_0)n^2(n^2-1)^2}{p-r_0(1+n^2)}, \quad (2.23)$$

$$\omega^2 = \frac{2J \sin^2 \theta (r-r_0)}{f^2} d\varphi, \quad (2.24)$$

where parameters c_1 , c_5 , s_1 , s_5 , r_0 , n and p are related to the mass, angular momentum and charges of the solution.

This specific reduced 4D fuzzball solution has an associated 4D effective fluid near the would-be horizon. The anisotropic pressure of the fluid is crucial to the horizonless geometry[279].

2.6 Aether Holes and Dark Energy

In 2009, Prescod-Weinstein, Afshordi, and Balogh [233] studied the spherically symmetric solutions of the Gravitational Aether proposal for solving the old cosmological constant problem [34, 46]. Surprisingly, they showed that if one sets Planck-scale boundary conditions for aether near the horizons of stellar mass BHs, its pressure will match the observed pressure of dark energy at infinity.

In the Gravitational Aether proposal [34, 46], the modified Einstein field equation is given by

$$\frac{1}{8\pi G'} G_{\mu\nu} = T_{\mu\nu} - \frac{1}{4} T^\alpha{}_\alpha g_{\mu\nu} + T'_{\mu\nu}, \quad (2.25)$$

$$T'_{\mu\nu} = p'(u'_\mu u'_\nu + g_{\mu\nu}), \quad (2.26)$$

where $G' = 4/3G_N$, and then energy-momentum tensor of aether is assumed to be a perfect fluid with stress-energy tensor $T'_{\mu\nu}$ without energy density. Here, quantum vacuum energy decouples from the gravity, as only the traceless part of the matter energy-momentum tensor appears on the right-hand side of the field equations. It can be shown that the Bianchi identity and energy-momentum conservation completely fix the dynamics, and thus the theory has no additional free parameters, or dynamical degrees of freedom, compared to General Relativity.

The modified Schwarzschild metric is the vacuum solution with spherical symmetry in modified equations, and identical to a traditional equations sourced by the aether perfect fluid. Far away from the would-be horizon but close enough to the origin ($2M \ll r \ll |p_0|^{-1/2}$), the solution has the form

$$ds^2 = -(1 + 4\pi p_0 r^2)dt^2 + dr^2 + r^2 d\Omega^2 \quad (2.27)$$

which can be compared to the de Sitter metric

$$ds^2 = -(1 - \frac{8}{3}\pi\rho_\Lambda r^2)dt^2 + (1 - \frac{8}{3}\pi\rho_\Lambda r^2)^{-1}dr^2 + r^2 d\Omega^2 \quad (2.28)$$

We see that assuming $p_0 = -2/3\rho_\Lambda$, the g_{tt} 's agree with each other. Therefore, the Newtonian observers (for $2M \ll r \ll |p_0|^{-1/2}$) will experience the same acceleration as in the de-Sitter metric with the cosmological constant. However, on larger scales, one has to take into account the effects of multiple black holes and other matter in the Universe. The Planckian boundary conditions at the (would-be) horizon relates the pressure of the aether to the mass of the astrophysical BHs, $-p_0 \sim M^{-3}$ [233]. In particular, the BH masses within the range $10 M_\odot - 100 M_\odot$, which correspond to the most astrophysical BHs in galaxies, yield aether pressures comparable to the pressure of Dark Energy, inferred from cosmic acceleration. Moreover, Ricci scalar is inversely proportional to g_{tt} , so the event horizon where $g_{tt} = 0$ has a curvature singularity, which is reminiscent of the firewall and fuzzball proposals discussed above.

In particular, the fuzzball paradigm is a good approach to remove the singularity. On the one hand, fuzzball gives an extra anisotropic matter field similar to the aether theory, which stands as a good evidence that quantum effects can modify the Einstein field equation with extra sources of 4d energy-momentum like aether. Furthermore, fuzzball is a regular and horizonless geometry, which might indicate the singularity is removable in the full quantum picture of BHs.

2.7 2-2 holes

In general relativity, gravitational collapse of ordinary matter will always leads to singularities behind trapping horizons [227]. In [152], Holdom and Ren revisited this problem with the asymptotically free quadratic gravity, which could be regarded as a UV completion of general relativity [152]. The quantum quadratic gravity (QQG), whose action is given by

$$S_{\text{QQG}} = \int d^4x \sqrt{-g} \left(\frac{1}{2} \mathcal{M}^2 R - \frac{1}{2f_2^2} C_{\mu\nu\alpha\beta} C^{\mu\nu\alpha\beta} + \frac{1}{3f_0^2} R^2 \right), \quad (2.29)$$

is famously known to be not only asymptotically free, but also perturbatively renormalizable [257, 275, 121, 47]. However, it suffers from a spin-2 ghost due to the higher derivative terms, which is commonly regarded as a pathology of the theory. In [152], it is proposed that the ghost may not be problematic when \mathcal{M} is sufficiently small, so that the poles in the perturbative propagators fall into the non-perturbative regime, and the perturbative analysis of ghosts is not reliable. Then it is conjectured [151] that the full graviton propagator in the IR, when $\mathcal{M} \lesssim \Lambda_{\text{QQG}}$, the spin-2 ghost pole is absent in an analogy with the quantum chromodynamics (QCD) where the gluon propagator, describing off-shell gluons, also does not have a pole. Here Λ_{QQG} is a certain critical value in QQG, analogous to confinement scale Λ_{QCD} in QCD. Based on this conjecture, the asymptotically free quadratic action in (2.29) may involve small quadratic corrections at super-Planckian scale, and so the super-Planckian gravity might be governed by the classical action

$$S_{\text{CQG}} = \frac{1}{16\pi} \int d^4x \sqrt{-g} (M_{\text{Pl}}^2 R - \alpha C_{\mu\nu\alpha\beta} C^{\mu\nu\alpha\beta} + \beta R^2). \quad (2.30)$$

Since gravitational collapse would involve the super-Planckian energy scale, applying the classical action (2.30) to such a situation is interesting from a point of view of the quantum gravitational phenomenology. Then the authors in [152] found a solution of horizonless compact object, so-called 2-2 hole, in the classical quadratic gravity. 2-2 holes have an interior with a shrinking volume and a timelike curvature singularity at the origin. It also has a thin-shell configuration, leading to non-zero reflectivity at the would-be horizon, which may cause the emission of GW echoes [99]. Recently, 2-2 holes sourced by thermal gases were also investigated in [149, 238].

2.8 Non-violent Unitarization

A separate class of possible approaches to the BH information paradox involves a violation Postulate 2 in BH complementarity, i.e. non-locality of field equations well outside the

stretched horizon, which is dubbed as “nonviolent unitarization” by Steve Giddings [128]. Such a possibility would allow for transfer of information outside horizon around the Page time (e.g., [52, 53]), but could also lead to large scale observable deviations from general relativistic predictions in GW and electromagnetic signals [129]. However, it is not clear whether this non-locality is only limited to BH neighborhoods, and if not, how it could affect precision experimental/observational tests in other contexts. Moreover, in contrast to GW echoes that we shall discuss next, it is hard to provide concrete predictions for astrophysical observations in the nonviolent unitarization scenarios.

Chapter 3

Black Hole Echology

3.1 Introduction

As discussed in early chapters, motivated by the BH information paradox and cosmological constant problems, it has been suggested that non-perturbative quantum gravitational effects may lead to Planck-scale modifications of BH horizons. Proposals to solve the BH information paradox include gravastars [195], fuzzballs [174, 175, 187, 188, 193], and firewalls [70, 40], amongst others [51, 159]. These QBHs all modify the standard structure of BH horizons, and should form by Page time $\sim M^3$, but can emerge as early as the “scrambling time” $\sim M \log M$ [145, 253].

Recent detections of gravitational waves from binary BH mergers by the LIGO-Virgo collaboration [13, 12, 127, 15, 14, 21, 18, 19, 17] provide a way to test the structure around the horizon scale. Shortly after LIGO’s first detection, GW150914, [81, 82] argued that introducing a wall to replace horizon might yield a similar ringdown waveform as GR BHs, but produce delayed echoes (see [84, 83] for a review) in the gravitational wave signal. Using a phenomenological template by truncating the GR merger waveforms, [29] carried out the first search for echoes and claimed a 2.5σ tentative evidence for them in the the first three (candidate) events in the LIGO public data (but see [45, 282] and [30] for a critique/rebuttal).

An independent search [99], using a different methodology, has recently found evidence for echoes in each of LIGO’s merger events (with the notable exception of GW150914) at $\sim 3\sigma$ significance level. However, we should note that the echoes reported in [29] and [99] are for different events, even though they are both broadly consistent with the

hypothesis of near-horizon Planck-scale structure. In particular, [30, 282] fail to find echoes in GW151226, which has the most significant evidence for echoes in [99], suggesting that the two methods capture different parts of the echo waveform.

Most recently, [?] claim a tentative detection of (lower harmonics of) echoes, at 4.2σ level, from a “black hole” remnant in the aftermath GW170817 binary neutron star merger.

While one may consider other phenomenological echo templates (e.g., [185]), more realistic templates for fitting data may be found by solving (linearized) Einstein equations with modified boundary conditions near the horizon. Along this direction, most studies have at that time focused on Schwarzschild BHs (e.g., [81, 82, 235, 183, 277, 276]). In this chapter, we extend this to Kerr metric as realistic BHs have spin. [197] also presented echo templates by modelling the reflectivity of the angular momentum barrier in the Kerr spacetime. We, however, model the propagation in the full spacetime which provides a more realistic treatment at lower frequencies.

Another related work at that time is [76] which studies the echoes of scalar Gaussian wavepackets in Kerr-like wormholes. In contrast, we study generic propagation in Kerr spacetime, with arbitrary boundary conditions, which can be applied not only to scalar fields ($s=0$), but also massless Dirac ($s = \pm 1/2$), electromagnetic ($s = \pm 1$), or gravitational ($s = \pm 2$) fields. Interestingly (but not surprisingly), we come to some similar conclusions, e.g., *i*) Spinning QBHs give rise to unstable modes which, however, do not affect the echoes till very late times (depending on whether the initial frequency range is within the superradiance regime). *ii*) It is hard to make a model-independent prediction for the first echo.

A related phenomenological issue that arises when we replace the horizon with a wall is the emergence of superradiant instability for horizonless ergoregions [122, 86, 102]. While this might suggest long-term instability of spinning QBHs, which may be in conflict with astrophysical spin measurements for BHs [198], it was suggested by [177] that an absorption rate of the wall as small as 0.4% is sufficient to quench the instability completely.

We organize this chapter as follows: Sec 3.2 provides the linear Einstein equations and boundary conditions used. Instead of normal boundary condition with no outgoing wave on the horizon, we put a wall standing just outside the would-be horizon. The reflection rate of the wall depends on the specific model of quantum BHs. Sec 3.3 presents echo solutions for different positions of a perfect wall and time-delays of a geometric formula given in [29], while Sec 3.4 discusses how superradiance of Kerr geometry is manifested in echo templates. In Sec 3.5, we provide an analytic fit to the echo templates, based on solutions in Sec 3.3. We explore a soft wall with frequency-dependent reflection, as well as nonlinear corrections to initial conditions in Sec 3.6 for a more realistic picture. In

Table 3.1: Corresponding field ψ for different spin weight s in Master equation, where $\rho^{-1} = -(r - ia \cos \theta)$.

s	0	-1/2, 1/2	-1, 1	-2, 2
ψ	Φ	$\chi_0, \rho^{-1}\chi_1$	$\phi_0, \rho^{-2}\phi_2$	$\Psi_0, \rho^{-4}\Psi_4$

Sec 3.7, we briefly discuss ergoregion instability developed in the presence of a perfect wall. While in principle the instability is significant at high spins, we show that these instabilities do not affect the first several echoes of typical binary merger events. Finally, Sec 3.8 concludes our work.

For concreteness, we use the best fit properties and waveforms resulting from the GW150914 merger event, provided by the LIGO-Virgo collaboration [13, 12]¹. In particular, the detector frame mass and reduced spin parameter of the remnant used for the echo calculation are $M_{\text{fin}} = 67.6 M_{\odot}$ and $a = 0.67$. Echo templates for other final masses can be found by rescaling our analytic templates, as long as the dimensionless binary properties are not too different from those of GW150914.

3.2 Propagation and Boundary Conditions in Kerr spacetime

We study the propagation of gravitational waves using linearized Einstein equations in Kerr geometry which describes the spacetime of a spinning BH. In order to model a QBH, we simply replace the Kerr event horizon with a wall, where boundary conditions for linear perturbations are modified. The initial condition here is an incoming wavepacket h_{in} from infinity, and we calculate the outgoing wavepacket h_{out} by solving the linear Einstein equations. As usual, we use the Newman-Penrose (NP) Formalism which greatly simplifies perturbation in Kerr metric, reducing to only a single master equation (known as the Teukolsky equation) which describes propagation of all scalar ($s = 0$), massless Dirac ($s = \pm 1/2$), electromagnetic ($s = \pm 1$) and gravitational ($s = \pm 2$) fields (see [262] for details):

¹<https://losc.ligo.org/events/GW150914/>

$$\begin{aligned}
& \left[\frac{(r^2 + a^2)^2}{\Delta} - a^2 \sin^2 \theta \right] \frac{\partial^2 \psi}{\partial t^2} + \frac{4Mar}{\Delta} \frac{\partial^2 \psi}{\partial t \partial \varphi} + \left(\frac{a^2}{\Delta} - \frac{1}{\sin^2 \theta} \right) \frac{\partial^2 \psi}{\partial \varphi^2} \\
& - \Delta^{-s} \frac{\partial}{\partial r} \left(\Delta^{s+1} \frac{\partial \psi}{\partial r} \right) - \frac{1}{\sin \theta} \frac{\partial}{\partial \theta} \left(\sin \theta \frac{\partial \psi}{\partial \theta} \right) - 2s \left[\frac{a(r-M)}{\Delta} + \frac{i \cos \theta}{\sin^2 \theta} \right] \frac{\partial \psi}{\partial \varphi} \\
& - 2s \left[\frac{M(r^2 - a^2)}{\Delta} - r - ia \cos \theta \right] \frac{\partial \psi}{\partial t} + (s^2 \cos^2 \theta - s) \psi = 0, \tag{3.1}
\end{aligned}$$

where the field ψ for each spin weight s corresponds to NP quantities presented in Table 3.1. The Teukolsky equation (3.1) is separable in coordinates in the frequency domain and can be decomposed into 4 ODEs. Furthermore, the symmetries in time and azimuth, allows for Fourier space decomposition in t and φ :

$$\psi = \frac{1}{2\pi} \int d\omega e^{i(-\omega t + m\varphi)} S[\theta] R[r], \tag{3.2}$$

$$\Delta^{-s} \frac{d}{dr} \left(\Delta^{s+1} \frac{dR}{dr} \right) + \left[\frac{K^2 - 2is(r-M)K}{\Delta} + 4is\omega r - \lambda \right] R = 0, \tag{3.3}$$

$$\begin{aligned}
& \frac{1}{\sin \theta} \frac{d}{d\theta} \left(\sin \theta \frac{dS}{d\theta} \right) = \\
& - \left(a^2 \omega^2 \cos^2 \theta - \frac{m^2}{\sin^2 \theta} - 2a\omega s \cos \theta - \frac{2ms \cos \theta}{\sin^2 \theta} - s^2 \cot^2 \theta + s + A_{slm} \right) S, \tag{3.4}
\end{aligned}$$

where $K = (r^2 + a^2)\omega - am$ and $\lambda = A_{slm} + a^2\omega^2 - 2am\omega$. The solution for the angular mode is spin-weighted spheroidal harmonic (full discussion can be found in [61]). We solve the radial mode numerically based on [71], with publicly available Mathematica code, which was developed to study superradiance in Kerr metric ². Eq 3.3 has the following asymptotic solutions ((see [262] for details)):

$$R = \mathcal{T} \Delta^{-s} e^{-ik_{\text{h}} r^*} + \mathcal{O} e^{ik_{\text{h}} r^*}, r \rightarrow r_+, \tag{3.5}$$

$$R = \mathcal{I} \frac{e^{-i\omega r^*}}{r} + \mathcal{R} \frac{e^{i\omega r^*}}{r^{2s+1}}, r \rightarrow \infty, \tag{3.6}$$

where r^* is tortoise coordinate (defined as $r^* = \int (r^2 + a^2)/(r^2 - 2Mr + a^2) dr$ that approaches $-\infty$ at horizon), $k_{\text{h}} = \omega - am/(2Mr_+)$ and $r_+ = M + \sqrt{M^2 - a^2}$. Here \mathcal{T} and \mathcal{O} are the reflective and transmissive amplitude near horizon, while \mathcal{I} and \mathcal{R} are ones at infinity.

²<https://centra.tecnico.ulisboa.pt/network/grit/files/amplification-factors/>

In classical General Relativity, everything that reaches the horizon will fall into the BH, and thus there is no outgoing wave at $r \rightarrow r_+$, i.e. $\mathcal{O} = 0$. However, for QBHs we assume that quantum gravity effects replace the horizon with (partially) reflective wall standing the order of Planck length proper distance outside the (would-be) horizon. We shall assume that this modifies the boundary condition, so that the wall reflects the incoming energy flux (see [197] for definition of energy near horizon) with a rate R but does not change the phase:

$$|\mathcal{O}|^2 = R_{\text{wall}} \left| \frac{C}{D} \right|^{s/2} |\mathcal{T}|^2, \quad \arg[\mathcal{T} \Delta^{-s} e^{-ik_{\text{h}} r^*}] = \arg[\mathcal{O} e^{ik_{\text{h}} r^*}] \quad r \rightarrow r_{\text{wall}}, \quad (3.7)$$

$$C = B \{-36a^2\omega^2 + 36am\omega + [\lambda + (s+1)s - 2]^2\} + \{2[\lambda + (s+1)s] - 1\} \\ \times (96a^2\omega^2 - 48am\omega) + 144\omega^2 (M^2 - a^2), \quad (3.8)$$

$$B = [\lambda + s(s+1)]^2 + 4maw - 4a^2\omega^2, \quad (3.9)$$

$$D = 256k_{\text{h}}^2 (2Mr_+)^8 \left[k_{\text{h}}^2 + \frac{4(M^2 - a^2)}{(4Mr_+)^2} \right]^2 \left[k_{\text{h}}^2 + \frac{16(M^2 - a^2)}{(4Mr_+)^2} \right]. \quad (3.10)$$

$R_{\text{wall}} = 1$ would correspond to a perfectly reflective wall, but the actual reflectivity and phase change depend on the specific quantum gravity model for QBHs. In the rest of the paper, we will present solutions to these equations with different choices of the reflectivity and discuss the important properties of solutions, such as echo templates, time-delays and superradiant instability.

3.3 Making Echoes

Realistic predictions for Echo waveforms requires nonlinear simulations of the mergers of binary QBHs in full general relativity. As a consistent covariant formulation for dynamics of QBHs is yet non-existent, we have to rely on approximate methods to produce realistic echo templates. In order to do this using linear theory, we instead custom-design an ingoing wavepacket \hat{h}_{in} at infinity, so that the outgoing waveform matches the LIGO best-fit template \hat{h}_{LIGO} (without a wall). The higher frequencies will go across the barrier and fall into BH, as shown in Fig 3.1 (left), while the lower frequencies are reflected. We thus assume

$$\hat{h}_{\text{LIGO}}(\omega) = R_{\text{BH}}(\omega) \hat{h}_{\text{in}}(\omega), \quad (3.11)$$

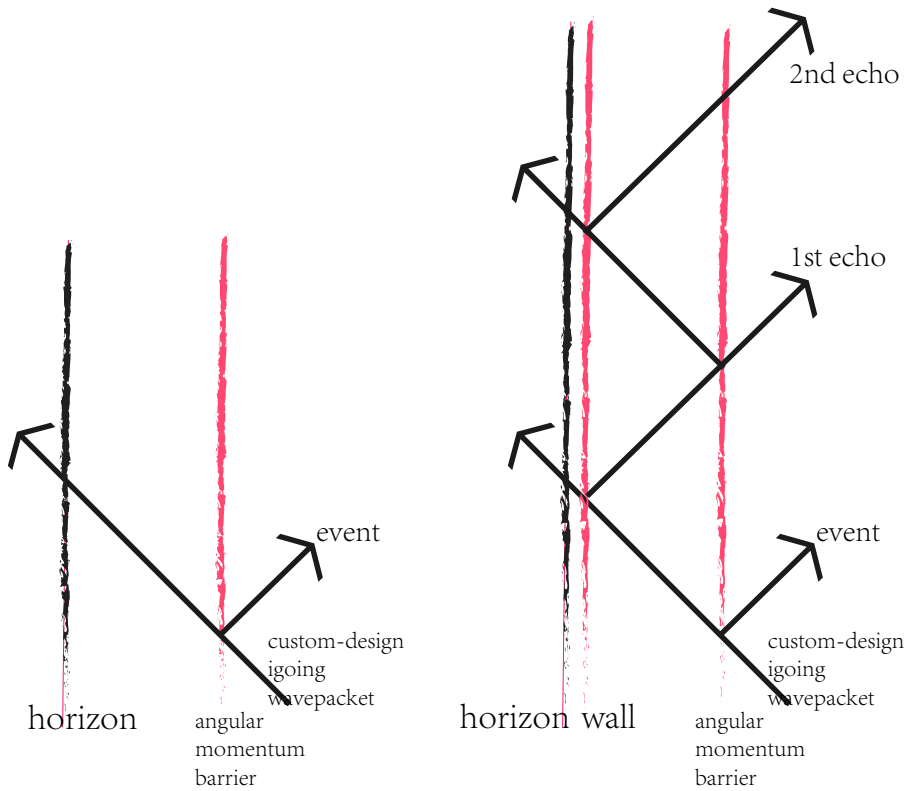


Figure 3.1: BHs and QBHs with an ingoing wavepacket. For BHs, angular momentum barrier reflects low frequency modes but higher frequencies cross the barrier and fall through the horizon. For QBHs with a wall standing the order of Planck length proper distance outside the (would-be) horizon, modes with intermediate frequencies can be trapped between the wall and the angular momentum barrier, slowly leaking out as repeating echoes.

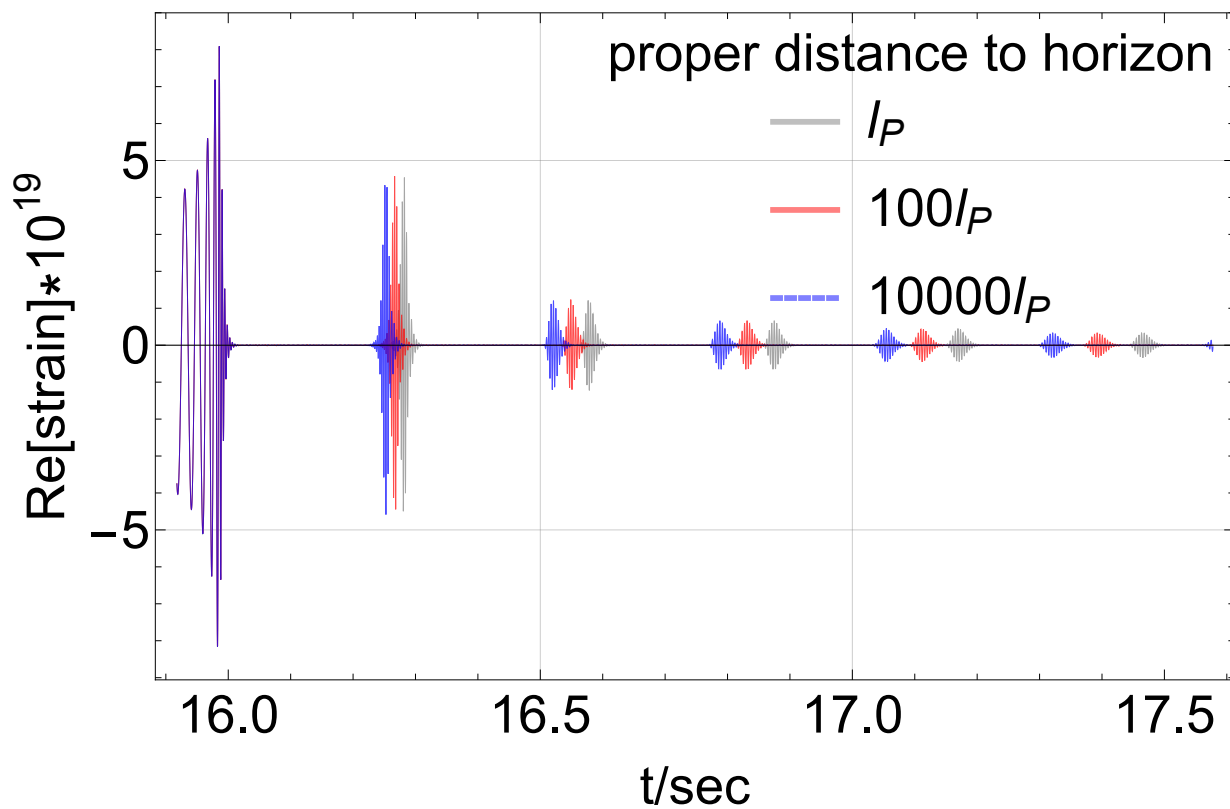


Figure 3.2: Echoes with different wall positions. Changing the positions of wall doesn't influence the shape of echoes a lot, but when putting wall closer to the would-be horizon and away from angular momentum barrier, the time-delay becomes bigger.

where $R_{\text{BH}}(\omega)$ is the reflectivity of the Kerr angular momentum barrier. For an QBH, however, we have one more barrier near the would-be horizon as shown in Fig 3.1 (right). Wavepackets with intermediate frequencies can now be trapped between two barriers and leak slowly every time when they hit the angular momentum barrier. Therefore, QBHs would have a similar ringdown waveform as classical BHs, but they are followed by delayed slowly decaying echoes.

$$\hat{h}_{\text{out}}(\omega) = R_{\text{QBH}}(\omega)\hat{h}_{\text{in}}(\omega) = R_{\text{QBH}}(\omega)\frac{\hat{h}_{\text{LIGO}}(\omega)}{R_{\text{BH}}(\omega)}f_{\text{cutoff}}(\omega), \quad (3.12)$$

where $f_{\text{cutoff}}(\omega)$ is a low-pass filter introduced to suppress numerical noise at high frequencies, as the reflectivity of the Kerr angular momentum barrier $R_{\text{BH}}(\omega)$, in the denominator, vanishes at high frequencies. Luckily, high frequencies leak out quickly in the first echo, and have small effect on the subsequent echoes. Our choice of f_{cutoff} does not affect the second and later echoes, but it changes the first echo slightly by cutting the high frequency noise:

$$\hat{h}_{\text{out,fin}} = \hat{h}_{\text{out}}f_{\text{cutoff}}, \quad (3.13)$$

$$f_{\text{cutoff}} = \exp\left[-\frac{1}{2}\left(\frac{2\pi f(\text{Hz})-299.495}{1347.73}\right)^{16}\right], \quad (3.14)$$

where $\omega = 2\pi f$.

We note here that the drawback assuming ingoing wave scattering at the barrier is that the real initial condition is actually highly nonlinear. That's why later we include estimation with pure outgoing wave inside barrier, which is still not ideal. At the end, we introduce hybrid method at Chapter. 6 and numerical simulations(ongoing but not included in the thesis) to deal with the highly nonlinear initial condition.

With the equations and boundary conditions given in the last section, we can numerically solve for R_{BH} and R_{QBH} as a function of frequency. We use LIGO event GW150914 with $a = 0.67$, $M = 62 M_{\odot}$ and $z = 0.09$. The mass is measured in the source frame and the final mass used in our calculation is the mass in the detector frame $M_{\text{fin}} = (1 + z)M$. The waveform is dominated by the $(l, m) = (2, 2)$ mode, which we shall focus on for the rest of the paper ³

The time dependence of the waveform can then be obtained by Fourier transforming $\hat{h}_{\text{out}}(\omega)$, and is shown in Fig 3.2. We see that changing the position of the wall changes

³Given the symmetries of Eqs. (3.3-3.4), we can easily extend the solution to $m = -2$ case using $R_{slm}[\omega] = R_{sl-m}^*[-\omega]$.

the time-delay between the echoes, but does not affect the individual echo waveforms significantly (as long as the wall is close the would-be horizon). As we see in Fig. 3.1, in the geometric optics approximation, the time delay between echoes, $\Delta t_{\text{echo,geom}}$ is given by the travel time from the angular momentum barrier to the wall and back [29]:

$$\begin{aligned} \Delta t_{\text{echo,geom}} &= 2r_* \Big|_{r_{\text{wall}}}^{r_{\text{barrier}}} = 2 \int_{r_{\text{wall}}}^{r_{\text{barrier}}} dr \frac{r^2 + a^2 M^2}{r^2 - 2Mr + a^2 M^2} \\ &= 2r_{\text{barrier}} - 2r_{\text{wall}} + 2 \frac{r_+^2 + a^2 M^2}{r_+ - r_-} \ln \frac{r_{\text{barrier}} - r_+}{r_{\text{wall}} - r_+} \\ &\quad - 2 \frac{r_-^2 + a^2 M^2}{r_+ - r_-} \ln \frac{r_{\text{barrier}} - r_+}{r_{\text{wall}} - r_-}. \end{aligned} \quad (3.15)$$

This can be well approximated by the following fitting function:

$$\Delta t_{\text{echo,geom}} = 2 \frac{r_+^2 + a^2 M^2}{r_+ - r_-} \ln \frac{M}{r_{\text{wall}} - r_+} + MG(a), \quad (3.16)$$

$$G(a) \simeq \frac{0.335}{a^2 - 1} + 4.77 + 7.42(a^2 - 1) + 4.69(a^2 - 1)^2, \quad (3.17)$$

$$r_{\text{wall}} - r_+ = \frac{\sqrt{1 - a^2} d_{\text{wall}}^2}{4M(1 + \sqrt{1 - a^2})}, \quad (3.18)$$

where we find the fit of $G(a)$ for the angular momentum barrier of $l = m = 2$ mode, while d_{wall} is the proper distance from the wall to the would-be horizon. The latter is expected to be comparable to Planck length for QBHs of quantum gravitational nature, but Δt_{echo} only depends on the exact value of d_{wall} logarithmically (see Fig. 3.2).

The echoes in both time and frequency domain for the LIGO event GW150914 are shown in Fig. 3.3 and 3.4 with perfect wall standing a Planck length proper distance outside the (would-be) horizon. Here, we show the Amplitude Spectral Density (ASD), which is the square root of the power spectral density. The latter is the average of the square of the fast Fourier transforms of the model. In the next section, we will study the structure of the echo in the frequency domain and present how superradiance affect the structure of echo.

3.4 Superradiance

Scattering off Kerr BH can lead to superradiance of modes with frequency $0 < \omega < m\Omega_{\text{H}}$, which can extract energy from a spinning background [234]. Adding a (partially) reflective

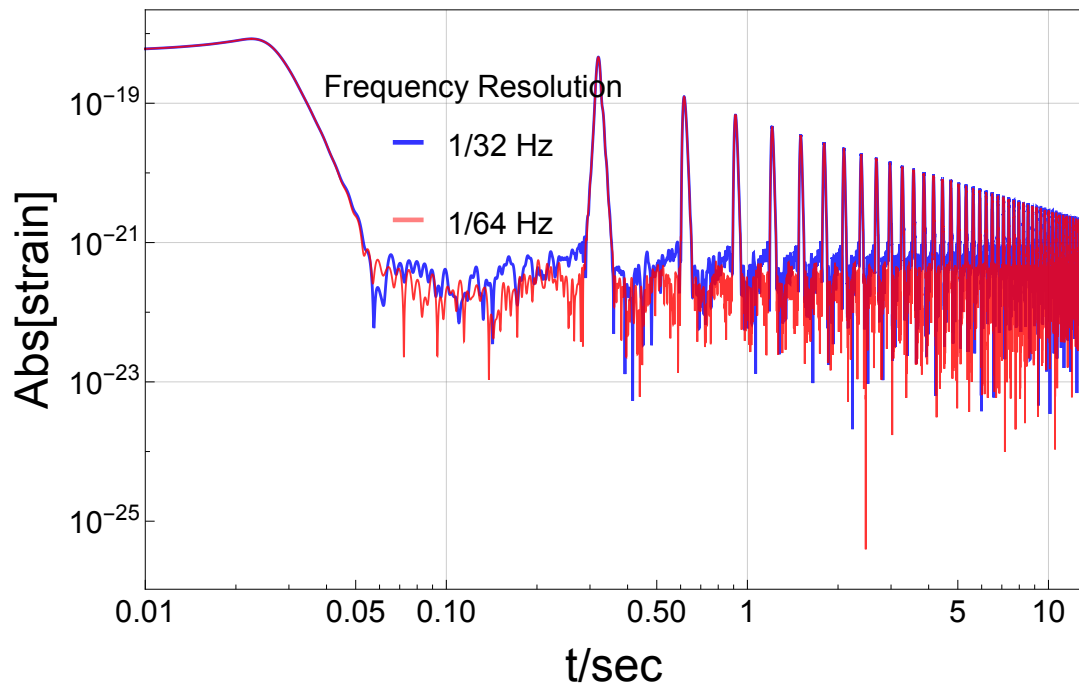


Figure 3.3: Predicted echoes for LIGO event GW150914 in the time domain with different resolution, assuming a perfect wall at a Planck length proper distance outside the horizon

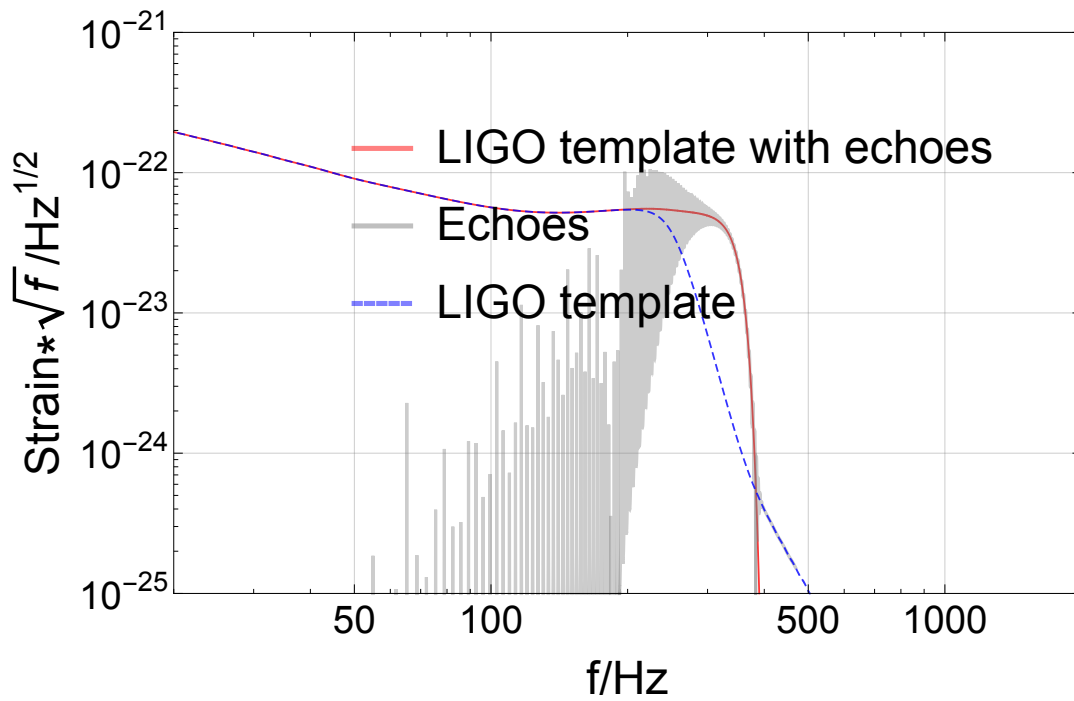


Figure 3.4: Predicted echoes for LIGO event GW150914 in the frequency domains, assuming a perfect wall at a Planck length proper distance outside the horizon. ⁵

wall near horizon could turn this amplification to an instability, since modes trapped between the wall and the angular momentum barrier can extract the spin energy repeatedly [122, 86]. In this section, we study this effect for the echoes in frequency domains.

There is an odd looking spike in Fig. 3.4 frequency domain around 183 Hz (see top panel in Fig. 3.5 for a zoom-in). Indeed, this is exactly the threshold frequency for the superradiance. This is demonstrated in the middle panel of Fig. 3.5, which shows the scattering amplification with the horizon, perfect wall and soft wall around that frequency. The vertical axis is the relative energy, extracted from around black hole by scattered gravitational waves. The blue dashed line shows superradiance slowly turning off with increasing the frequency, and we confirm that it ends exactly at frequency $f_{\max} = am/[2\pi(r_+^2 + a^2)] = 183$ Hz, for $m = 2$ as shown in the plot. In contrast, superradiance by soft wall (grey and thin curve) occurs at resonance peaks, corresponding to the ergoregion trapped mode (for more details, see Appendix 3.7). Since superradiance ends at 183Hz, the resonance peaks shift the direction, which is the reason we have an odd spike in the Fig. 3.4 and 3.5 top panel.

The perfect wall (the red thick curve) in Fig. 3.5 middle panel is a constant zero without any resonance peaks, since a perfect reflective wall kills superradiance, as all the energy that goes in, comes out eventually (see Appendix 3.7 for a subtlety in this argument). However, the odd spike structure remain in the amplitudes, as shown in Fig. 3.5 bottom panel, where we change the vertical axis to real part of outgoing to ingoing wave at infinity. We still see the sign flip in resonance structure at 183 Hz.

In the next section, we study the echo templates resulting from solving the linearized Einstein equations, which improves the simplistic geometric picture in Fig. 3.1.

3.5 Minimal Echo templates

Now that we have numerical predictions for echoes, we would like to provide simple fitting functions that could be used for quick visualization and data-fitting purposes. We call these fitting functions, templates. In order to find our templates, we define echoes in the time domain by the regions that surround the peaks of $|h(t)|$ and exceed a limit: $\ln[|h(t)|/|h|_{\max,n}] > -1, -1.5$ or -2 . $|h|_{\max,n}$ is the height of the n^{th} peak of $|h(t)|$, which we call the n^{th} echo. Then we fit the n^{th} echo to a complex Gaussian

$$h_n(t) = \exp[\Psi_n(t) + I\Phi_n(t)], \quad (3.19)$$

$$\Psi_n(t) = a_0 + a_1 t + a_2 t^2, \quad (3.20)$$

$$\Phi_n(t) = b_0 + b_1 t, \quad (3.21)$$

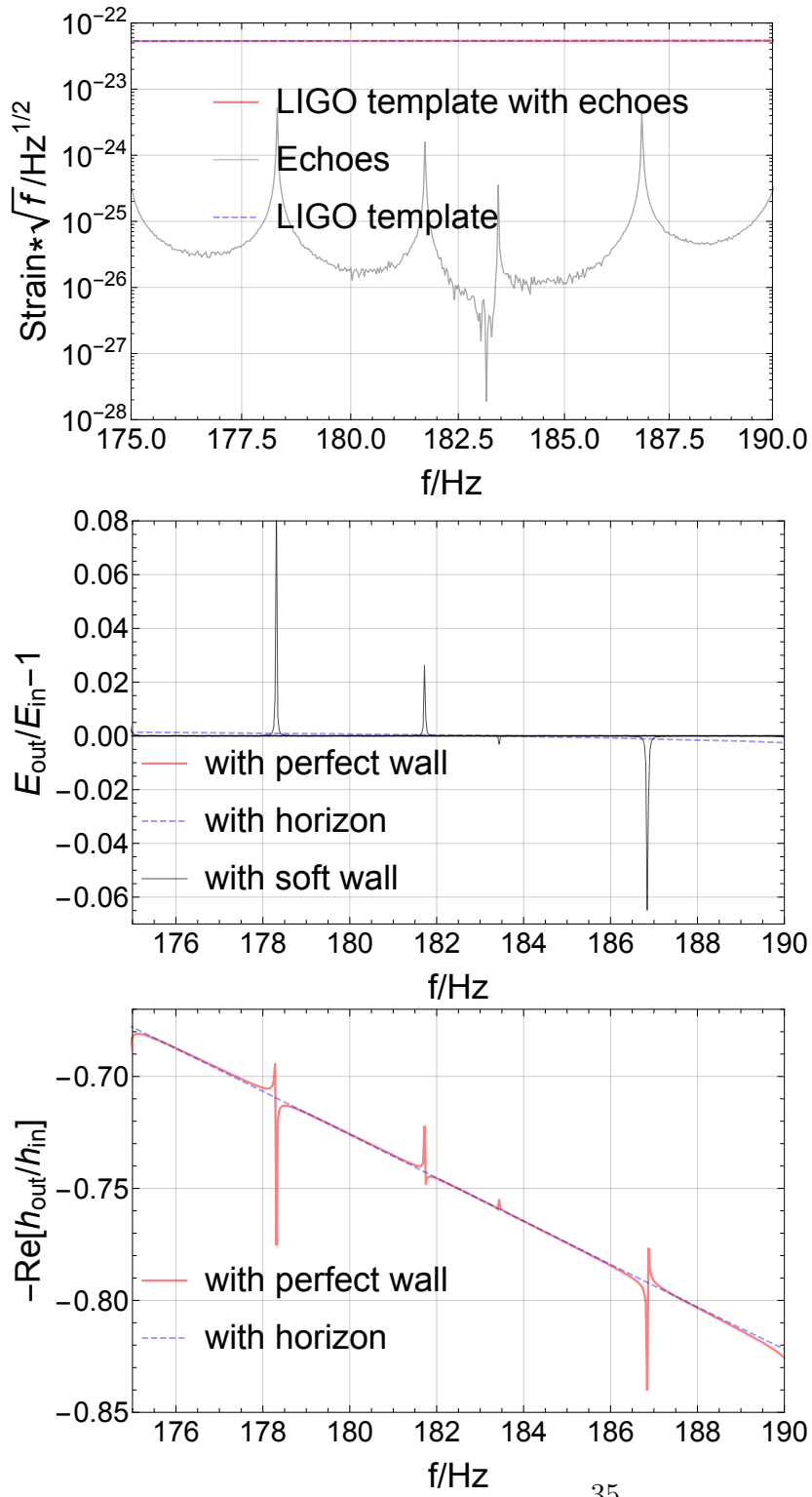


Figure 3.5: Superradiance in frequency domain for BHs and QBHs.

Table 3.2: Some physical quantities of a single echo defined by the five parameters from the gaussian echo template (Eq. 3.20)

	width	center	peak amplitude
time	$\sqrt{-1/(2a_2)}$	$-a_1/2a_2$	$\exp[a_0 - a_1^2/4a_2]$
frequency	$\sqrt{-2a_2}/(2\pi)$	$b_1/(2\pi)$	$\exp[a_0 - a_1^2/4a_2 - 1/2 \log[2\sqrt{a_2^2}]]$
overall phase	$b_0 - b_1 a_1/(2a_2)$		

Table 3.3: Best fit gaussian echo template quantities (see Table 3.2 and Fig. 3.7) , for our minimal model of GW150914

peak amplitude in time / strain	$2.91 \times 10^{-19}/n^{1.32}$
width in time / msec	$4.29 + 0.883n$
correction to $\Delta t_{\text{echo,geom}}$ / msec	$1.52 + 1.71/(1 + n)$
peak frequency / Hz	$177 + 102/n^{0.3}$
Overall phase	$-7.26 + 27.1n^{0.945} + 22.6n$

where a_0, a_1, a_2, b_0 and b_1 are real numbers. This form is same as fitting the n^{th} echo to $A \exp[(t - t_0)^2/(2\sigma^2)]$, where A and t_0 are complex, while the width σ is real.

As an example, Fig 3.6 compares the numerical solutions and gaussian fits for the 2^{nd} , 10^{th} , and 30^{th} echoes, with time origin shifted to center of each echo, and fitting the region with $\ln [|h(t)|/|h|_{\text{max},n}] > -1.5$.

Within this approximation, there are five real parameters for every echo that quantify its amplitude, width and center, both in time and frequency domain, as well as the overall phase at the center of the echo, as shown in Table 3.2.

Table 3.3 provides the best fit parameters of our echo templates for all echoes, based on the LIGO event GW150914 and averaging over the best fit functions with different echo domains $\ln [|h(t)|/|h|_{\text{max},n}] > -1, -1.5$ or -2 .

The best fits for each echo domain is also provided in Fig. 3.7. For correction to $\Delta t_{\text{echo,geom}}$, we define time-delay as $\Delta t_n = t_n - t_{n-1}$. For all other plots, first echo is not included since it is very sensitive to the properties of the wall, as well as nonlinear effects from early stage of merger (see details in Sec. 5.5). The top three panels in Fig. 3.7 show the time domain properties as a function of the echo number. Starting from the left, peak echo amplitudes in time are all well fit by decaying power laws([100] argue that the decay of echoes at early stages is polynomial). Middle are the width of the echoes, becoming wider for later echoes in the time domains, as the high frequency modes leak out more quickly. The top right panel gives correction to $\Delta t_{\text{echo,geom}}$ (3.16), while the bottom left

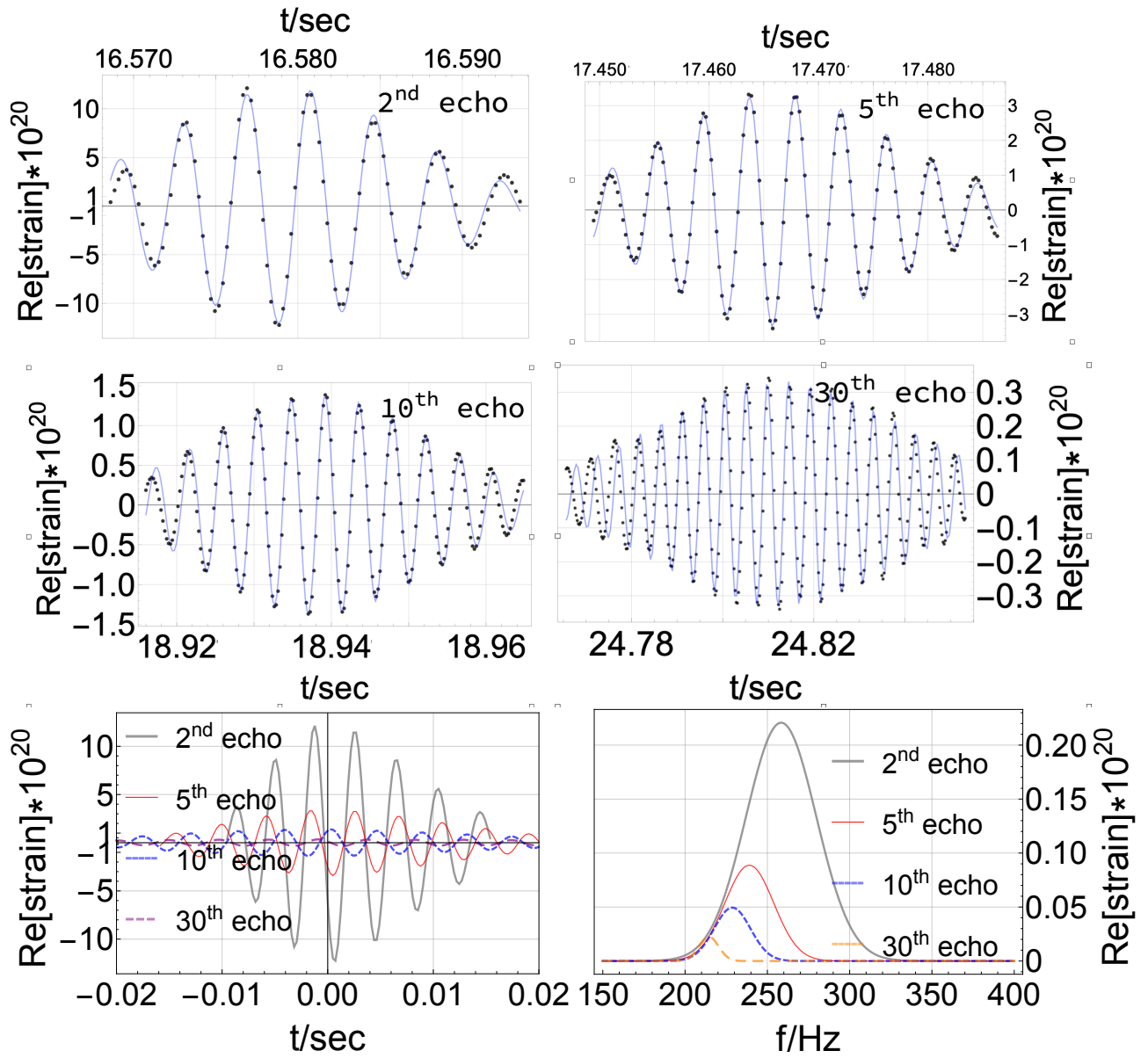


Figure 3.6: Best fit gaussians to the 2nd, 5th, 10th and 30th echoes within $\ln[|h(t)|/|h|_{\max,n}] > -1.5$. We see that as high frequency modes leak out faster, later echoes decay in amplitude and become wider in time domain, and high frequency is cut in the frequency domain.

panel shows the decay of the mean echo frequency. The bottom middle and right provide overall phase at t_{center} and the residuals of the best fit for the phase. We only show the residuals for the phase, as the numerical error for the phase is relatively big.

To visualize the quality of the template to fit data, Fig. 3.8 shows the $\text{SNR}_{\text{temp}}/\text{SNR}_{\text{model}}$, where $\text{SNR}_{\text{model}}$ is the predicted signal-to-noise ratio for our numerical solution of echoes (assuming white noise), while SNR_{temp} is a reduced value, if we use our Gaussian approximations of Fig. 3.6 (gray circles in Fig. 3.8). Using a second fit for how properties (i.e. width, center and amplitude) of $\Psi_n(t) = \log |h_n(t)|$ depend on n (Table 3.3) further reduces SNR_{temp} (red triangles in Fig. 3.8). We notice that the quality of Gaussian fit drops for later echoes, which could be either due to build-up of numerical error or systematic deviations from a single gaussian fit. The secondary fit for Ψ_n vs n further reduces SNR as the width in time and time delay, shown as Fig. 3.7, do not have a simple behavior. However, the power law fit to the peak amplitude in time $\propto n^{-4/3}$ is surprisingly good. Also, as we discussed before, since the shapes of first few echoes are much more dependent on the initial conditions, it might be better to use independent Gaussians to fit them in data. Finding a reasonable fit for phase information Φ_n vs n proves even more challenging, as a small change in phase leads to a significant change in echo profiles. Fortunately, model-agnostic searches (e.g., [99]) based on cross-correlating different detectors can be done independent of the phase information.

3.6 Beyond the minimal model

While our minimal model for echoes has only one free parameter (wall distance to the horizon, d_{wall}) in addition to those of GR, the reality can be more complicated. Here, we explore the two main deviations expected from the minimal model due to nonlinear effects in GR and quantum gravity.

3.6.1 Nonlinear Mergers Effects

Our assumption of a custom-designed incoming wavepacket, as a placeholder for black hole binary merger, is almost certainly too naive to provide a realistic echo template, as it misses the nonlinear nature of the merger. While numerical simulations can now provide realistic waveforms for black hole mergers in GR, a covariant formulation of QBHs that could produce realistic echo waveforms is currently missing. However, we can get an idea about the extent of nonlinear corrections to linear results by noticing that the Kerr

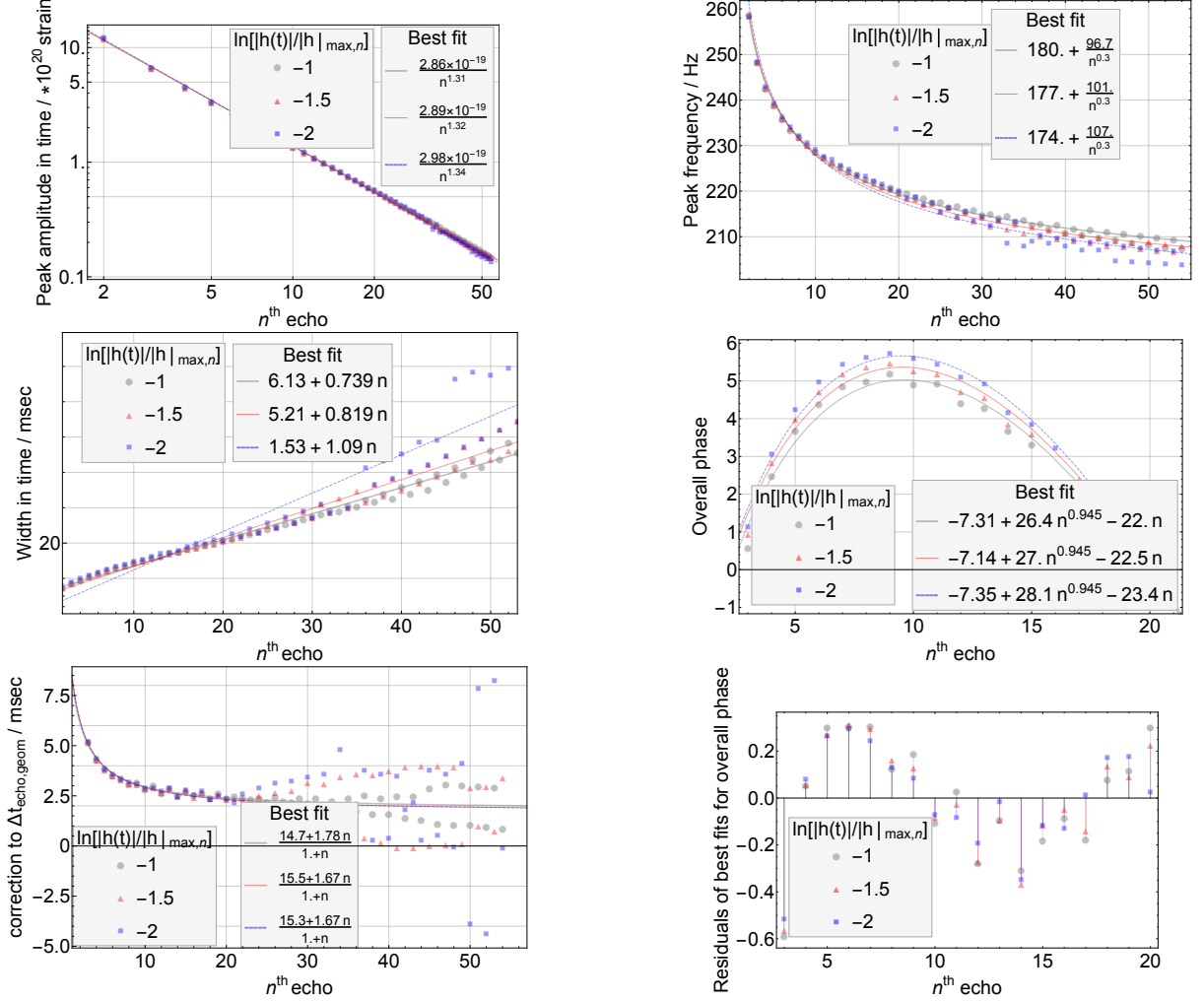


Figure 3.7: Best fit Gaussian template parameters (for $\ln[|h(t)|/|h|_{\text{max},n}] > -1, -1.5$ or -2), in our minimal model of LIGO event GW150914, showing second and later echoes. The top three panels are in the time domains. Starting from left, peak amplitudes of echoes in time are well fit by power laws. Middle panel is the width of the echoes, which become wider in time, as the high frequencies leak out more quickly. For the same reason, the peak frequency (bottom left) also decays with time. The top right panel gives corrections to $\Delta t_{\text{echo,geom}}$ (Eq. 3.16). Finally, the bottom middle and right provide the overall phase at t_{center} of each echo and the residuals of the best fit. This is the only plots we show the residuals since the numerical error for the phase is relatively big.

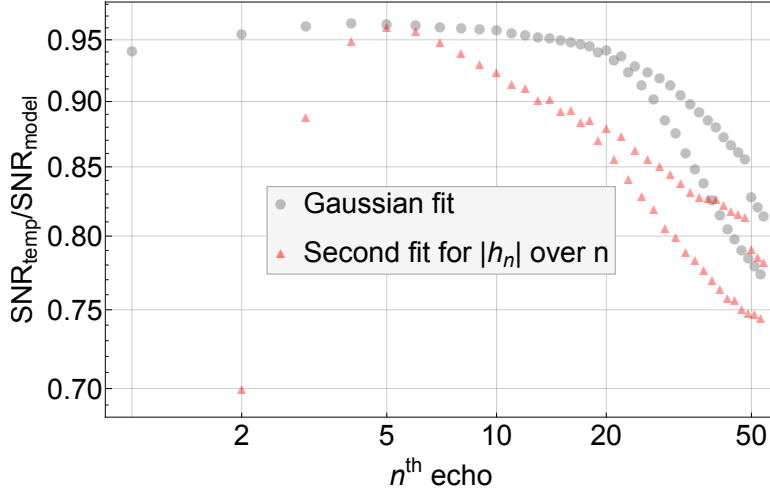


Figure 3.8: SNR_{temp} compared to $\text{SNR}_{\text{model}}$, showing the quality of gaussian templates.

background for Teukolsky equation (3.1) is dynamical during the merger event, and thus the frequencies can be shifted by $\mathcal{O}(30\%)$, between the ingoing and outgoing waves at merger⁶. We shall explore the extent of this effect on echoes by introducing a blueshift parameter s , in the ingoing linear initial conditions:

$$\hat{h}_{\text{LIGO,shifted}}[f] = \hat{h}_{\text{LIGO}}[f/s]. \quad (3.22)$$

As shown in Fig. 3.9, redshifted (blueshifted) initial conditions give echoes which damp more slowly (quickly), since low frequencies leak more slowly through the angular momentum barrier. This also dramatically changes the amplitude of first few echoes. Blueshift parameter s can be a free parameters for data fitting purposes.

The effect is clearer if we compared SNR of echoes to first echo, as shown in Fig. 3.10. SNR_n^2 is SNR^2 of our numerical solution of n^{th} echo and we trimmed a single echo with $\ln[|h(t)|/|h|_{\text{max},n}] > -1.5$. We assume white gaussian noise $\sigma_\omega = 1$ so that

$$\text{SNR}_n^2 = \sum_{\omega} \frac{|\hat{h}_{n,\omega}|^2}{\sigma_\omega^2} = \sum_t |h_n|^2. \quad (3.23)$$

$$(3.24)$$

⁶For example, the best-fit for the dominant quasinormal mode frequency for GW150914 is 10-20% offset from the linear theory predictions for the best-fit Kerr metric (Fig. 5 in [16]).

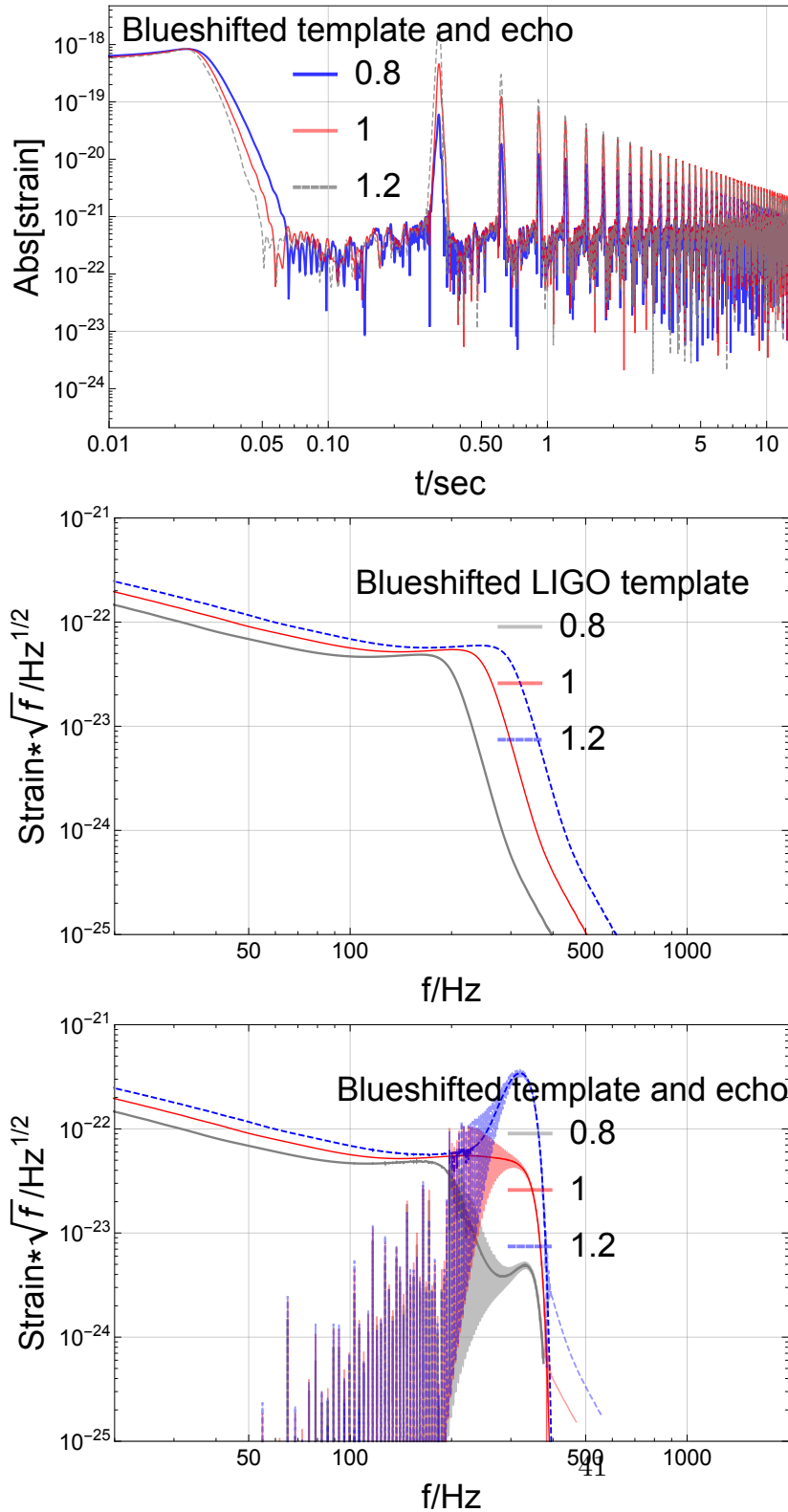


Figure 3.9: Echoes predicted for GW150914, expected for redshifted (blueshifted) initial conditions with respect to our minimal model. We see that lower frequency initial conditions lead to lower amplitude, but more persistent, echoes as they cannot penetrate the angular momentum barrier efficiently.

Table 3.4: Same as Table 3.3, but contrasting with redshifted/blueshifted initial conditions, fitted within $\ln[|h(t)|/|h|_{\max,n}] > -1.5$.

blueshift factor s	0.8	1	1.2
peak amplitude in time / strain	$5.91 \times 10^{-20}/n^{1.14}$	$2.92 \times 10^{-19}/n^{1.33}$	$5.31 \times 10^{-19}/n^{1.54}$
width in time / msec	$3.91 + 0.678n$	$5.5 + 0.808n$	$9.48 + 0.711n$
correction to $\Delta t_{\text{echo,geom}}$ / msec	$-47.8 - 57.0/(1+n)$	$15.4 + 1.64/(1+n)$	$76.2 + 60.4/(1+n)$
peak frequency / Hz	$227 + 95.2/n^{0.3}$	$175 + 104/n^{0.3}$	$144 + 97.8/n^{0.3}$
Overall phase	$-3.06 + 30.2n^{0.945} - 25.9n$	$-6.65 + 28.5n^{0.945} - 23.8n$	$-12.7 + 35.2n^{0.945} - 29.4n$

Fig 3.10 (right panel) shows that later echoes contain more (less) information in redshifted (blueshifted) templates, since they decay more slowly (quickly). The left panel also shows the relative SNR of 1st echo compared to the trimmed main event in our model. The fact that this number can change by more than 1.5 orders of magnitude suggests that the amplitude of 1st echo is very sensitive to the nonlinear merger physics and cannot be reliably predicted. [137] simulates a binary black hole merger and finds the ratio of the energy falling into the black hole to the energy out is around 1:1, which can be used as a normalization of amplitude of echoes.

Table 3.4 and Fig. 3.11 compare the best fit echo parameters for different blueshift factors. We see in the left panels that the blueshifted initial condition ($s = 1.2$) has a transient excess in amplitude that decays quickly and falls in line the minimal model. In contrast, the redshifted model ($s = 0.8$) has a significantly smaller but more persistent amplitude. Surprisingly, the middle panels show that the redshifted echoes remain narrower in time. Even more puzzling is that the redshifted initial conditions have higher frequency echoes as shown in Fig. 3.11 the bottom left panel. This is due to the fact that the echo peak frequency depends on the slope (and not the amplitude) of the spectral density $\hat{h}_{\text{out}}(\omega) = R_{\text{QBH}}(\omega)\hat{h}_{\text{LIGO}}(\omega)f_{\text{cutoff}}(\omega)/R_{\text{BH}}(\omega)$ from Eqn. 3.12, which involve several complicated components. As we see in the middle panel of Fig. (3.9), this slope is not monotonic which leads to the counterintuitive behavior, even though the amplitude of the redshifted model is smaller compared to the blueshifted.

3.6.2 Soft Wall

Motivated by quantum models of black holes, the wall must at least partially absorb the energy incident on the wall [29]. For example, in fuzzball models [193] high energy particles (with $\hbar\omega \gg kT_{\text{H}}$, where T_{H} is the Hawking temperature) excite the fuzzball microstates and thus will be absorbed by the wall. On the other hand, particles with $\hbar\omega \leq kT_{\text{H}}$ may

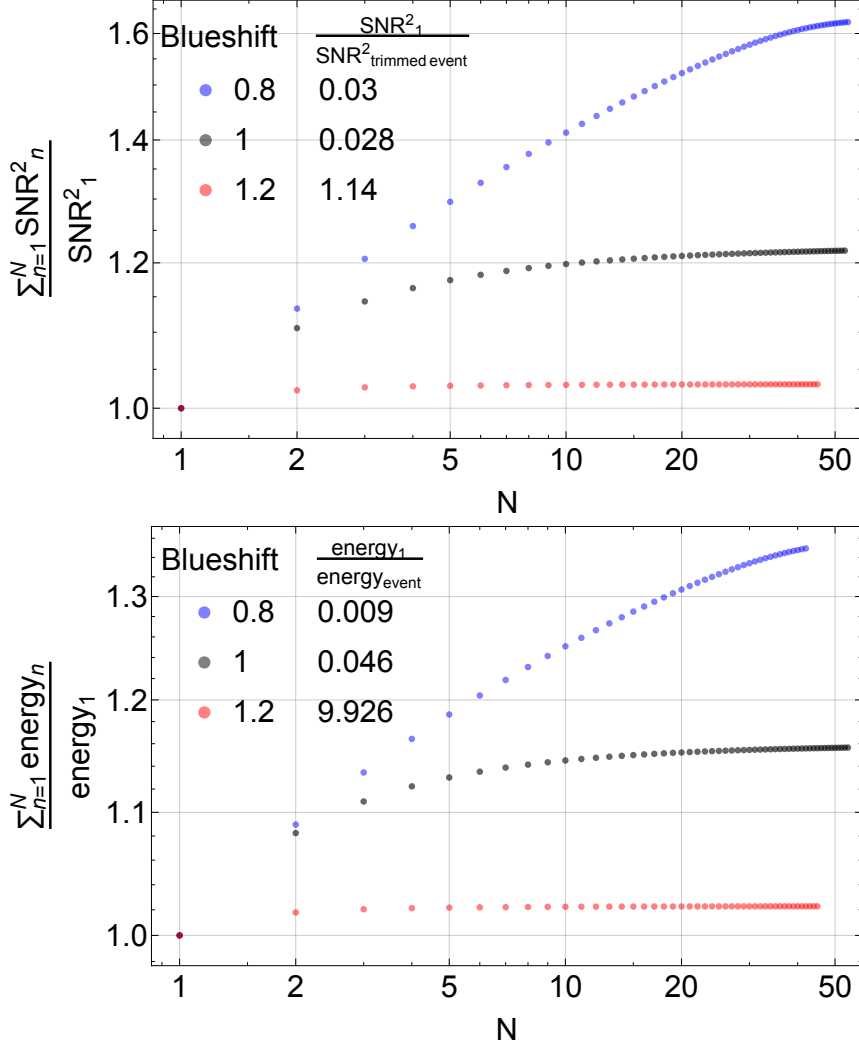


Figure 3.10: Signal-to-noise ratios(SNR) and energy for blueshifted echoes compared with the first echo. We see that there is more (less) information in subsequent echoes for lower (higher) frequency initial conditions. Furthermore, the amplitude of first echo is hard to predict and can change by more than 1.5 orders of magnitude. We also list SNRs and energy for blueshifted first echoes compared with the event. Since we assume white noise to calculate the SNR in time domain, we trim the merger template at around 0.076 seconds before the peak (similar to the LIGO noise whitening for GW150914 template).

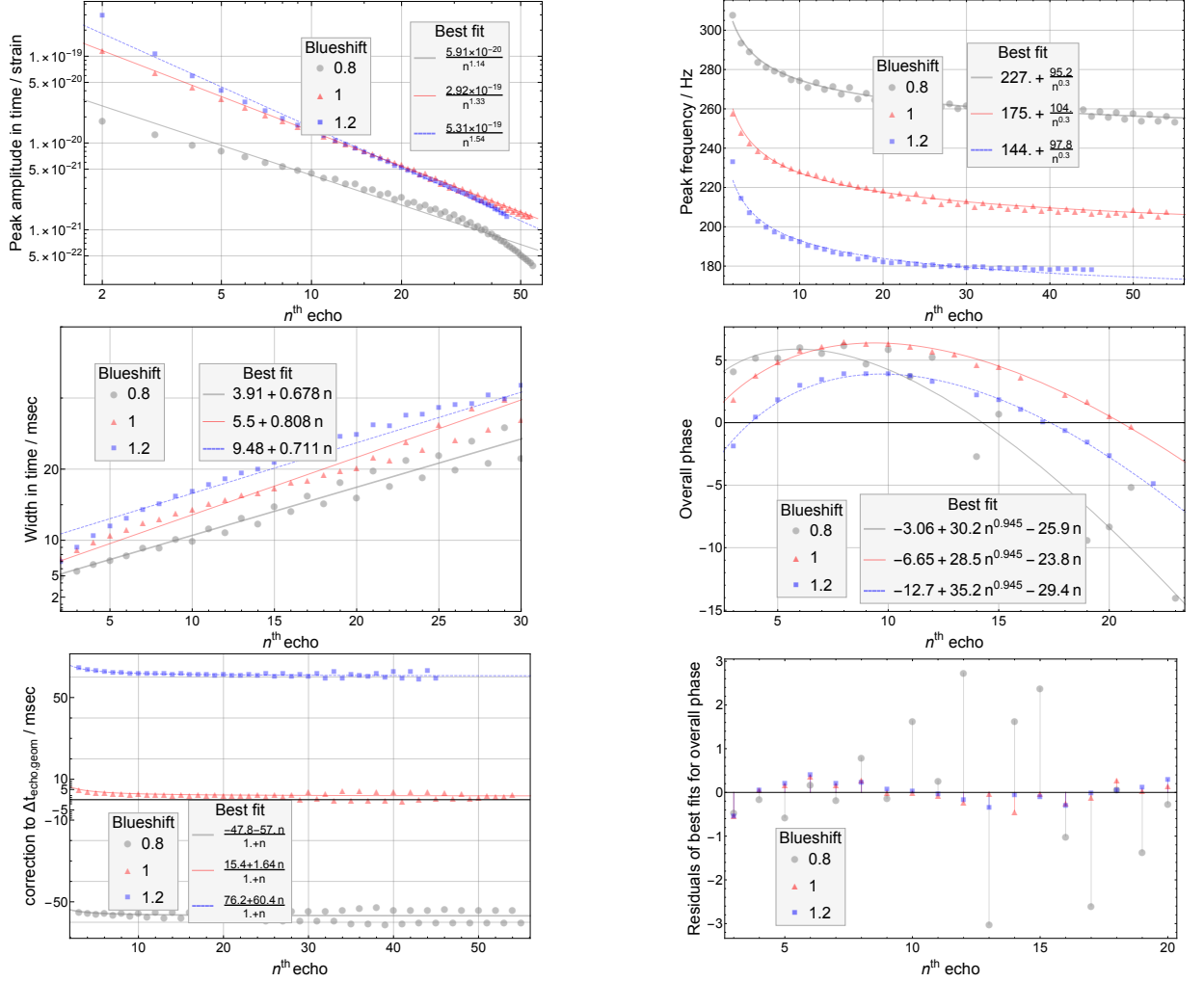


Figure 3.11: Same as Fig. (3.7), but using the different blueshift factors s (Eq. 3.22) for echo initial conditions (fitted for $\ln [|h(t)|/|h|_{\max,n}] > -1.5$). We see that redshifted initial conditions yield weaker, but more persistent echoes (see text for details).

be (at least partially) reflected (but see [136] for recent counter-arguments). Ringdown phase of mergers of two BHs is in the intermediate range (~ 100 Hz for GW150914). Therefore, a realistic quantum gravity model for the echoes is expected to involve a *soft* wall. For example, frequency of electromagnetic emissions from accretion into BHs is much higher, which is expected to be absorbed by the wall [72, 73]. However, possible loopholes that could lead to astrophysical observables from quantum effects have been exploited in [226, 36].

A wall that absorbs high frequency modes will dramatically decrease the amplitude of the first echo, since these modes leak out quickly every time the wavepacket hits the angular momentum barrier. Therefore, the first echo contains most of the high frequency modes which, as shown in the top left panel in Fig 3.14, would be absorbed for a soft wall.

Of course, the actual frequency-dependent reflection of the wall depends on the specific quantum theory of black holes. We explore a phenomenological model for the wall with a Gaussian-like energy reflection rate

$$R_{\text{wall}}(\omega) \simeq \exp \left[- \left(\alpha \frac{\omega}{T_{\text{H}}} \right)^q \right], \quad (3.25)$$

where $T_{\text{H}} = r_+^2 - a^2 / [4\pi r_+(r_+^2 + a^2)]$ is the Hawking temperature for Kerr BH. While smooth R_{wall} 's, such as gaussian or Boltzmann reflectivity ($q = 2$ or 1 , respectively) may appear natural, they do tend to essentially wipe out the echoes, unless $\alpha \ll 1$, which is inconsistent with the tentative echoes found in [29]. In contrast, a sharper function with, e.g., $q = 12$ then can damp the first echo, but not significantly influence later echoes, as shown in Fig 3.13 ⁷. We can also compare these reflectivity functions with that of the angular momentum barrier of the Kerr BH, for the same spin and mass, as shown in Fig 3.12, which provides another motivation for sharper R_{wall} 's.

Table 3.5 and Fig. 3.14 compare the template for the perfect and soft walls, similar to Figs. (3.7) and (3.11). We see in the top left panel that, due to absorption of high frequency modes, the power law fit to the amplitudes could be extended to first echo for the soft walls. More generally, echoes decay faster for a softer wall. As echoes for a wall with $R_{\text{wall}} = \exp[-(0.06\omega/T_{\text{H}})^8]$ decay too fast, we only focus on the $R_{\text{wall}} = \exp[-(0.055\omega/T_{\text{H}})^{12}]$ case in subsequent panels of Fig. 3.14, and provide numerical fits for echo properties in Table 3.5. With this choice, the evolution of echo properties is similar to those in Figs. (3.7) and (3.11), with the notable difference that peak frequency decays more rapidly as the soft wall absorbs high frequencies.

⁷Fig 3.13 also shows that if the wall absorbs too much, the late echoes will stop decaying. This is due to superradiant instability which we shall discuss in the next section.

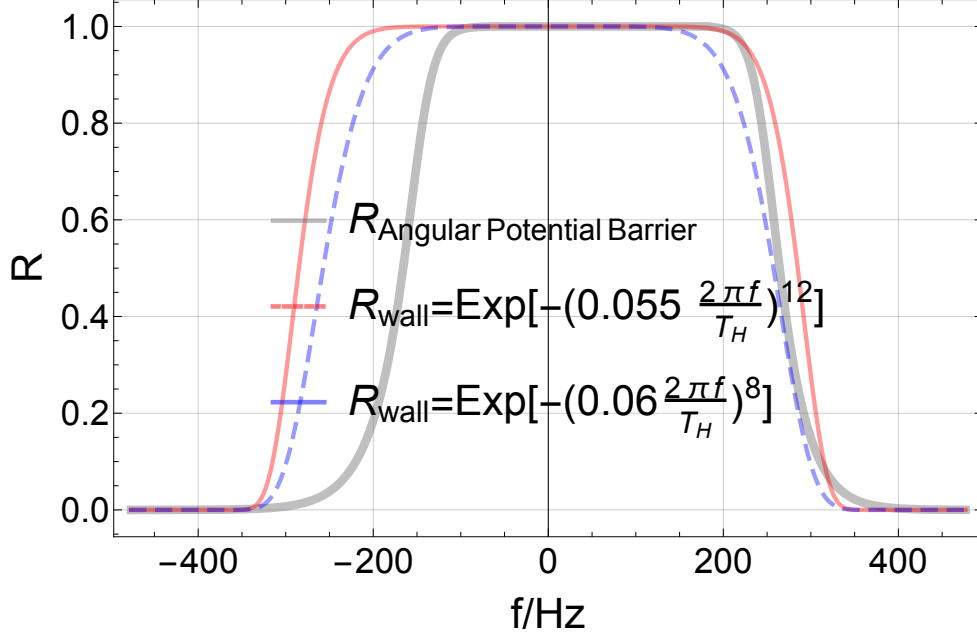


Figure 3.12: Comparison of soft wall reflectivity coefficients that we use, with that of the Kerr angular momentum barrier [197]. The thin and dashed lines are the two reflectivity rates used in Fig 3.13.

Table 3.5: Same as Table 3.3, but contrasting perfect ($R_{\text{wall}} = 1$) and soft ($R_{\text{wall}} = \exp[-(0.055 \frac{\omega}{T_H})^{12}]$) walls, fitted within $\ln[|h(t)|/|h|_{\text{max},n}] > -1.5$.

wall type	perfect	soft
peak amplitude in time / strain	$2.78 \times 10^{-19}/n^{1.31}$	$2.33 \times 10^{-19}/n^{1.36}$
width in time / msec	$5.5 + 0.808n$	$8.17 + 0.659n$
correction to $\Delta t_{\text{echo,geom}}$ msec	$15.4 + 1.64/(1+n)$	$14.3 + 1.52/(1+n)$
peak frequency / Hz	$175 + 104/n^{0.3}$	$177 + 96.8/n^{0.3}$
Overall phase	$-6.65 + 28.5n^{0.945} - 23.8n$	$-5.2 + 26.8n^{0.945} - 22.6n$

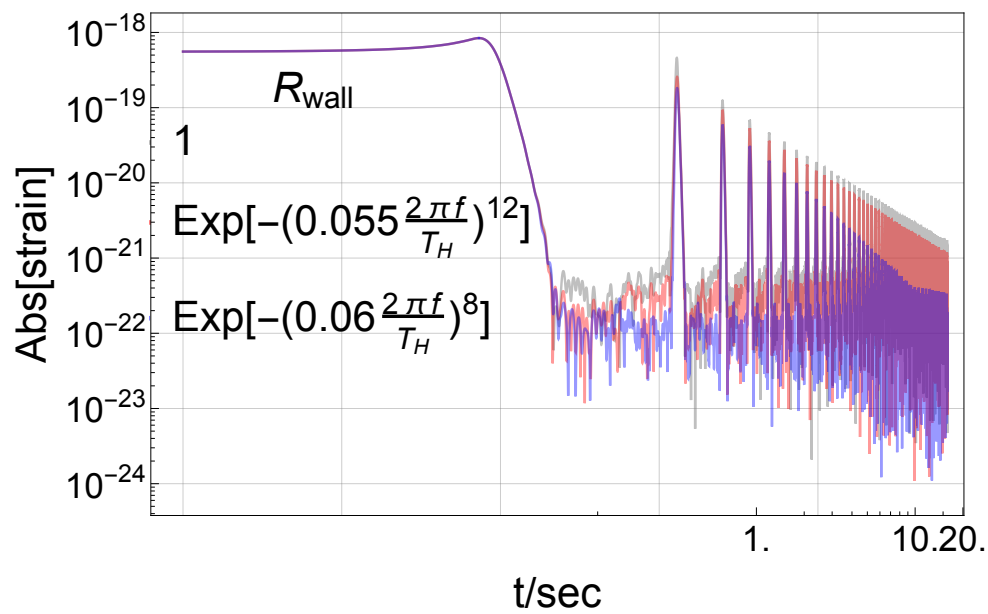


Figure 3.13: Echoes for GW15014, for soft vs. perfect walls. The top (gray) curve assumes a perfect wall/mirror, while the lower curves show soft walls with different energy reflectivity coefficients.

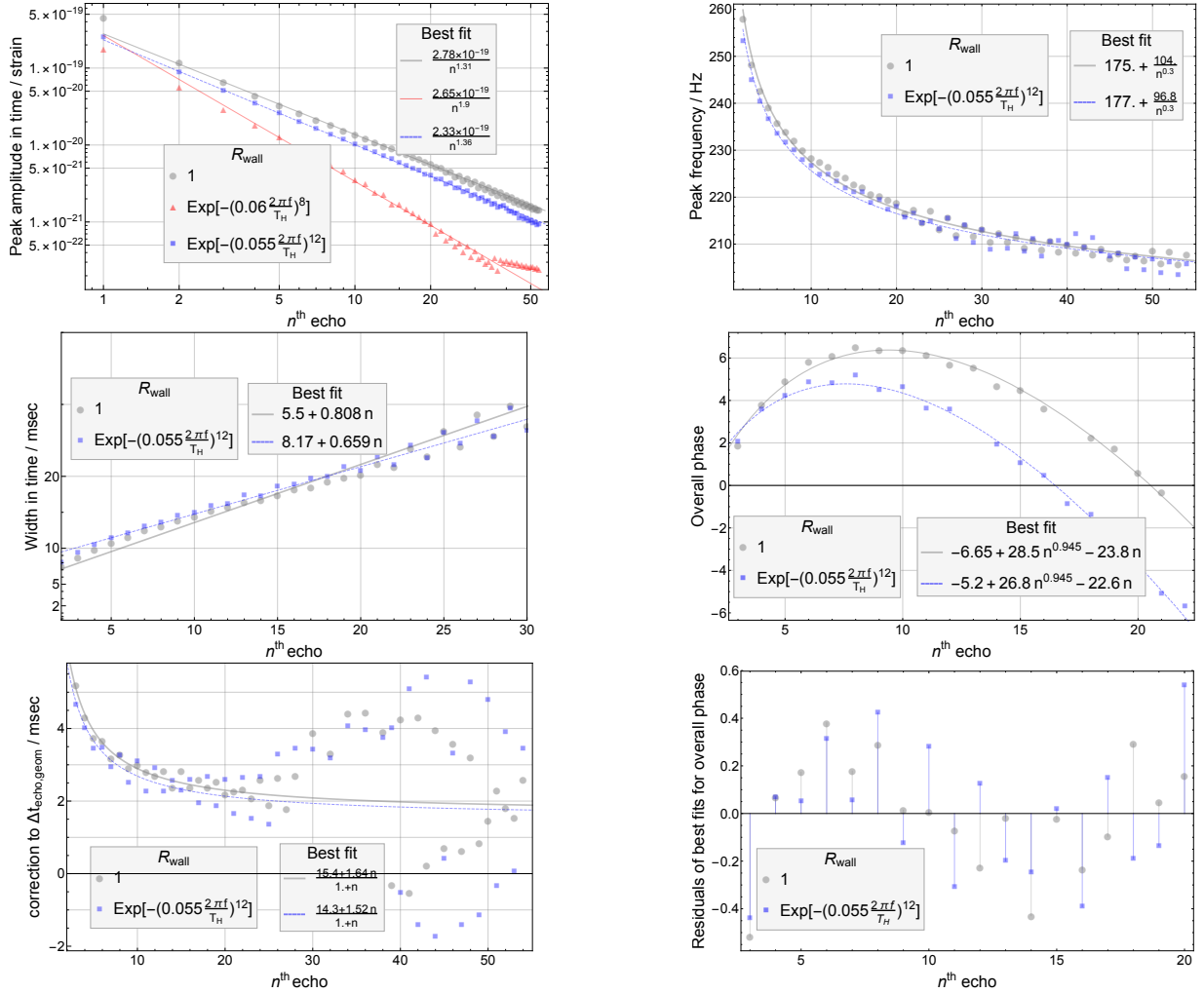


Figure 3.14: Same as Fig. (3.7), comparing walls with different energy reflectivity coefficients (fitted for $\ln[|h(t)|/|h|_{\text{max},n}] > -1.5$). We see that echo amplitudes and peak frequencies decay more quickly for softer walls (see text for details).

Table 3.6: Integrals of superradiance profiles in Fig.3.15, up to the superradiance threshold for different wall positions δ , or absorption R_{wall} . We see that the integrated superradiance appears to have a universal value, independent of wall presence or properties. The same is likely to be the case of the perfect wall (last row), but cannot be resolved numerically due to infinitely sharp resonance structure.

$\delta =$	0.05	0.015	0.0005
$R_{\text{wall}} = 0$	0.2202	0.2202	0.2202
0.2	0.2226	0.2226	0.2225
0.4	0.2246	0.2246	0.2243
0.6	0.2260	0.2260	0.2256
0.8	0.2223	0.2276	0.2190
1	0.0000	0.0000	0.0000

3.7 Ergoregion Instability

In this section, we further discuss the emergence of superradiance and ergoregion instability in QBHs.

Fig 3.15 shows the superradiance in the frequency domain. The resonance peaks are signal of superradiance⁸, and these peaks become sharper with increasing the reflectivity of wall. However, the curve for perfect wall $R_{\text{wall}} = 1$ doesn't show any peaks in the plot, which is not intuitive. So we integrate the plots over superradiance range for different reflectivity of the wall, shown as Table 3.6. The area is roughly conserved for all soft walls and equal to the area of a classical BH. Hence, we conclude that when approaching $R_{\text{wall}} = 1$, we still have the superradiance and thus the peaks, but only at discrete frequencies. The zero of both Fig. 3.15 and Table 3.6 are just because of finite resolution in the frequency domain, and we are not able to see the infinitely sharp resonances when approaching $R_{\text{wall}} \rightarrow 1$.

Fig 3.16 shows that resonance superradiant peaks disappear as $a \rightarrow 0$, while Fig 3.17 shows that they shift when we shift the position of the wall, as expected.

Note that, even in the absence of dissipation, there could still be instabilities that manifest themselves as the poles of the amplification in the upper complex plane of frequency space. Indeed, ergoregion instability was predicted in [122] in the absence of horizons and/or dissipation.

However, we do not see any significant growth, at least in the first 50 echoes we predict

⁸For simplicity, we present results with scalar mode $(l, m, s) = (2, 2, 0)$, but we have confirmed the same results for gravitational waves.

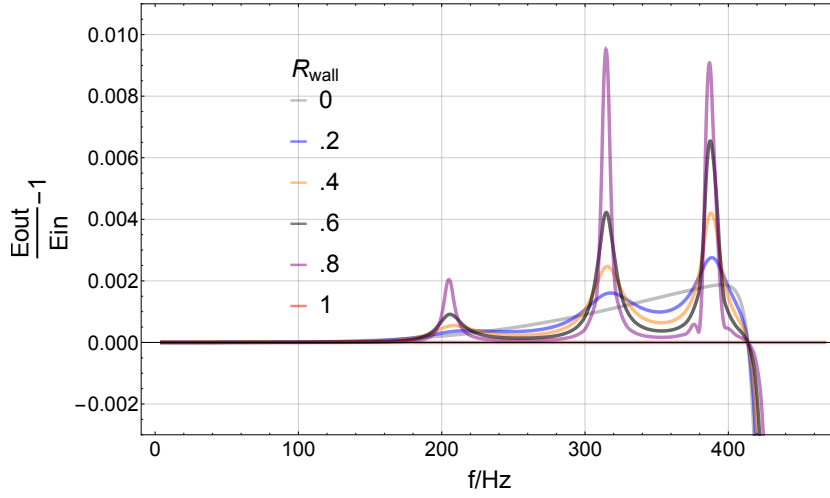


Figure 3.15: Superradiance by a spinning ECO/BH with $a = 0.99$ and $M = 67.6M_{\odot}$, assuming different wall reflection coefficients R_{wall} , with wall position $r_{\text{wall}} = r_{\text{h}}(1 + \delta)$, $\delta = 0.05$. For simplicity, we present results with scalar mode $(l, m, s) = (2, 2, 0)$, but we have confirmed the same results for gravitational waves. The horizontal axis is frequency, while the vertical axis is the relative energy extracted from ECO/BH. $R_{\text{wall}} = 0$ is the classical BH (with no reflection on horizon), showing a smooth response with superradiance at low frequencies. A soft wall with $0 < R_{\text{wall}} < 1$ shows several peaks, corresponding to the resonance frequencies of the cavity formed by the wall and the angular momentum barrier, which amplify superradiance. A perfect reflective wall kills superradiance by definition, as all the energy that goes in, comes out eventually.

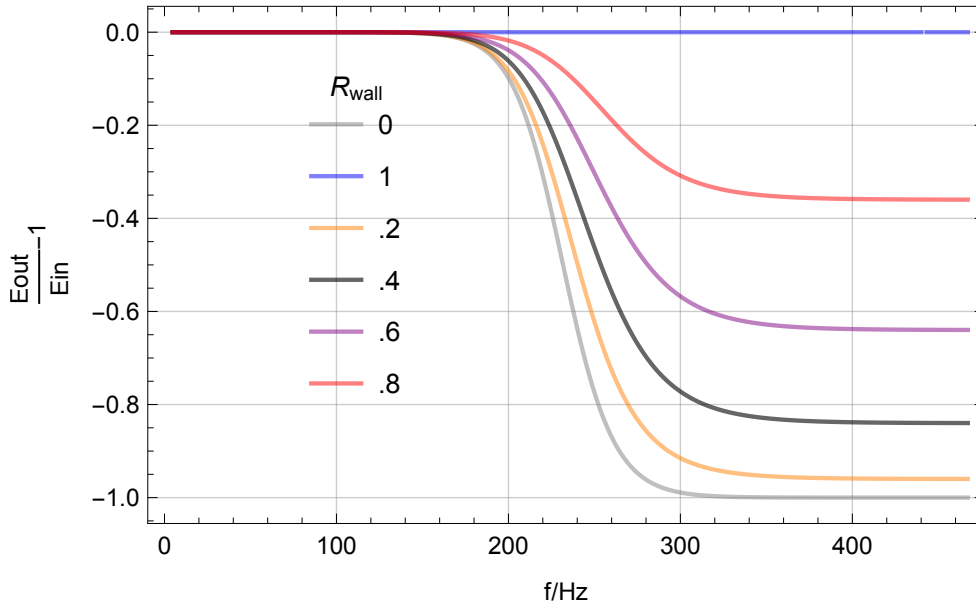


Figure 3.16: Same as Fig. 3.15, but with $a = 0$. We see that superradiance, and superradiant resonance peaks disappear as spin goes to zero.

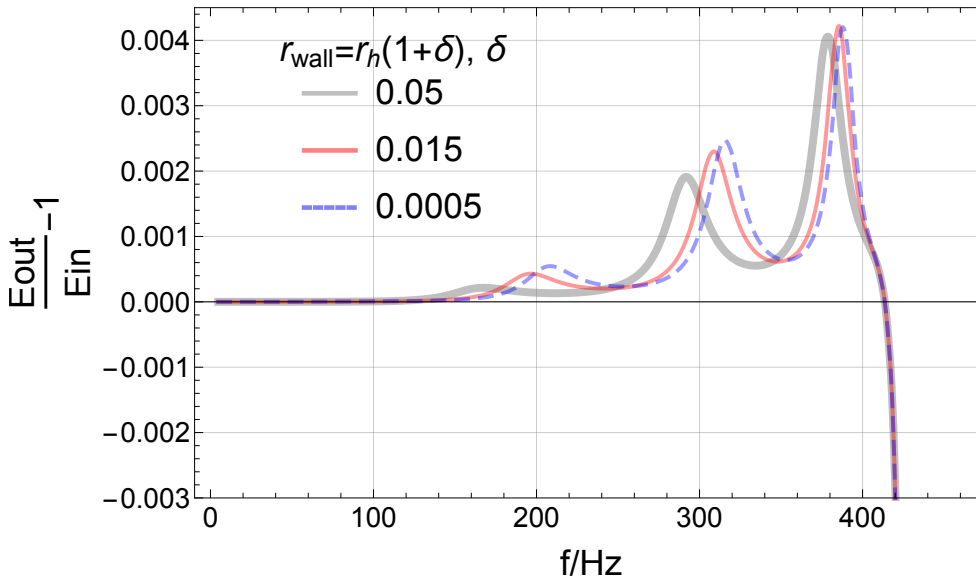


Figure 3.17: Same as Fig. 3.15, but with different wall positions (fixing $R_{\text{wall}}=0.4$). We see that this shifts the resonance frequencies.

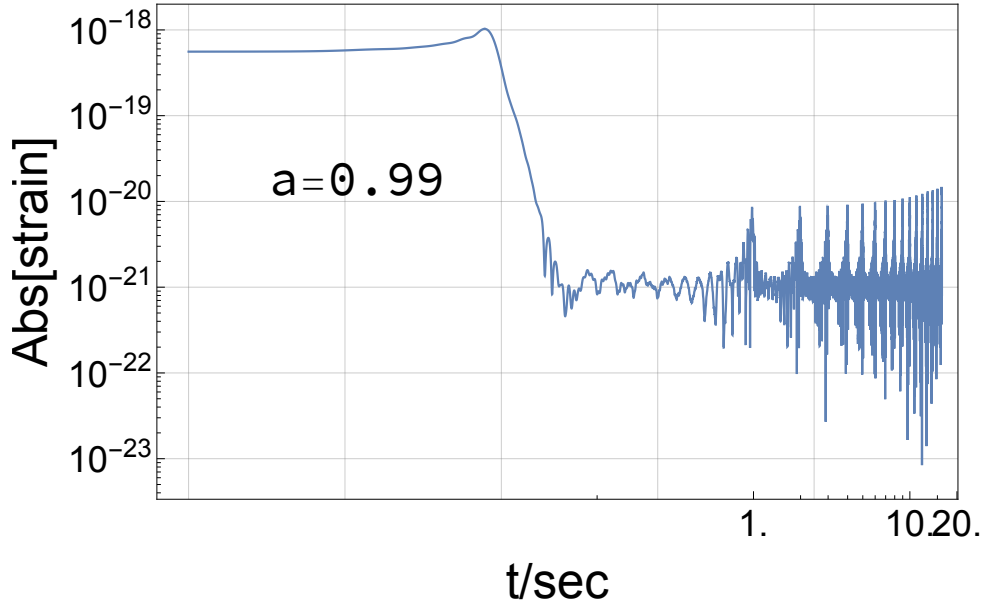


Figure 3.18: Occurrence of ergoregion instability in later echoes in QBHs with higher spin (near extremal Kerr).

for GW150914 in Fig. 3.3. This can be understood by noticing that, as shown in Fig 3.7, the echoes are dominated by frequencies $f \gtrsim 210$ Hz, but superradiance happens at $f < m\Omega_H \simeq 180$ Hz for this event. Hence, the instability does not take over until peak frequency drops below this limit.

We can increase the spin to see the superradiant instability develop faster, as shown in Fig 3.18. For spin $a = 0.80$, the echoes stop decaying at some point and for $a = 0.99$, they start to increase. While this example does demonstrate the appearance of ergoregion instability, it should be treated as a toy model, as the initial wavepacket was designed to reproduce the merger/ringdown template LIGO event GW150914 with $a = 0.67$.

As we mentioned in Sec. 5.1, whether or not ergoregion instability acts in nature depends on the wall absorption properties [177]. Indeed, observation of astrophysical black holes at significant spins [198] does suggest that the instability must be suppressed.

3.8 Conclusions

We have provided realistic templates for echoes of BH mergers by numerically solving the linearized Einstein equation (or Teukolsky equation) in Kerr spacetime with boundary conditions at a Planck length proper distance outside the (would-be) event horizon. We obtain analytic approximations for the echo waveforms and time-delays, and explore their dependence on the softness of the wall (or frequency-dependence of the reflection rate), as well as nonlinear effects during merger event. These analytic templates should be useful in echo searches in current and future gravitational wave data. Finally, we studied the occurrence of superradiant instability and showed that it has negligible effect, for the first few dozen echoes of in typical BH mergers such as GW150914.

Let us close with some open questions and future directions:

- The strain is dominated by mode $l = 2, m = \pm 2$. We only show mode $m = 2$ here and solution of $m = -2$ can easily be found by $R_{slm}[\omega] = R_{sl-m}^*[-\omega]$. More realistic templates should combine all other modes by appropriate weight.
- We cannot provide a reliable waveform for the first echo as it is too sensitive to the *ad hoc* cutoff function (3.14) that we use to set up our initial conditions. This highlights the need for a covariant numerical implementation of QBHs within a dynamical spacetime, which could provide realistic nonlinear initial conditions for echoes.
- Another big uncertainty is the expected softness of the wall. While this is ultimately a question for the quantum models of black holes, it highlights the need for a covariant and causal description of the wall dynamics. It might be possible to describe this dynamics in terms of the properties of a surface (2+1d) fluid and Israel junction conditions (e.g., see [248]).
- The computation of the echo phase beyond ~ 20 echoes is limited by numerical precision and frequency resolution. This can be improved in the future, by either brute force or novel numerical/analytic methods.

Chapter 4

Boltzmann Reflectivity

In this chapter, we discuss another possible universal quantity – surface reflectivity of quantum BHs– and show that *from independent aspects of* detailed balance, the fluctuation-dissipation theorem, and CP-symmetry of the BH final state – the reflectivity is given by the thermal Boltzmann factor. We then briefly discuss the physical implications for the late-time ringdown of gravitational waves from a spinning quantum BHs, as well as for ergoregion stability and viscosity in the membrane paradigm.

4.1 Boltzmann reflectivity from Detailed Balance

From a quantum mechanical point of view, we can consider an isolated BH as an excited multilevel quantum system (e.g., a giant atom), which de-excites by emitting Hawking radiation. We will now show that gravitational waves (GWs) infalling into a BH must be reflected near the horizon with the Boltzmann factor $\mathcal{R} = \exp(-\hbar\omega/(kT_H))$, where ω is the near-horizon frequency, and T_H is the Hawking temperature.

Let us suppose that ingoing (large amplitude and low-frequency) GWs, of which the spectral energy density is denoted by $\rho(\omega)$, can stimulate the BH in a perturbative manner, and excite the quantum system from state 1 to state 2, where $E_2 - E_1 = \hbar\omega > 0$ ¹. The reflectivity of the BH can be characterized by the Einstein coefficients for spontaneous emission, stimulated emission, and absorption, denoted by $A_{21}(\omega)$, $B_{21}(\omega)$, and $B_{12}(\omega)$,

¹Note that this derivation only applies to $\hbar\omega > 0$, as real photons/gravitons have positive energy. If a further assumption of time-reversal symmetry in the horizon-frame is made, we can switch $\omega \rightarrow |\omega|$.

respectively [114]. The net rate of transition from state 1 to state 2 is given by:

$$R_{1\rightarrow 2} - R_{2\rightarrow 1} = B_{12}n_1\rho - A_{21}n_2 - B_{21}n_2\rho, \quad (4.1)$$

where $R_{1\rightarrow 2}$ ($R_{2\rightarrow 1}$) is rate of transition from state 1 to 2 (2 to 1). The detailed balance condition $R_{1\rightarrow 2} = R_{2\rightarrow 1}$ would guarantee that the BH remains in thermal equilibrium with a blackbody radiation $\rho(\omega)$ given by:

$$\rho_{\text{BB}}(\omega) = \frac{2\hbar\omega^3}{\pi c^3 \left[\exp\left(\frac{\hbar\omega}{kT_{\text{H}}}\right) - 1 \right]}, \quad (4.2)$$

with $n_2/n_1 = \exp(\hbar\omega/(kT_{\text{H}}))$ ². The equilibrium constrains Einstein coefficients as $B_{12}(\omega) = B_{21}(\omega) = \pi c^3 A_{21}(\omega)/(2\hbar\omega^3)$ [114].

Now, imagine a classical incident GW with a much bigger energy flux than Hawking radiation, i.e. $\rho(\omega) \gg \rho_{\text{BB}}(\omega)$. In this limit, we can ignore spontaneous emission (or Hawking radiation, i.e. 2nd term on the RHS of Eq. 4.1), to find the reflectivity of the membrane³

$$\mathcal{R} = \frac{B_{21}(\omega)n_2\rho(\omega)}{B_{12}(\omega)n_1\rho(\omega)} = \frac{n_2}{n_1} = \exp\left(-\frac{\hbar\omega}{kT_{\text{H}}}\right). \quad (4.3)$$

In other words, the slow decay of the quantum BH via Hawking radiation is stimulated by incident GWs for $\hbar\omega \lesssim kT_{\text{H}}$, leading to $\mathcal{O}(1)$ reflectivity (see Fig. 4.1). In contrast, in the opposite limit of geometric optics, $\hbar\omega \gg kT_{\text{H}}$, the quantum BHs are indeed *black*, consistent with the *fuzzball complementarity* conjecture [193, 96].

For the sake of brevity, in the remainder of this chapter we shall use natural units with $\hbar = k = c = 1$ and we define $r_g \equiv 2GM$ where M is the mass of the BH.

4.2 Boltzmann reflection and CP-symmetry.

We here briefly show that the Boltzmann reflectivity is equivalent to the CP-symmetry of the BH state. Let us consider a mixture of ingoing and outgoing plane waves in Rindler

²While there could be many other energy levels in the quantum system, they will not be involved in the *detailed balance* condition for these two states, as long as their energy gaps do not match $E_2 - E_1$. We should note that *detailed balance* is a stronger condition than *balance* as we assume transition from any state to any other state is balanced, while “balance” would only require net transition to any state to vanish. For N states, the former leads to $N(N - 1)/2$ conditions, while the latter is only N conditions.

³Motivated by the quantization of BH area, Cardoso et al. [80] discussed the reflectivity of quantum black holes to calculate the echo GWs. The reflection rate they used, however, differs from the Boltzmann reflection rate we derived in (4.3). This is because they assume that the reflection rate is given by $B_{21}(\omega)$.

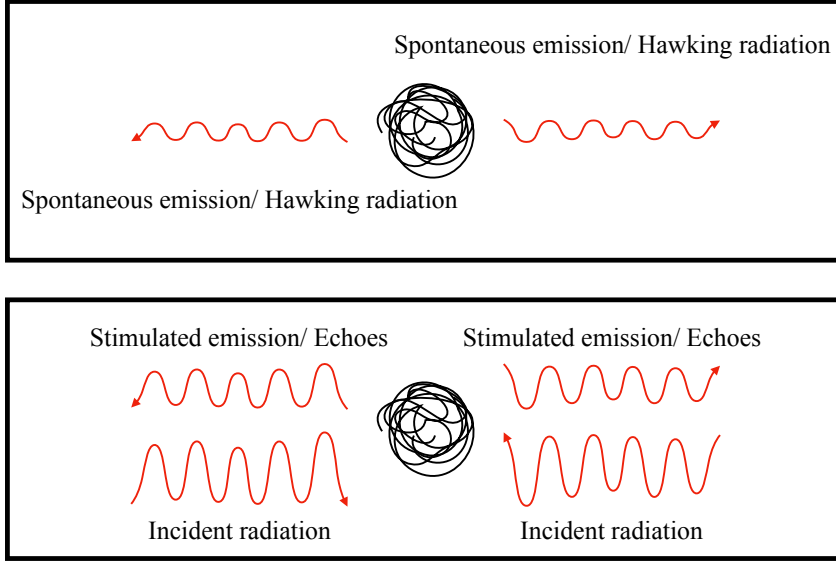


Figure 4.1: Analogy between spontaneous emission and Hawking radiation for isolated BHs, in contrast to stimulated emission caused by incident radiation, that could lead to echoes (see text; note that, for this cartoon we ignore the angular momentum barrier).

metric (4.12):

$$\psi(x, t) = A_{\text{in}} e^{-i\omega(t+x)} + A_{\text{out}} e^{-i\omega(t-x)}. \quad (4.4)$$

$\psi(x, t)$ can be rewritten in the Minkowski coordinates which are related to the Rindler coordinates as

$$T = \kappa^{-1} e^{\kappa x} \sinh \kappa t, X = \kappa^{-1} e^{\kappa x} \cosh \kappa t, \quad (4.5)$$

where κ is the surface gravity of a BH, and then we have

$$\psi(x, t) = A_{\text{in}} [\kappa(T + X)]^{-i\omega/\kappa} + A_{\text{out}} e^{-\pi\omega/\kappa} [\kappa(T - X)]^{i\omega/\kappa}. \quad (4.6)$$

Imposing the CP-symmetry, $\psi(T, X) = \psi^*(T, -X)$, one has the following conditions for the coefficients

$$A_{\text{in}} = e^{-\pi\omega/\kappa} A_{\text{out}}^*, \quad (4.7)$$

$$A_{\text{out}} = e^{\pi\omega/\kappa} A_{\text{in}}^*. \quad (4.8)$$

This again leads to the Boltzmann reflectivity of $\mathcal{R} \equiv |A_{\text{out}}/A_{\text{in}}|^2 = e^{-\omega/T_{\text{H}}}$ once we properly treat branch-cut ⁴.

Note that this analysis could have been equivalently done in terms of Kruskal/Schwarzschild coordinates. $X \rightarrow -X$ antipodal identification of Kruskal metric is known as a RP^3 topological geon [173]. While this spacetime is classically indistinguishable from a BH outside the event horizon, outside quantum measurements can potentially distinguish the two, as the quantum states have different analytic structures [199]. However, forming an RP^3 geon from e.g., stellar collapse requires a non-perturbative change of topology, which can (in principle) happen through quantum tunneling [192].

4.3 Boltzmann reflectivity and Fluctuation-Dissipation theorem

Although the previous two derivations, based on the detailed balance and CP-symmetry, give the Boltzmann reflectivity, they remain ambiguous about the sign of frequency, or the phase of the reflected amplitude. We then next consider a more concrete model motivated by the possible dissipative effects near a BH horizon, which uniquely determines both the amplitude and the phase of reflectivity.

Classical linear perturbations in BH spacetimes obey the equation [237, 288]

$$\left[\frac{d^2}{dx^2} + \omega^2 - V_\ell(x) \right] \psi_\omega(x) = 0, \quad (4.9)$$

where $V_\ell(x)$ is the angular momentum barrier located outside the horizon and ℓ is a angular harmonic number. The asymptotic behavior of the (quasinormal) mode function of GWs in the Schwarzschild BH background is

$$\lim_{x \rightarrow \pm\infty} \psi_\omega = e^{\pm i\omega x}. \quad (4.10)$$

However, we know that quantum effects near BH horizon lead to a thermal behavior at temperature T_{H} . According to fluctuation-dissipation theorem [166], this should modify the classical field equations via additional fluctuation and dissipation terms, resulting from interaction with quantum/thermal fields. Therefore, we shall posit that Eq. (4.9) is modified to:

⁴Mathematically, one finds $\mathcal{R} = \exp(\pm\omega/T_{\text{H}})$, depending on the choice of branch-cut. However, only one choice is physically sensible (and consistent with detailed balance and fluctuation-dissipation theorem).

$$\left[-i \frac{\gamma \Omega(x)}{E_{\text{Pl}}} \frac{d^2}{dx^2} + \frac{d^2}{dx^2} + \omega^2 - V(x) \right] \psi_\omega(x) = \xi_\omega(x), \quad (4.11)$$

where ξ_ω is a stochastic fluctuation field, while γ is a dimensionless dissipation parameter, $\Omega(x) \equiv \omega/\sqrt{|g_{00}(x)|}$ is the blueshifted (or proper) frequency, and E_{Pl} is Planck energy. The form of the dissipation term (which is similar to viscous dissipation for sound waves [169]⁵) is expected from the fact that gravitational coupling constant is given by Ω/E_{Pl} . Therefore, dissipation terms coming from gravitational interactions must be suppressed by this factor. In other words, only when the blueshift effect is so intense that the proper frequency is comparable to the Planck energy (i.e. near horizon), $\Omega \sim E_{\text{Pl}}$, the dispersion relation is drastically modified ⁶.

Moreover, the membrane paradigm [264, 156], the fluctuating geometry around a BH [223, 55] and the minimal length uncertainty principle [74] lead to the dissipative effects near the apparent horizon. From the point of view of the phenomenology of quantum gravity, constraints on the spacetime viscosity, ν , was also discussed by adding the viscous term of the Navier-Stokes equation, $-i(4/3)\nu\Omega\nabla^2$ [170], as we did in (4.11). Of course, in lieu of a theory of quantum gravity, there is no clear guiding principle to add dissipation to the dispersion relation, but our choice follows naturally if one follows the analogy between viscous fluids and quantum spacetime.

According to fluctuation-dissipation theorem, the balance of fluctuation ξ_ω and dissipation should lead to a thermal spectrum for the field ψ_ω [166]. Otherwise, for classical fluctuations, $\omega^2|\psi_\omega| \gg |\xi_\omega|$, far from the horizon, $\Omega \ll E_{\text{Pl}}$, we recover the classical Eq. (4.9).

Let us calculate the mode function near the horizon where the blueshift effect is most significant ⁷. In the near-horizon limit, the exterior metric can be approximated as Rindler

$$ds^2 = e^{2\kappa x}(-dt^2 + dx^2) + dy^2 + dz^2, \quad (4.12)$$

⁵The dispersion relation for sound waves that dissipate via fluid (kinematic) viscosity ν is: $(4\nu/3)\nabla^2\partial_t p + c_s^2\nabla^2 p - \partial_t^2 p = 0$.

⁶One might wonder if the perturbative approach can be valid even when the Planck energy is involved in (4.11). Since the gravitational blue shift does not enhance the amplitude of the incoming GWs, but just increases its frequency, using the wave equation (4.11) is still valid. Furthermore, in the near-horizon regime, the backreaction of transverse traceless GWs can be quantified using the GW stress tensor $T_{\mu\nu} \propto \partial_\mu h^{\alpha\beta} \partial_\nu h_{\alpha\beta}$, which remains finite in the locally flat coordinates, as derivatives are only non-vanishing in the longitudinal direction. Whether there could be nonlinear effects at higher orders is an interesting question that we defer to future work.

⁷We shall focus on large amplitude perturbations, and thus ignore the fluctuation term ξ_ω .

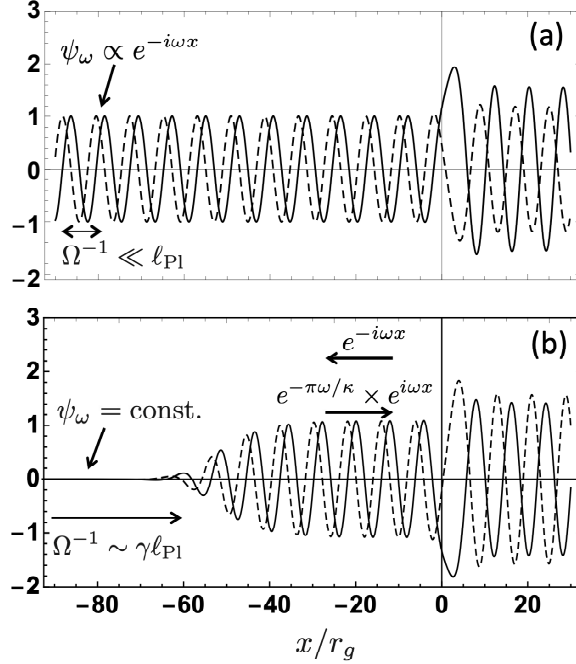


Figure 4.2: (a) The mode function $\psi_\omega(x)$ with the Regge-Wheeler potential, for which the ingoing boundary condition is imposed in the near-horizon limit as in the classical BHs. (b) The mode function $\psi_\omega(x)$ with the Regge-Wheeler potential and the dissipation term added in (4.11). We take $\gamma = 10$ and $\kappa = (2r_g)^{-1}$. In both (a) and (b) we take $\ell = 2$, $s = -2$, and $r_g\omega = 0.8$. Solid and dashed lines show $\Re[\psi_\omega]$ and $\Im[\psi_\omega]$, respectively.

where $\kappa = 2\pi T_H$ is the surface gravity. The modified wave function (4.11) has an analytic solution near the horizon

$$\lim_{x \rightarrow -\infty} \psi_\omega(x) = {}_2F_1 \left[-i\frac{\omega}{\kappa}, i\frac{\omega}{\kappa}, 1, -i\frac{E_{\text{Pl}}e^{\kappa x}}{\gamma\omega} \right], \quad (4.13)$$

where ${}_2F_1(a, b, c, z)$ is the hypergeometric function. In the limit of $x \rightarrow -\infty$, this mode function is constant. The physical meaning of this boundary condition is that the energy flux carried by the ingoing GWs cannot penetrate the horizon, and is either absorbed or reflected. In this sense, this boundary condition is consistent with the picture according to a distant observer in the context of BH complementarity [260] or the membrane paradigm [264, 106], in which there is virtually no BH interior to propagate into. In the range of $-\log[E_{\text{Pl}}/(\gamma\omega)] \ll \kappa x \ll -1$, the function can be expressed by the superposition of

outgoing and ingoing modes

$$\psi_\omega = e^{\pi|\omega|/(2\kappa)} A e^{-i\omega x} + e^{-\pi|\omega|/(2\kappa)} A^* e^{i\omega x}, \quad (4.14)$$

$$A \equiv \frac{\left(\frac{\gamma\omega}{E_{\text{Pl}}}\right)^{i\omega/\kappa} \Gamma(-2i\omega/\kappa)}{\Gamma(-i\omega/\kappa)\Gamma(1-i\omega/\kappa)}. \quad (4.15)$$

Therefore, we again recover the Boltzmann reflectivity (4.3):

$$\mathcal{R} = \left| \frac{e^{-\pi|\omega|/(2\kappa)} A^*}{e^{\pi|\omega|/(2\kappa)} A} \right|^2 = e^{-|\omega|/T_{\text{H}}}. \quad (4.16)$$

Remarkably, the flux reflectivity \mathcal{R} is independent of the dissipation parameter γ in Eq. (4.11), even though the approximate position of the reflection x_{echo} (where $\gamma\Omega \sim E_{\text{Pl}}$), and hence echo time delays [209], does depend on it ⁸:

$$\Delta t_{\text{echo}} = 2|x_{\text{echo}}| = 2\kappa^{-1} \ln [E_{\text{Pl}}/(\gamma\omega)]. \quad (4.17)$$

4.4 GW Echoes and absence of ergoregion instability.

A non-vanishing horizon reflectivity will lead to echoes from the ringdown of a perturbed BH (e.g., [81, 82, 197, 280, 78, 209]). Indeed, tentative (albeit controversial) evidence for these echoes have been claimed in the literature [28, 99, 22]. Here we outline the basic features of GW echoes from Boltzmann reflectivity, while next chapter examines these predictions and implications for BH quasinormal modes in more detail [281]. We further show that (consistent with current observational bounds [49]), ergoregion instability is not expected for spinning BHs, due to imperfect reflectivity.

In order to investigate how the dissipation term change the ringdown GWs propagating from a spinning quantum BH, we start with the Sasaki-Nakamura (SN) equation [249] including the dissipation term. Although there is no unique choice of wave equation around a Kerr BH, we here choose the SN equation that describes the wave propagation in the co-rotating coordinates, and so there is no time-asymmetry due to the rotation of background spacetime. As such, the only terms that break time-asymmetry are dissipative terms near horizon, where propagation is governed by near-horizon Rindler geometry, and is fully fixed by surface gravity $\kappa = 2\pi T_{\text{H}}$.

⁸Note that since we can only derive the phase of reflectivity from our Equation (4.11), its derivation is more model-dependent than that of Boltzmann reflectivity for the energy.

In the near-horizon limit, one can obtain the mode function (as we did before) by satisfying the no-flux condition ($\psi_\omega(x) = \text{const.}$ for $x \rightarrow -\infty$), yielding the Boltzmann reflectivity of Eq. (4.16) (see the Appendix A).

An example of a full waveform ⁹ can be obtained by starting with a Gaussian wavepacket

$$\psi(x, 0) = \exp \left[-\frac{(x - x_c)^2}{\sigma^2} - \frac{ix}{\sigma_h} \right], \dot{\psi}(x, 0) = 0, \quad (4.18)$$

where a dot denotes the derivative with respect to t , σ and σ_h^{-1} characterize the width and mean wavenumber of the wavepacket, while x_c is its initial position. Fig. 4.3 shows numerical integration of Eq. (A.1) to find the GW strain amplitude seen by a distant observer. In addition to the original ringdown, as expected, we see echoes with a time-delay given by Eq. (4.17), with a spin-dependent amplitude. In particular, in the extremal limit $a \rightarrow 1$ for fixed initial conditions, echoes are highly suppressed (and delayed), since $T_H \rightarrow 0$, and thus the reflectivity is exponentially suppressed except for a narrow range around $\omega_\infty = m\Omega_H$ (see Fig. 4.4). This is enough to suppress ergoregion instability, even for a rapidly spinning BH [176].

4.5 Conclusions.

We have provided three independent derivations for a Boltzmann reflectivity of quantum BH horizons, $\mathcal{R} = e^{-\omega/T_H}$, based on

1. Thermodynamic detailed balance,
2. CP-symmetry, or RP^3 topology, of extended BH spacetime, and
3. Fluctuation-dissipation theorem.

Therefore, although a concrete picture of microscopic structure of a quantum BH is still missing, macroscopic properties such as entropy, temperature, and now, its energy flux reflectivity, may be independent of the details.

Assuming this universal property of the quantum BHs, we numerically investigated the GW echoes and showed that the echo is strongly suppressed, and delayed, for a rapidly

⁹Since we calculate the waveform by solving the SN equation, which reduces to the Regge-Wheeler equation in the limit of $a \rightarrow 0$, our waveform corresponds to axial perturbations of a black hole.

spinning BH, $0 < 1 - a \ll 1$, due to the decrease of its Hawking temperature. This leads to the absence of the ergoregion instability since the frequency dependence of the Boltzmann reflectivity is sharply peaked around $\omega_\infty \simeq m\Omega_H \pm T_H$ and is exponentially suppressed outside this range. Finally, we discussed the implication for the fluid viscosity in the membrane paradigm, finding that it should vanish at low frequencies.

The synergy of our three, seemingly independent, derivations all leading to a Boltzmann reflectivity may help us draw a clearer picture of what a quantum black hole might look like (as long as we assume validity of linear perturbation theory):

The central assumption underlying our key result, Eq. (4.3), is that black holes are not classical spacetimes, but rather quantum objects, obeying standard rules of unitary quantum mechanics and thermodynamics. For one, this implies that they cannot be perfectly absorbing, as it would violate unitarity. Furthermore, as typical de-excitation of BH state leads to emission of Hawking photons/gravitons, it is reasonable to assume that typical absorption happens at similar frequencies, and thus photons/gravitons at much lower frequencies, $\hbar\omega \ll kT_H$ cannot excite *local* membrane degrees of freedom. As such, they should be reflected, which is exactly what is predicted by Boltzmann reflectivity (4.3). In other words, quantum BHs must be “optically thin” at $\hbar\omega \ll kT_H$.

The latter point is further underscored by the fluctuation-dissipation derivation, as lower frequency waves are reflected farther away from the horizon, where gravity is weaker. It also suggests that this universality might be a low-energy property, as higher powers of Ω/E_{Pl} can modify the dispersion relation at higher frequencies [209]. However, this may not be a significant correction since reflectivity is already highly suppressed for $\hbar\omega \gtrsim kT_H$.

Finally, the equivalence of the CP-symmetry, or RP^3 topology, of the BH spacetime with Boltzmann reflectivity suggests that a drastic transition from classical to quantum BHs is necessary. This is clearly not something that would emerge from e.g. classical collapse of a star, and requires a change of topology through non-perturbative quantum tunneling, similar to what is advocated in the fuzzball proposal [192]. Therefore, even though we rely on perturbation theory outside stretched horizon in our analysis, from a global perspective, a non-perturbative transition is necessary to take a classical BH to a quantum BH spacetime.

Let us end by noting that, as we discuss in next chapter [281], our concrete predictions for GW echoes from quantum BHs are imminently testable using current and upcoming GW observations. May we suggest that we hold other proposals for quantum black holes to the same standard?

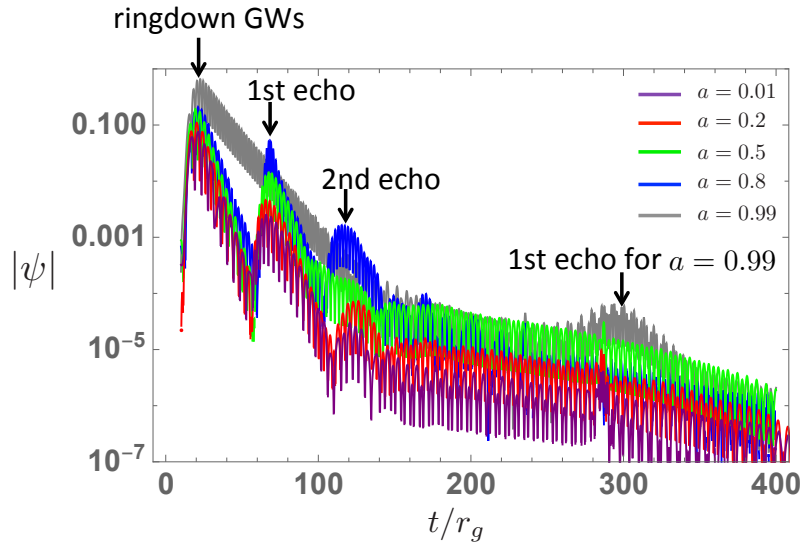


Figure 4.3: The ringdown signals followed by the echo GWs with $\sigma = 2r_g$, $\sigma_h = 0.45r_g$, and $x_c = 0$ seen by an observer at $x = 25r_g$. For illustrative purposes, we take $r_g = 10^5 \ell_{\text{Pl}}$ and $\gamma = 10$. The spin parameter is $a = 0.01$ (purple), $a = 0.2$ (red), $a = 0.5$ (green), $a = 0.8$ (blue), and $a = 0.99$ (gray).

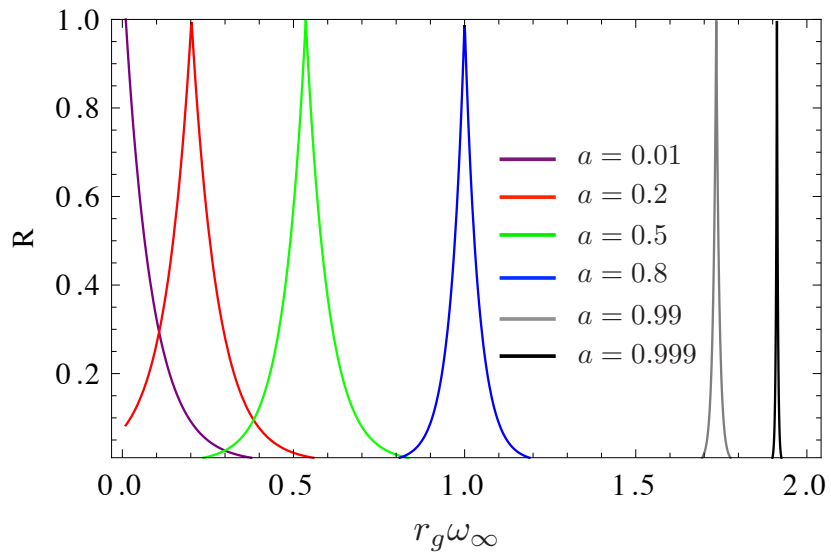


Figure 4.4: The frequency dependence of the Boltzmann reflectivity (for $m = 2$ mode) assuming a spinning BH with spin parameters $a = 0.01, 0.2, 0.5, 0.8, 0.99,$ and 0.999 .

Chapter 5

Echoes from Boltzmann Reflectivity

5.1 Introduction

In the frequency dependence of the Boltzmann reflectivity last chapter, we study this question assuming that BHs are quantum systems that follow standard rules of quantum mechanics and thermodynamics [211]. There, we found that independent arguments based on thermodynamic detailed balance, fluctuation-dissipation theorem, and CP-symmetry of the extended BH spacetime, remarkably all lead to a universal Boltzmann energy flux reflectivity:

$$\frac{E_{\text{out}}}{E_{\text{in}}} = \exp\left(-\frac{\hbar|\tilde{\omega}|}{k_B T_{\text{H}}}\right), \quad (5.1)$$

where $\tilde{\omega}$ is the horizon-frame frequency and T_{H} is the Hawking temperature. Here we investigate the quasinormal modes (QNMs) of these quantum BHs, and show how their excitation can be related to QNMs of classical BHs. This result can be used to make predictions for GW echoes from quantum BHs, which we verify using numerical and analytic calculations. We further study the detectability of these echoes, and show that ergoregion instability is suppressed, consistent with astrophysical [198] and GW observations [49].

We organize this chapter as follows: Sec. 5.2 calculates the QNMs from a Boltzmann boundary condition analytically, using the tools developed in [176]. Next, Sec. 5.3 presents echoes in the time domain both numerically and analytically, and confirms the QNMs calculated in Sec.5.2 with numerical results. Also the importance of the initial condition is manifested in the time domain. Then, in Sec. 5.4, we discuss how the ergoregion instability is quenched, and draw conclusions in Sec. 5.5.

If not specified, $\tilde{\omega}$ is the near horizon frequency while ω is the frequency at infinity.

5.2 Quasinormal modes

In this section, we investigate the QNMs based on the fluctuation-dissipation theorem for quantum BHs, that we introduced in the last chapter. We use two analytic methods: the geometric optics approximation, or the asymptotic matching method based on [176], which both yield the same analytic formula.

We introduce Detweiler's function [109]

$${}_sX_{lm} = \Delta^{s/2}(r^2 + a^2)^{1/2} \left[\alpha_s R_{lm} + \beta \Delta^{s+1} \frac{d_s R_{lm}}{dr} \right], \quad (5.2)$$

where α and β are radial functions and the different choices of them influence the $V(r, \omega)$ in Eq. (5.3). Specifically, we focus on Sasaki-Nakamura (SN) equation in this chapter (the explicit form of the functions α and β is given in [254]). The radial master equation becomes a simple non-singular wave equation with two independent asymptotic solutions X_s^+ and X_s^- , where we omit indices l and m :

$$\frac{d^2 {}_sX_{lm}}{dx^2} - V(r, \omega) {}_sX_{lm} = 0, \quad (5.3)$$

$$X_s^+ = \begin{cases} B_+ e^{-i\tilde{\omega}x}, & x \rightarrow -\infty \\ e^{+i\omega x} + A_+ e^{-i\omega x}, & x \rightarrow \infty \end{cases} \quad (5.4)$$

$$X_s^- = \begin{cases} e^{+i\tilde{\omega}x} + A_- e^{-i\tilde{\omega}x}, & x \rightarrow -\infty \\ B_- e^{+i\omega x}, & x \rightarrow \infty \end{cases} \quad (5.5)$$

where x is the tortoise coordinate (defined as $x = \int (r^2 + a^2)/(r^2 - 2Mr + a^2) dr$, approaching $-\infty$ at horizon), while $\tilde{\omega} = \omega - am/(2Mr_+)$ and $r_+ = M + \sqrt{M^2 - a^2}$. The potential $V(r, \omega)$ can be found in [176].

Now, we apply the fluctuation-dissipation theorem [211]. With the modified Einstein equation from the theorem ¹, the boundary condition obtained for the asymptotic solution X_s^- near horizon is fixed by Eq. (5.1):

$$A_- = R_{\text{wall}}^{-1} = e^{+\frac{\tilde{\omega}}{2T_H}} (\gamma |\tilde{\omega}|)^{\frac{i\tilde{\omega}}{\pi T_H}}, \quad (5.6)$$

where γ was the free parameter that quantified dissipation in the fluctuation-dissipation theorem. We further assume that the imaginary part of frequency is much smaller than its real part, thus

$$A_- \simeq e^{+\frac{|\tilde{\omega}|}{2T_H} + \frac{i\tilde{\omega}}{\pi T_H} \ln(\gamma |\tilde{\omega}|)}. \quad (5.7)$$

¹Here we ignore the potential term since we only need to consider the near horizon range for calculating reactivity of the wall, which is far away from angular potential barrier

We can compare this result to [176] with a Neumann boundary condition, $dX_s^-/dx = 0$, at $r_0 = r_+(1 + \epsilon)$: They find $A_- = e^{2i\tilde{\omega}x_0}$, with $x_0 = x(r_0)$. We can thus identify $(\gamma\tilde{\omega})^{i\tilde{\omega}/(\pi T_H)} = e^{2i\tilde{\omega}x_0}$ or

$$x_0 \equiv \frac{\ln(\gamma|\tilde{\omega}|)}{2\pi T_H}, \quad (5.8)$$

as the effective position of the reflecting wall. In the following focus on $\gamma \sim 1$ in Planck units. Moreover, as discussed above, the energy flux reflectivity of the wall is exactly given by a Boltzmann factor $e^{-|\tilde{\omega}|/T_H}$.

Since the effective position of the wall changes very slowly as the $\ln(\tilde{\omega})$ (for $\tilde{\omega} \ll 1$ in Planck units), it can be translated to an approximately constant time delay between subsequent echoes:

$$\Delta t_{\text{echo}} \equiv 2|x_0| = -\frac{\ln(\gamma|\tilde{\omega}|)}{\pi T_H}. \quad (5.9)$$

Let us now find the QNMs for the quantum BH. Fig. 3.1 shows the geometric ‘‘optics’’ picture for the echology, which is valid as long as $|\tilde{\omega}| \gg |x_0|^{-1}$. In this limit, following [183], we can obtain the quantum BH response by using R_{BH} and T_{BH} (R_{BH}^* and T_{BH}^*), the reflectivity and transmissivity of classical BHs’ angular momentum barrier with an ingoing (outgoing) wavepacket from outside (inside):

$$\begin{aligned} \left(\frac{h_{\text{out}}}{h_{\text{in}}}\right)_{\text{outside}} &= R_{\text{BH}} + \sum_{n=1}^{\infty} |T_{\text{BH}}|^2 R_{\text{wall}}^n R_{\text{BH}}^{*(n-1)} \\ &= R_{\text{BH}} + \frac{|T_{\text{BH}}|^2 R_{\text{wall}}}{1 - R_{\text{wall}} R_{\text{BH}}^*}, \end{aligned} \quad (5.10)$$

$$\begin{aligned} \left(\frac{h_{\text{out}}}{h_{\text{in}}}\right)_{\text{inside}} &= T_{\text{BH}}^* + \sum_{n=1}^{\infty} T_{\text{BH}}^* R_{\text{wall}}^n R_{\text{BH}}^{*n} \\ &= T_{\text{BH}}^* + \frac{T_{\text{BH}}^* R_{\text{BH}}^* R_{\text{wall}}}{1 - R_{\text{wall}} R_{\text{BH}}^*}. \end{aligned} \quad (5.11)$$

The first term of each equation is the initial observed event as in Fig. 5.1, which is the same for classical BHs and quantum BHs. The subsequent terms in Eqs. (5.10) and (5.11) represent the first echo, second echo, etc., which can be summed as a geometric series. The QNMs are poles of the response function, or the zero’s of the denominator, $1 - R_{\text{wall}} R_{\text{BH}}^* e^{-2i\tilde{\omega}x_0} = 0$, where $R_{\text{wall}} = e^{-|\tilde{\omega}|/(2T_H)}$ for our quantum BHs. Near $\tilde{\omega} \simeq 0$, we have the least-damped modes, which we shall focus on next. We numerically confirm $R_{\text{BH}}^* \simeq \pm 1$ for $|\tilde{\omega}| \ll T_H$, where plus (minus) is for $s = -1$ ($s = 0, -2$), corresponding to axial perturbations of a black hole. Hence, $\tilde{\omega}_q$ for QNMs satisfy:

$$e^{-2i\tilde{\omega}x_0 - \frac{|\tilde{\omega}|}{T_H}} = \pm 1, \quad (5.12)$$

$$\tilde{\omega}_n = \frac{q\pi}{2x_0} \left[1 - \frac{\text{sgn}(q) \times i}{4x_0 T_H} \right], \quad (5.13)$$

where $q = 2n + 1$ for $s = 0, -2$, and $q = 2n$ for $s = -1$, with $n \in \mathbb{Z}$. We arrive at the same result via the asymptotic matching method used in [176]. Since we prove that the ratio of outgoing and ingoing waves of solution of Eq. (3.3) (denoted as C_1/C_2 in [176]) is proportional to A^{-1} , just simply multiplying the extra Boltzmann reflectivity by Eqs. (A9) and (A13) in [176] recovers Eq. (5.12), hence the QNMs.

Let us note that, here we approximated the final stage of nonlinear binary merger event as a scattering problem of a final black hole with wave from inside or outside. Intuitively, the outside source might be activated first by the binary merger event. However, with the data and our linear model it is not clear how these two signals actually combine to produce the main event and echoes due to highly nonlinear initial conditions. Hence, in this work, we consider pure inside/outside condition independently. As the signal sent in from outside decays quickly, its inclusion cannot affect the morphology of the echo templates significantly, and can only impact the relative amplitude of echoes to the main merger event.

5.3 Real time Echoes

QNMs are crucial to the structure of echoes in the real time. Our analytic derivation of QNMs, in Sec. 5.2 above, is only valid for $|\tilde{\omega}| \ll T_H$, but might be sufficient to encode information for the real time echoes since the least-damped mode is in the same range. In this section, we calculate the echoes numerically in the geometric optics limit (Eqs. (5.10) and (5.11)), and analytically from the QNMs found in Sec 5.2, confirming that two calculations are consistent.

5.3.1 Numerical Echoes from geometric optics approximation

While the realistic behavior of echoes should come from the nonlinear evolution, starting with two inspiraling BHs, we can imitate this by linear initial conditions with a wavepacket hitting the angular momentum barrier, from inside *or* outside, producing exactly the same ringdown waveform as in the LIGO template for GW150914, denoted as h_{LIGO} . We can

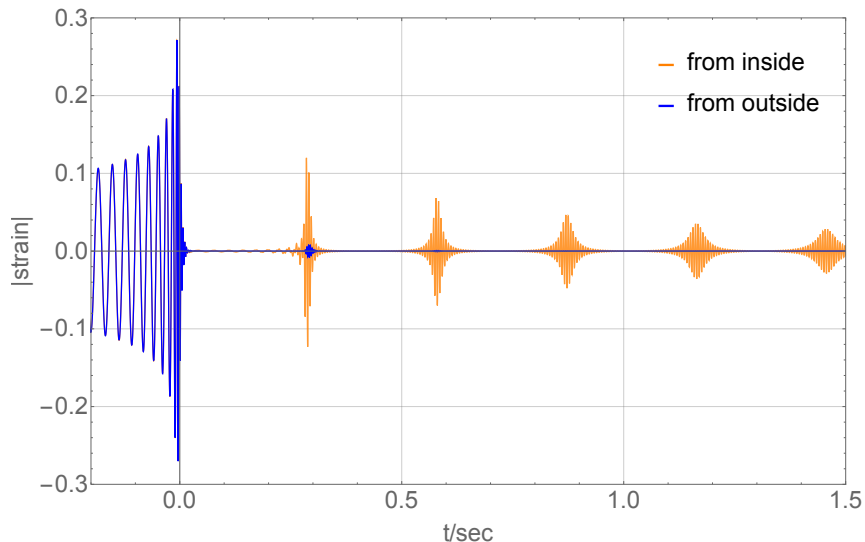


Figure 5.1: Real time echoes from the geometric optics approximation, and $\gamma \sim 1$ (in Planck units). By construction, the first burst is exactly the same as in the LIGO template for GW150914 (only with strain rescaled for comparison with the analytic solution in Fig. 5.4). Purple (orange) is for the initial wavepacket coming from outside (inside). Note that our calculation uses linear perturbation theory and does not capture the nonlinear physics during inspiral and merger phases.

then use Eqs. (5.10) and (5.11) to predict echo waveform, using linear initial conditions and geometric optics limit, in frequency space:

$$h_{\text{out}} = h_{\text{LIGO}} (1 + \mathcal{K}_{\text{echo}}), \quad (5.14)$$

$$R_{\text{wall}} = \exp\left(-\frac{|\tilde{\omega}|}{2T_{\text{H}}}\right) e^{-2i\tilde{\omega}x_0}, \quad (5.15)$$

$$\mathcal{K}_{\text{echo}}^{(\text{outside})} = \frac{|T_{\text{BH}}|^2}{R_{\text{BH}}} \frac{R_{\text{wall}}}{1 - R_{\text{wall}} R_{\text{BH}}^*}, \quad (5.16)$$

$$\mathcal{K}_{\text{echo}}^{(\text{inside})} = \frac{R_{\text{BH}}^* R_{\text{wall}}}{1 - R_{\text{wall}} R_{\text{BH}}^*}, \quad (5.17)$$

Reflectivity and transmissivity of classical BHs can be found numerically by solving the Teukolsky equation². Fig. 5.1 shows the prediction for real-time echo waveforms, by Fourier

²Here, we use the numerical solutions from Conklin:2017lwb [99].

transforming Eq. (5.15). By construction, the first burst has the exact same waveform as the LIGO template for GW150914 (note that we rescale the strain for later comparison with analytic result in Fig. 5.4). The outside initial condition produces smaller echoes than the inside since reflection rate of BH is near 1 around the main frequency (around $\tilde{\omega} \sim 0$, where $R_{\text{wall}} \sim 1$), and the transmission is around 0. Hence, $\mathcal{K}_{\text{echo}}^{(\text{outside})}$ is much smaller than $\mathcal{K}_{\text{echo}}^{(\text{inside})}$, and so are the echoes. Another feature is that the echoes become broader over time, as they become more sharply peaked in frequency, around $\omega \simeq 2\Omega_H$.

5.3.2 On the accuracy of the geometric optics approximation

Let us now discuss the validity of the geometric optics approximation (Figure 3.1 and Equations 5.10-5.11). Since the calculation of R_{BH} assumes plane waves at $x_0 \rightarrow -\infty$, the geometric optics approximation may fail at low frequencies, where $\tilde{\omega}|x_0| \sim 1$. We numerically integrate the full SN equation with the inclusion of the dissipative term proposed in [211] and the boundary condition of $\lim_{x \rightarrow -\infty} \psi_{\tilde{\omega}}^{(\text{regular})}(x) \rightarrow 1$. Then we calculate the Fourier mode of GWs, $h_{\text{out}}^{(N)}$, which is given by

$$h_{\text{out}}^{\text{SN}}(\omega) = \int dx' \frac{S(\omega, x') \psi_{\tilde{\omega}}^{(\text{regular})}(x')}{W_{\text{BH}}}, \quad (5.18)$$

where $S(\omega, x')$ is the source term and W_{BH} is the Wronskian of $\psi_{\tilde{\omega}}^{(\text{regular})}$ and a purely outgoing solution at $x \rightarrow \infty$, $\psi_{\tilde{\omega}}^{(\text{outgoing})}$. Assuming a simple source term of $S = \delta(x - x_s)$ at $x_s \ll x_0$, Eq. (5.18) reduces to

$$h_{\text{out}}^{\text{SN}}(\omega) = \frac{1}{2i\omega A_{\text{in}}}, \quad (5.19)$$

and the Fourier mode based on the geometric optics approximation $h_{\text{out}}^{\text{GO}}$ is given by

$$h_{\text{out}}^{\text{GO}}(\omega) = \frac{e^{-i\tilde{\omega}x_s}}{2i\omega} T_{\text{BH}}^* \left(1 + \mathcal{K}_{\text{echo}}^{(\text{inside})} \right). \quad (5.20)$$

In Fig. 5.2, we plot transfer functions, $1/|A_{\text{in}}|/T_{\text{BH}}^*$ and $|1 + \mathcal{K}_{\text{echo}}^{(\text{inside})}|$, for comparison. Although one finds small deviation between them, both are almost consistent at high frequency.

5.3.3 On the γ -dependence of echo spectrum

Although γ does not change the reflectivity of the would-be horizon, it does change the time-interval of echoes, Δt_{echo} , and so the peak frequencies in the spectrum of echo GWs are useful to put constraint on the value of γ from the observations. The dissipative effect becomes dominant when the blue-shifted frequency Ω reaches the energy of E_{Pl}/γ . To give a few examples, we calculate the spectra of echo GWs by implementing the inverse Fourier transform of (5.14) in the cases of $\gamma = 1$ and 10^3 (Fig. 5.3), for which the relevant energy scales are the Planck and Grand Unified Theory scales, respectively. Here we plug the ringdown spectrum [63] into h_{LIGO} in (5.14) to obtain Fig. 5.3. Therefore, one can see only the ringdown spectrum (black dashed line in Fig. 5.3) when $\gamma = 0$ that is the GR limit.

5.3.4 Analytic Echoes from QNMs

QNMs are the pure outgoing solution as X_s^- in Sec 5.2. Hence, we should also be able to recover the numerical real-time echo solution with the analytic QNMs calculated in Sec 5.2. We assume that the solution is a sum over QNMs:

$$h_{\text{out}}(t) \simeq \sum_{n=-\infty}^{\infty} B_n e^{-i(\tilde{\omega}_n + \frac{a}{Mr_+})t}, \quad (5.21)$$

where B_n 's are the complex amplitudes of the QNMs, and we use $l = m = 2$ for the dominant QNMs.

For event GW150914, the classical ringdown is well-modelled by a single dominant QNM (or a Lorentzian template) with $\omega_* \simeq 1470 - i250$ rad/s [16]:

$$\begin{aligned} h_{\text{Lorentz}}(t) &= \Theta(t) e^{-i\omega_* t} = \frac{1}{2i\pi} \int \frac{e^{-i\omega t}}{\omega - \omega_*} d\omega \\ &\simeq \frac{1}{2ix_0} \int \frac{1}{\tilde{\omega}_n + \frac{a}{Mr_+} - \omega_*} e^{-i(\tilde{\omega}_n + \frac{a}{Mr_+})t} dn, \end{aligned} \quad (5.22)$$

where we used Eq. (5.13) to approximate $\tilde{\omega}_n$, and ignored the imaginary part of $\tilde{\omega}_n$ ³.

Now, comparing Eq. (5.21) and Eq. (5.22), we notice that the dominant QNM of the classical BH can be simply written as the sum over the QNMs of the quantum BH, by

³Note that $\left| \frac{\Im \tilde{\omega}}{\Re \tilde{\omega}} \right| = -\frac{\pi}{2 \ln(\gamma |\tilde{\omega}|)} \ll 1$

replacing $\int dn \rightarrow \sum_n$:

$$h_{\text{out}}(t) \simeq \sum_{n=-\infty}^{\infty} \frac{e^{-i(\tilde{\omega}_n + \frac{a}{Mr_+})t}}{2ix_0 \left(\tilde{\omega}_n + \frac{a}{Mr_+} - \omega_* \right)}, \quad (5.23)$$

In other words, we assume that, in the $x_0 \rightarrow -\infty$ limit, the classical and quantum BHs have identical waveforms. However, for finite x_0 , if we ignore the imaginary part of $\tilde{\omega}_n$'s, all QNMs have a common period of $\Delta t_{\text{echo}} = 2|x_0|$, leading to periodic echoes after this time. However, the fact that $\Im \tilde{\omega} < 0$ implies that subsequent echoes will decay.

Fig. 5.4 compares the analytic prediction from Eq. (5.23) with the numerical result from (Fourier transform of) Eq. (5.15), for a wavepacket coming from inside the barrier (which is expected to be expandable in terms of quantum BH QNMs). The red dashed curve is the analytic solution, which matches very well with the orange curve from the numerical calculation. They both decay as $1/t$ at the beginning (first ~ 20 echoes), but then start to fall off exponentially. Note that we rescale the amplitude of LIGO template for GW150914 in the numerical calculation, to match the first echoes in both numerical and analytic solutions ⁴.

It is easy to understand this behavior analytically. Since only modes with $|\tilde{\omega}| \lesssim T_{\text{H}}$ survive for many echoes, the denominator of Eq. (5.23) is approximately constant, and can be factored out of the sum. The rest of the sum can be decomposed into two geometric series, and has a closed form:

$$h_{\text{out}}(t) \simeq \frac{ie^{-\frac{iat}{Mr_+}} \cos\left(\frac{\pi t}{2x_0}\right) \sinh\left(\frac{\pi t}{8x_0^2 T_{\text{H}}}\right)}{2x_0 \left(\frac{a}{Mr_+} - \omega_*\right) \left[\cos\left(\frac{\pi t}{x_0}\right) - \cosh\left(\frac{\pi t}{4x_0^2 T_{\text{H}}}\right) \right]}, \quad (5.24)$$

At the peak of the k -th echo $t = k \times \Delta t_{\text{echo}}$, corresponding to the echo, the cosines becomes ± 1 and thus the echo amplitudes can be further simplified:

$$|h_{\text{out}}(t = k \times \Delta t_{\text{echo}})| \propto \frac{1}{\sinh\left(\frac{\pi t}{8x_0^2 T_{\text{H}}}\right)}, \quad (5.25)$$

which indeed, as we see in Fig. 5.4, transitions from $1/t$ to exponential decay after:

$$k_{\text{tran}} \sim \frac{8x_0^2 T_{\text{H}}}{\pi \times 2|x_0|} = -\frac{2 \ln(\gamma|\tilde{\omega}|)}{\pi^2} \simeq 19, \quad (5.26)$$

⁴Hence, if we rescale them to have the same initial event, then the numerical echoes are larger than analytic. This is due to the fact that in the analytic Lorentzian template, we only use a single QNM of the classical BH, but we use the full LIGO template in the numerical solution.

echoes, for $\gamma\tilde{\omega} = \mathcal{O}(10^2)$ rad/s. Heuristically, we can see that summing over many QNMs is responsible for the early power-law decay. However, since higher QNMs leak faster, the late-time behavior for $k \gtrsim 20$ is dominated by the least-damped QNM, which would decay exponentially.

We can also look at the behavior around the peak of each echo, for $k \ll k_{\text{tran}}$:

$$h_{\text{out}}(t) \propto \sum_k \frac{(-1)^k k e^{-\frac{iat}{Mr_+}}}{(t - k\Delta t_{\text{echo}})^2 + \left(\frac{\Delta t_{\text{echo}}}{\pi}\right)^2 \left(\frac{k}{k_{\text{tran}}}\right)^2}. \quad (5.27)$$

In other words, the amplitude of the first ~ 20 echoes can be well-approximated by a Lorentzian function *in time*, where the ratio of echo width σ_{echo} to echo spacing Δt_{echo} is given by:

$$\frac{\sigma_{\text{echo}}}{\Delta t_{\text{echo}}} = \frac{1}{\pi} \left(\frac{k}{k_{\text{tran}}} \right). \quad (5.28)$$

We see that the echoes are sharper initially, but start to merge for $k \sim k_{\text{tan}}$, which is where we effectively transition to a single damped QNM.

This behavior can be seen in Fig. 6.24, where we plot the 1st, 5th and 15th echo, individually. Again, we see that the amplitude decays as $1/k$ for the k -th echo, while its width grows as k . Here, we slightly shift the numerical solution to match the phases around the peaks, since it is hard to predict phases correctly due to rapid oscillations, and uncertainty on the start point of the echo templates, due to the nonlinear nature of the merger event.

Given the accuracy of the Lorentzian model in capturing echo properties, we can apply it to different spins, starting with their fundamental ($n = 1$) classical QNM for $s = -2, l = 2$ and $m = 2$ from the public source [11], fixing the mass to $67 M_{\odot}$. We see in Fig. 5.6 that quantum BHs with higher spins have longer Δt_{echo} , and slightly higher amplitudes (normalized to their classical QNM amplitude), while they all show a similar power law decay at the early times.

5.3.5 On detectability of Boltzmann echoes

To get a sense of the detectability of our Boltzmann echoes from a quantum BH, we study the signal to noise ratios (SNRs) of the echoes that we obtain from GR template of GW150914, and compare it to that of the binary black hole merger event. Here, $\text{SNR}^2 \equiv \sum_f |\hat{h}_f|^2 / \sigma_f^2$, where \hat{h}_f is strain in the frequency domain, and σ_f is the detection noise of

LIGO. Fig. 5.7 shows the strains in the frequency domain. Comparing the LIGO noise [4] curves with the echoes illustrates that they stand out of the noise around 100 Hz to 300 Hz, and reach the biggest amplitude at $\tilde{\omega} \sim 0$, where Boltzmann reflectivity reaches a maximum.

Using LIGO noise (combining Hanford and Livingston detectors), we calculate the expected ratio $\text{SNR}_{\text{echoes}}/\text{SNR}_{\text{event}}$, which is shown in Fig. 5.8. Here we red(blue)shift the LIGO BH template as in Fig. 5.7 to compare SNRs with different effective masses. The ratio peaks around $85 M_{\odot}$, close to the GW150914 event final mass of $67 M_{\odot}$.

Some words of caution are in order: First, we should remind the reader that all the calculations presented here use linear perturbation theory, while the initial conditions of binary black hole mergers are clearly non-linear. This uncertainty in initial conditions can be seen by the difference in the amplitude at $t \rightarrow 0$ between the Lorentzian and numerical model in Fig. 5.4: The ratio of 1st echo to main event peak is 0.44 for the numerical model, while it is 0.13 for the Lorentzian model. This factor of ~ 3 difference reflects the uncertainty that arises from (lack of) proper nonlinear modeling of the initial conditions. We expect that a more realistic prescription would use a smoother cutoff of the ringdown phase (instead of the Heaviside function, in the Lorentzian profile, e.g., [29]), and thus would lead to an en echo amplitude in-between these two extremes.

Another point is that, any echo model would have additional free parameters, such as γ or echo phases, which need to be fitted for, and effectively reduce the significance of echoes, if one properly accounts for the look-elsewhere effects.

5.4 Ergoregion Instability?

Potential ergoregion instability has been a concern for the models of exotic compact objects (ECOs), since a perfectly reflective wall with the angular barrier potential catching the modes in the superradiance frequency range might lead to instability for all the spinning ECOs [177, 176], in contradiction with observations [198, 49]. However, the quantum BHs that follow the fluctuation-dissipation theorem do not suffer from this instability since the superradiance is highly suppressed because of the Boltzmann reflectivity. This is illustrated in Fig. 5.9: the top panel is the standard superradiance for BHs and the bottom plots reflectivity of quantum BHs (for one reflection), which never exceeds 1 for different spins.

5.5 Conclusion

In the last chapter[211], we advanced independent arguments for why classical horizons must be replaced with stretched horizons with Boltzmann reflectivity for quantum BHs, which are only perfectly absorbent for frequencies much bigger than that of Hawking photon. Using the concrete boundary conditions that result from the fluctuation-dissipation theorem, we analyzed the QNMs of quantum BHs analytically, and confirmed that the resulting predictions are consistent with numerical real-time echoes (in linear perturbation theory), that result from mergers of binary BHs. The echo waveforms are computed, both from geometric optics approximation and a sum over QNMs (which has a closed analytic form).

Considering the uncertainty in modeling the nonlinear initial conditions of Boltzmann echoes and LIGO noise properties, we predict that the SNR for first (all) echo(es) is 13-44% (24-82%) of the SNR for the main binary merger event.

Finally, we argue that with the efficient absorption from the Boltzmann factor, ergoregion instability is suppressed for all spins.

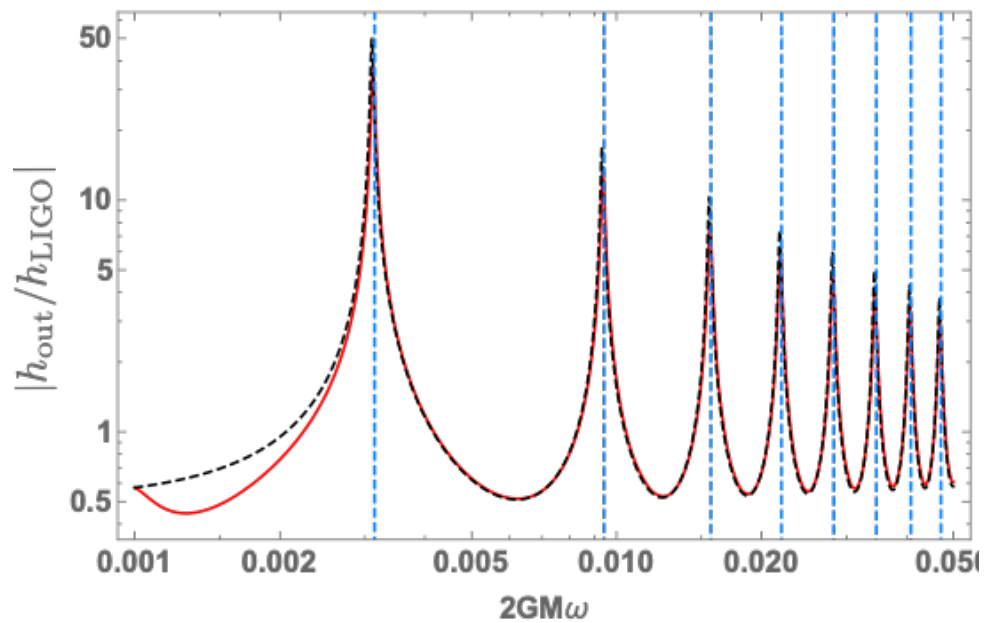


Figure 5.2: The expected ratio of outgoing GW amplitude (including both main event and echoes) to that of the main event $|h_{\text{out}}/h_{\text{LIGO}}|$ for $a = 0.8$ based on the geometric optics approximation (black dashed line) and the numerical integration of the SN equation (red line; see Sec. 5.3.2). Blue dashed lines show the real parts of the QNMs derived analytically in (5.13).

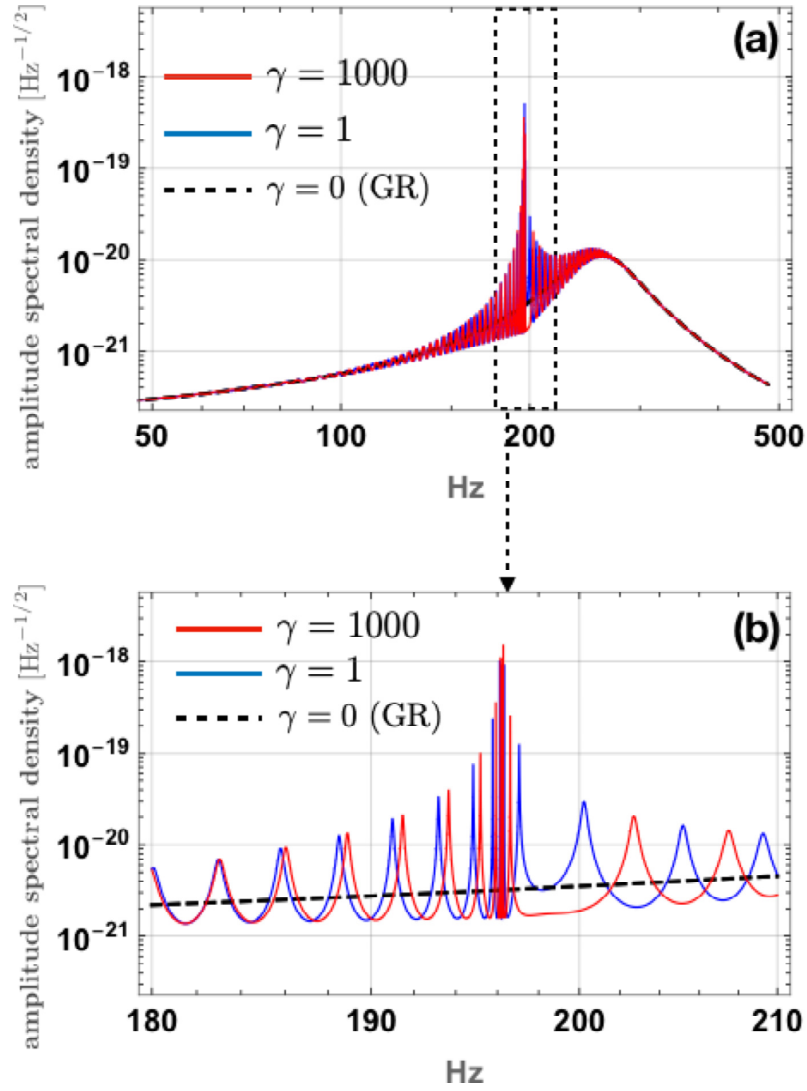


Figure 5.3: Amplitude spectral densities of ringdown+ echo GWs in the case of $a = 0.7$. The peak frequencies depend on the value of γ . We here take $M = 67.6M_{\odot}$ and $\bar{a} = 0.7$.

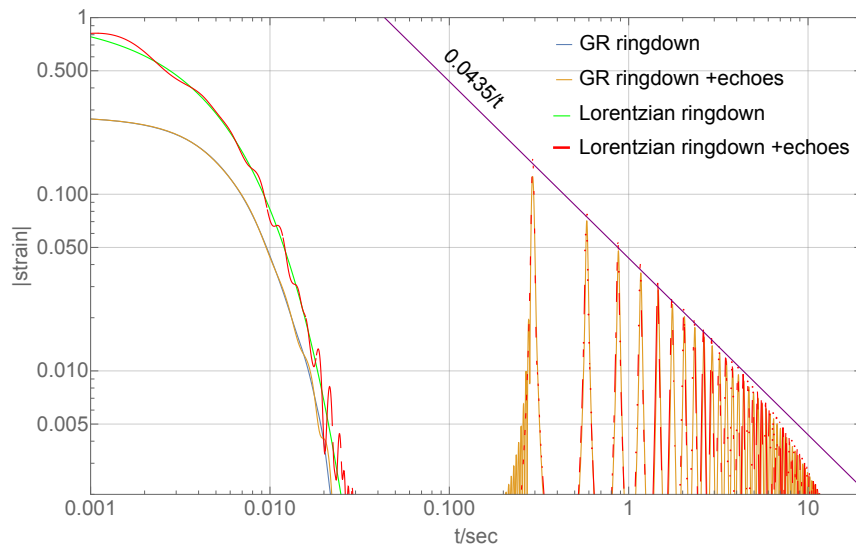


Figure 5.4: The real-time echoes from the geometric optics approximation applied to GR template for GW150914 (same as orange curve in Fig. 5.1), compared to the Lorentzian analytic approximation of QNMs. Note that the amplitude of the GR template is rescaled to make the first echoes match. The echoes initially decay as $1/t$, as many QNMs contribute to echoes. However, after ~ 20 echoes, only the least-damped QNM survives and thus strain starts to decay exponentially.

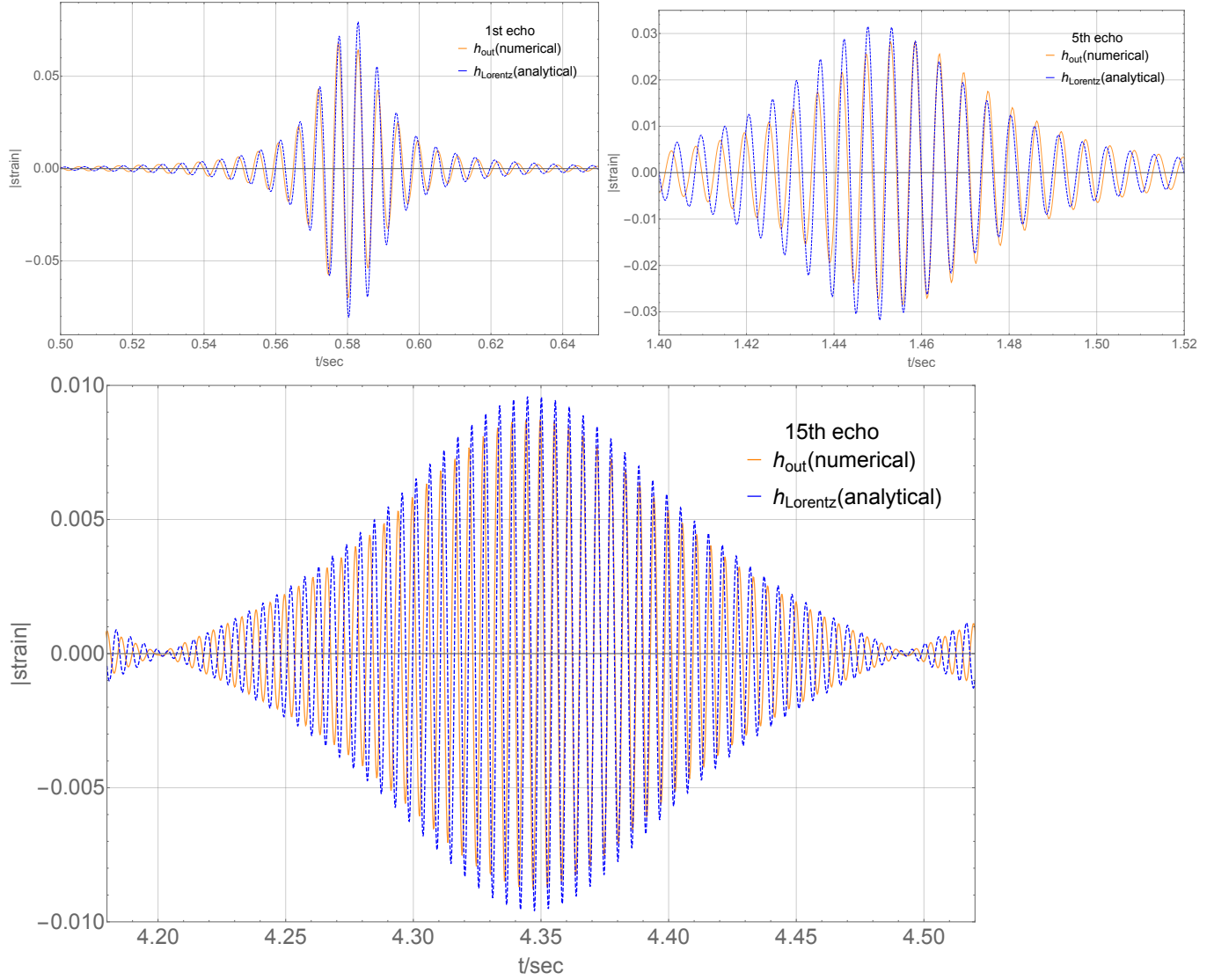


Figure 5.5: The single real time echoes from the numerical geometric optics approximation (applied to LIGO template), as well as the analytic Lorentzian model. The amplitudes match well, while phases are hard to predict due to rapid oscillation over long time. we shift the numerical solution for each echo to match the phases around the peak.

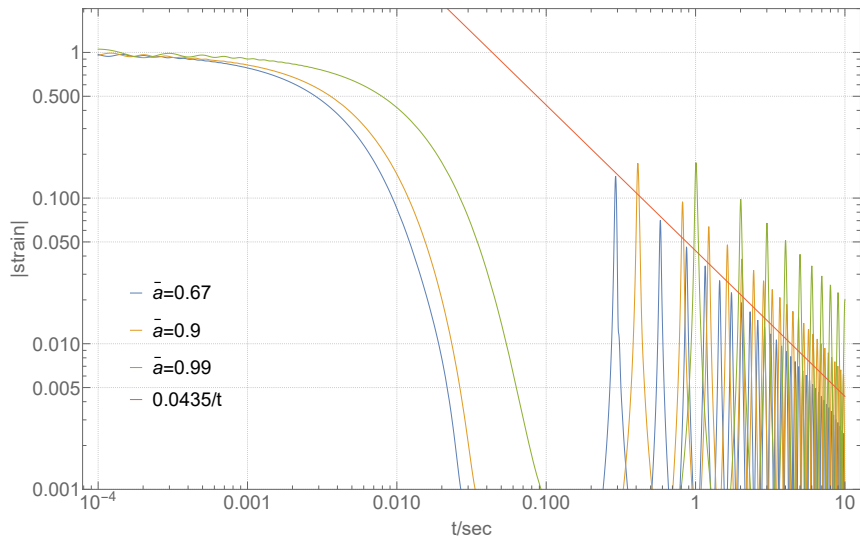


Figure 5.6: The real time echoes from the Lorentzian model for different spins with the same mass as GW150914, and $\gamma \sim 1$. Similar to Fig. 5.4, we see that they all decay as power laws at the early times.

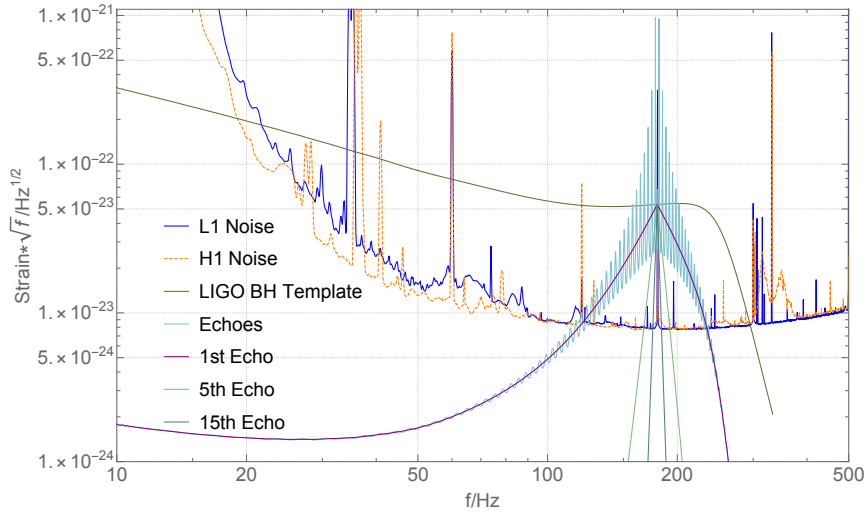


Figure 5.7: The echoes in the frequency domain compared to LIGO Hanford and Livingston noise around GW150914. Amplitude for the main, as well as expectation for the first, fifth, fifteenth, and all the echoes are shown. All the echo signals center at $\tilde{\omega} \simeq 0$ or $\omega \simeq a/(Mr_+)$ as expected. Note that echo amplitudes would be lower by a factor of ~ 3 , if we instead use the Lorentzian model in Fig. 5.4, and (approximately) fix the main event amplitude.

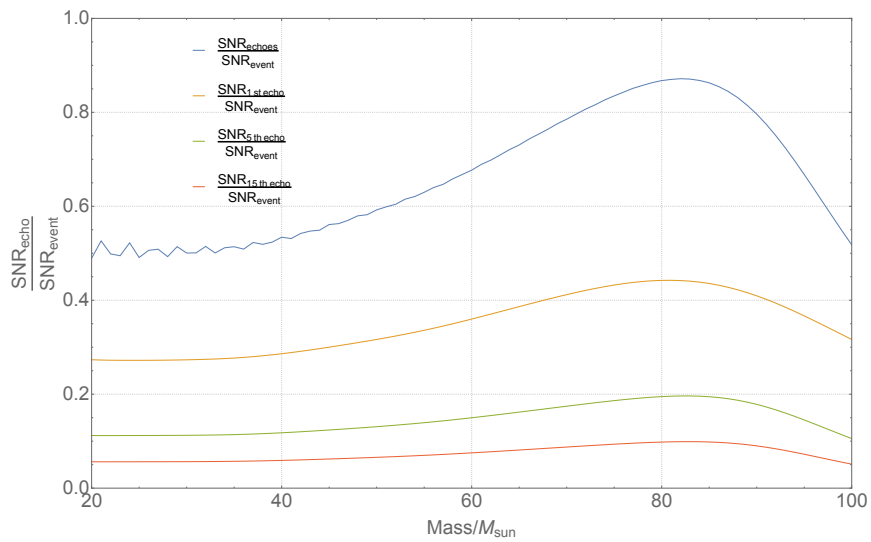


Figure 5.8: SNR of echoes over main event with the shifted mass (using GW150914 but shifting the data to effectively change the mass). Note that this ratio would be lower by a factor of ~ 3 , if we instead used the Lorentzian model in Fig. 5.4.

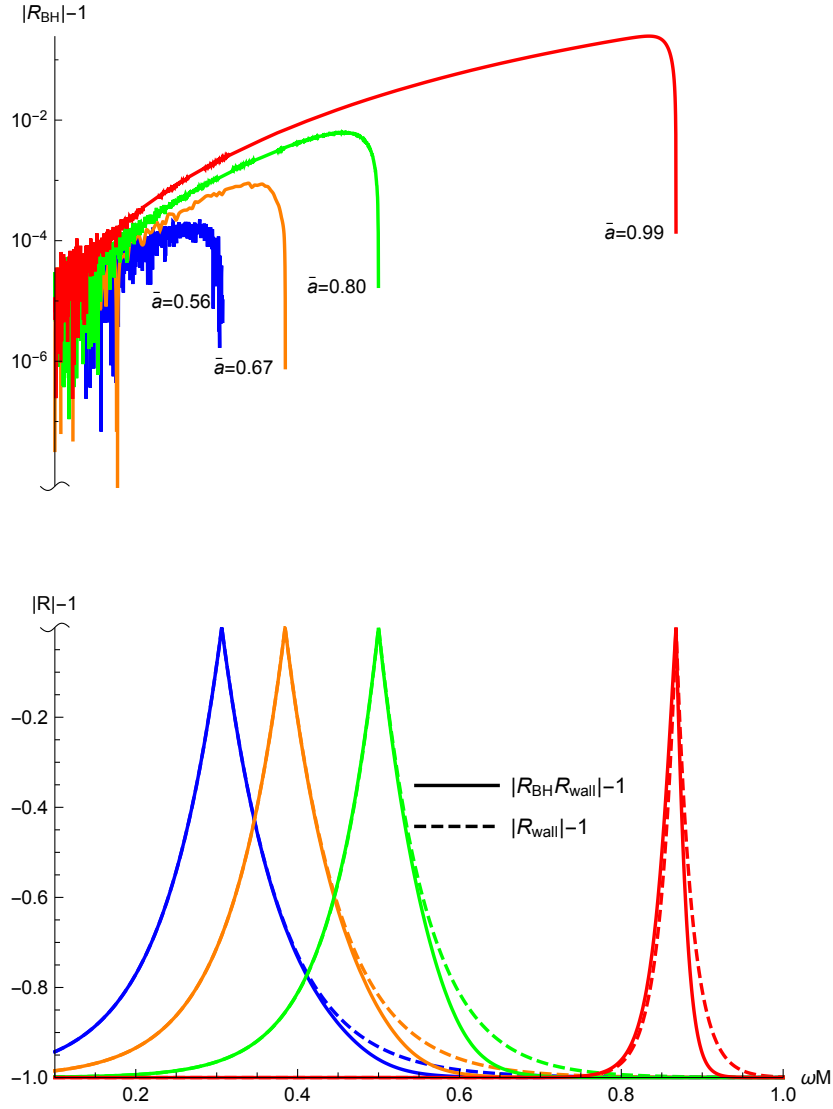


Figure 5.9: Comparison between reflectivity of angular momentum barrier for Kerr BHs (top panel) and Boltzmann reflectivity (bottom panel, dashed curves), and their product (bottom panel, solid curve) for different spins. We see that superradiance is highly suppressed by the Boltzmann factor.

Chapter 6

Hybrid Method

As we discuss in the previous chapters, the echoes are very sensitive to the initial condition. However, the condition is nonlinear in the real world with two black holes merging with each other. The next step, in the chapter, is to encode some nonlinear information into the echo analysis via hybrid method. Hybrid method is first developed in [200, 201]. We will extend it to Quantum BHs both with old hybrid method and a new hybrid green function method in this chapter.

6.1 Dividing the Binary BH collision spacetime into two regions

We decompose the entire, binary BH collision space time into two regions: the weak-perturbation region (region I) and the *strong-perturbation region* (region II). Note that a large part of the weak-perturbation region is still considered “strong gravity”.

It can be argued that from the waveform at future null infinity, we should be able to reconstruct the space-time geometry for region I. There is, of course, the issue that probably the Kerr geometry should have an evolving mass M and spin a . For the moment, let us just ignore these changes, and use M and a of the final black hole. This will be a limitation for this approach.

Let me also emphasize that the validity of such a division is not proven mathematically, but can be verified from numerical simulations.

Suppose we have a spherical shell, in the Boyer-Lindquist coordinate system, defined by the equation $t = T(r)$. We can *embed* region I in a full Kerr spacetime, with region I as *defined by* $t > T(r)$, and region II, as *replaced by* $t < T(r)$ region of the Kerr spacetime. We shall denote the world sheet of the shell by Σ_{SF} .

From now on, we shall only deal with this full Kerr spacetime. We need to keep in mind that the region II here is not the true strong-perturbation region, but what is necessary to make sure perturbations in region I matches the true BBH spacetime.

6.2 Kerr Spacetime

The value of ψ_4 (or Zerilli function X , which we might also choose to use in the Schwarzschild case), in the region II, can be *fully determined by* the waveform at future null infinity, as well as the absence of incoming waves from the past null infinity.

Let us take ψ_4 for example. Suppose ψ_4 at future null infinity is given by $-\omega^2 h(\omega)$. Here implicitly let us consider $l = m = 2$, and ignore the mixing between spherical and spheroidal harmonics.

6.2.1 Solution in Region I and Continuation to Region II

Let us define the *up*-mode homogeneous solution R_ω^∞ of the Teukolsky equation

$$R_\omega^\infty(r) \sim \begin{cases} r^3 D_\omega^\infty e^{i\omega r_*}, & r \rightarrow +\infty \\ D_\omega^{\text{out}} e^{ikr_*} + \Delta^2 D_\omega^{\text{in}} e^{-ikr_*} \end{cases} \quad (6.1)$$

where $k = \omega - m\Omega_+$. These D coefficients are available from standard BH perturbation literature.

In order to match our waveform at infinity with the actually numerically computed one, we simply need to *impose*

$$\psi_4 = -\frac{\omega^2 h(\omega)}{D_\omega^\infty} R_\omega^\infty \quad (6.2)$$

Here the value of ψ_4 exists for both $t > T(r)$ and $t < T(r)$. In region I, this corresponds to the actual BBH space-time, while in region II, this is analogous to an *image space-time*. If we get close to the horizon, we have

$$\psi_4 \sim -\left[\omega^2 \frac{D_\omega^{\text{out}}}{D_\omega^\infty} h(\omega)\right] e^{ikr_*} - \left[\omega^2 \frac{D_\omega^{\text{in}}}{D_\omega^\infty} h(\omega)\right] \Delta^2 e^{-ikr_*} \quad (6.3)$$

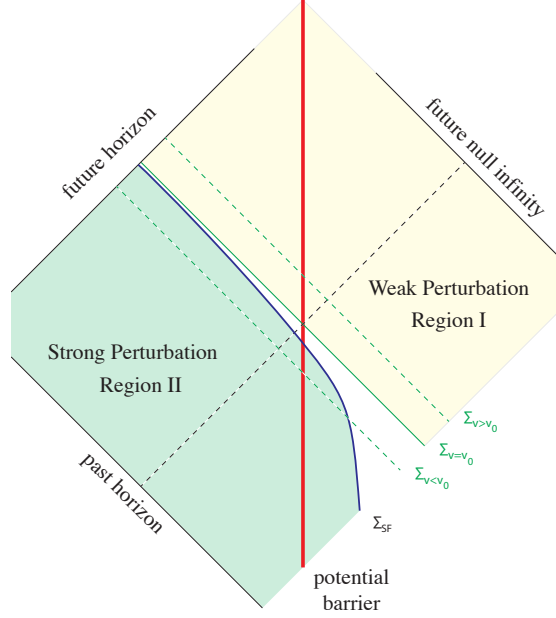


Figure 6.1: Waveform at future null infinity can be used to construct a solution of ψ_4 in region I, and continued to region II.

Here, the first term is one that goes up from the past horizon, while the second one it wave that travel toward the future horizon.

Since the past horizon lies completely within region II, this first term, which represents a wave that merges from the past horizon, exists only to drive the perturbation in region one. The second term exists partially in region I. It is this *portion* of the wave that will represent wave that travels toward the future horizon of the final black hole.

One can convert this into ψ_0 , by multiplying the relevant coefficient \mathcal{S}_ω in the frequency domain:

$$\psi_0^{\text{HH}}(r_*) = -\mathcal{S}_\omega \omega^2 \frac{D_\omega^{\text{in}}}{D_\omega^{\text{out}}} h(\omega) e^{-ikr_*} \quad (6.4)$$

We can convert this into the “time”-domain, where time is advanced time v .

Let us first ignore the need to window this ψ_0 to exclude the region II portion. Suppose at r_*^p , we simply feed this entirely into the out-going ψ_4 which emerges from the past horizon, with reflectivity \mathcal{R}_ω , we will get a first echo of

$$h^{\text{ECO}} = \mathcal{S}_\omega \frac{D_\omega^{\text{in}}}{D_\omega^{\text{out}}} e^{-2ikr_*^p} h(\omega) \quad (6.5)$$

Here the filtering out of region I can either be done with transforming into the time domain and then back, or simply applying a frequency-domain integral. We do note that the transition can be “abrupt”.

6.2.2 Data on Boundary Σ_{SF} between Region I and Region II

Let us propose a second approach, where we construct the wave in region I by applying a source term on the trajectory, imposing

$$\mathcal{L}_T R = F(r)e^{i\omega T(r)} \quad (6.6)$$

Here the RHS corresponds to the T/Δ^2 in the original Teukolsky equation.

In this way, we can write

$$R_\omega(r) = \frac{1}{W_T} \left[R_\omega^\infty(r) \int_{2M}^r R_\omega^H(r') F(r') e^{i\omega T(r')} dr' + R_\omega^H(r) \int_r^{+\infty} R_\omega^\infty(r') F(r') e^{i\omega T(r')} dr' \right] \quad (6.7)$$

Here the first term is waveform at future null infinity, and second term is waveform at future horizon. This can be a new way to generate $\psi_4^{+\infty}$ by posing data on the shell Σ_{SF}

For near the future null infinity, defining

$$u = t - r_* \quad (6.8)$$

we can write

$$\frac{\psi_4^{+\infty}(u)}{r^3} = \int_{2M}^{+\infty} dr' G(u, r') F(r') \quad (6.9)$$

with

$$G(u, r') \equiv \int_{-\infty}^{+\infty} \frac{d\omega}{2\pi} \frac{D_\omega^\infty R_\omega^H(r') e^{i\omega[T(r')-u]}}{W_T(\omega)} \quad (6.10)$$

This can in principle be inverted to obtain, from ψ_4^∞ the data $F(r)$ on the shell. This can then lead to wave that goes toward the future horizon.

6.3 Taking the Schwarzschild Special Case

In the Schwarzschild radial in-fall case, we can investigate the above approach more in a simple case. We can use the Zerilli function Z , which has better analytical properties near infinity and horizon.

Our Σ_{SF} will just be spheres that contain the particle's trajectory. We can first compute wave at future null infinity, obtain Z , both on Σ_{SF} and on the past horizon, and see how they behave. We can then evaluate Z on the Σ_v 's shown in the figure, and see whether there is a qualitative difference when v becomes less than the critical v_0 at which particle plunges into the future horizon.

For the Zerilli function, we have

$$Z_\omega^\infty = \begin{cases} e^{i\omega r_*}, & r_* \rightarrow +\infty \\ B_\omega^{\text{out}} e^{i\omega r_*} + B_\omega^{\text{in}} e^{-i\omega r_*} & r_* \rightarrow -\infty \end{cases} \quad (6.11)$$

and

$$Z_\omega^H = \begin{cases} A_\omega^{\text{out}} e^{i\omega r_*} + A_\omega^{\text{in}} e^{-i\omega r_*}, & r_* \rightarrow +\infty \\ e^{-i\omega r_*} & r_* \rightarrow -\infty \end{cases} \quad (6.12)$$

We also have

$$B_\omega^{\text{out}} = A_\omega^{\text{in}}, \quad B_\omega^{\text{in}} = -\bar{A}_\omega^{\text{out}}, \quad (6.13)$$

and

$$W_{\text{RW}} = 2i\omega A_\omega^{\text{in}} \quad (6.14)$$

From waveform at infinity h_ω^∞ , we directly obtain Zerilli function in the entire region I as $Z_\omega^\infty h_\omega^\infty$, hence, near the horizon

$$h_\omega^H = B_\omega^{\text{in}} h_\omega^\infty = -\bar{A}_\omega^{\text{out}} h_\omega^\infty \quad (6.15)$$

As it turns out, $\bar{A}_\omega^{\text{out}} \sim \omega^{-3}$ at low frequencies, but if we write

$$\bar{A}_\omega^{\text{out}} = (-i\omega)^{-3} \mathcal{M}(\omega) \quad (6.16)$$

then \mathcal{M} has a very simple shape both in time and frequency domain. In this way, we can write

$$h_\omega^H = (-i\omega)^{-3} \mathcal{M}(\omega) h_\omega^\infty \quad (6.17)$$

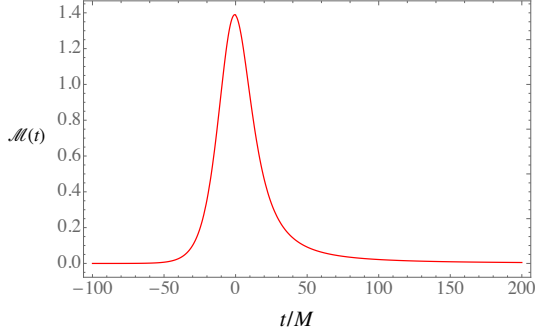


Figure 6.2: Plot of $\mathcal{M}(t)$ for a Schwarzschild black hole.

Here we need to be careful with the “time” variables associated with h^H and h^∞ ; because we have $e^{i\omega r^*}$ multiplying h^∞ and $e^{-i\omega r^*}$ multiplying h^H , the “time” is v for h^H and u for h^∞ .

Even though the ω^3 on the denominator seems to emphasize low-frequency components, we can still use this formula to obtain the region I portion of h^∞ , by resorting to the fact that all perturbation should die down at the end. We can first define

$$h^M(t) \equiv \int_{-\infty}^{+\infty} \mathcal{M}(t-t') h^\infty(t') dt', \quad (6.18)$$

and then start out at $t \rightarrow \infty$ and work our way backwards, we will be able to write

$$h^H(v) = \int_v^{+\infty} dt_1 \int_{t_1}^{+\infty} dt_2 \int_{t_2}^{+\infty} dt_3 h^M(t_3) \quad (6.19)$$

In the frequency domain, we shall denote the portion of wave we want as $[h_\omega^H]_{v>v_0}$.

We can see from there that the \mathcal{M} function, does not have much features at all, especially at the location of quasi-normal modes. This is because it comes from A_ω^{out} . We recall the relation that

$$|A_\omega^{\text{out}}|^2 - |A_\omega^{\text{in}}|^2 = 1 \quad (6.20)$$

and also the fact that

$$A_\omega^{\text{in}} = 0, \quad \omega = \omega_{lmn}^{\text{QNM}}. \quad (6.21)$$

In the Schwarzschild case, the function \mathcal{M} seems rather well-behaved as a kernel; therefore I speculate that in the Kerr case it will look rather similar. For the up-going wave, we

will have the issue that it will start rather abruptly, at $v = v_0$. However, this will be taken care of by \mathcal{R} , which will smooth out the start in the reflected wave.

Given $[h_\omega^H]_{v>v_0}$, we will get a reflected wave of

$$\frac{1}{A_\omega^{\text{in}}} \mathcal{R}_\omega [h_\omega^H]_{v>v_0} \quad (6.22)$$

this will be followed by more waves, of the form

$$h_\omega^{(n)} = \left(-\frac{\bar{A}_\omega^{\text{out}}}{A_\omega^{\text{in}}} \mathcal{R}_\omega \right)^n \frac{1}{A_\omega^{\text{in}}} \mathcal{R}_\omega [h_\omega^H]_{v>v_0}, \quad n = 0, 1, 2, \dots \quad (6.23)$$

Here, we might be somewhat worried about the triple integral in defining h^H ; in fact, if we apply Eq. (6.19) to any numerical waveform, it will lead to huge errors. However, this can be solved by carefully looking at Eq. (6.24). We note that both A^{in} and A^{out} scale as $\sim \omega^3$ at low frequencies. This way, we can take a triple derivative of h^H , and write

$$h_\omega^{(n)} = \left(-\frac{\bar{A}_\omega^{\text{out}}}{A_\omega^{\text{in}}} \mathcal{R}_\omega \right)^n \frac{1}{(-i\omega)^3 A_\omega^{\text{in}}} \mathcal{R}_\omega [h_\omega^M]_{v>v_0}, \quad n = 0, 1, 2, \dots \quad (6.24)$$

It is easy to verify that both h_ω^M and $1/[(-i\omega)^3 A_\omega^{\text{in}}]$ are well-behaved in the time domain.

6.4 Outlook

Following the methodologies discussed above, we are able to generate the echoes in Schwarzschild case. And we have verified in classical BH case, this hybrid green function method gives exactly same waveform in region I as the original hybrid method in [200, 201]. But our new hybrid green function method can be applied to Kerr metric, which will be our next step, while the old one is hard since it is not easy to separate the two regions in Kerr case.

In addition, we extend old hybrid method into quantum BHs case with an extra damping term. It can automatically generate echoes with whole spacetime numerical solution. We are comparing the result with the one generated in the new hybrid green function method to study if it can verify the geometrical optic approximation we have before.

Chapter 7

Future Prospects and Conclusion

7.1 Towards Synergistic Statistical Methodologies

As we summarized in the previous chapters, the past four years have witnessed hundreds of theoretical studies focusing on model-building for echoes, as well as dozens of observational searches and statistical methodologies. However, in spite of remarkable progress on both fronts, the theoretical and observational tracks have largely developed independently, due to the lack of good echoes template and noise of detections. However, it appears that both tracks have become mature enough, so much so that the time is ripe for a synergistic convergence. For example, Bayesian methods developed in [203, 171] applied to a superposition of QNMs of quantum BHs (as outlined in [281]) would put coherent methods developed by [99, 31] on more sound statistical *and* physical footings. The analogy will be with helio- or astro-seismology, where modeling a dense spectrum of QNM frequencies can be used to infer the int-renal structure of the compact objects [210].

The real challenge will be in allowing enough freedom in our best physical models, in order to capture all the remaining theoretical uncertainties, *but not any more!*

7.2 Echoes in Numerical Relativity

Most studies of echoes have so far focused on the linear perturbation theory around the final BH for simplicity, but in reality the mergers start with the highly nonlinear binary BH inspiral. Hence, we need a covariant numerical implementation of binary quantum

BHs within a highly-nonlinear dynamical spacetime to fully address the entire dynamics, especially the initial conditions. There are several possible approaches borrowed from numerical relativity which can be modified to either include the quantum boundary condition or the full dynamics of binary quantum BHs.

For instance, the effective one body (EOB) formalism [77, 104] is a concrete strategy which only needs to solve ordinary differential equations rather than to perform the costly 3d numerical relativity simulations. It uses higher-order post-Newtonian expansion in a resummed form (different from the usual the Taylor-expansion), to include the non-perturbative result using a conservative description of binary BHs dynamics, radiation-reaction and emitted GW waveform. One possible approach, that is currently underway, is to capture the nonlinear effects in echoes by modifying the boundary condition in the EOB codes to implement the quantum BH dynamics.

Another route is to directly modify numerical relativity codes that have successfully produced waveforms for BBH merger events. A concrete strategy could be incorporating the mock fuzzball energy-momentum tensor [24] as a source for Einstein equations, directly into the numerical relativity codes. If the fuzzball “fluid” manages to stay just outside the apparent BH horizons in a dynamical setting, then it can potentially generate echoes in a fully nonlinear numerical simulation of quantum BBH merger.

Recently, [207, 206] presented the first numerical simulation of BBH mergers in Chern-Simon gravity. They start with the modified action and predict the dynamics order by order. It is possible that a similar iterative approach can be applied to model boundary conditions at apparent horizons, or evolution of mock fuzzballs by adding modified matter term into second order after the classical simulation.

7.3 Quantum Gravity, Holography, and Echoes

As we discussed above, any modification of event horizons that could lead to echoes should be a non-perturbative modification of general relativity, and can only be fully captured by a non-perturbative description of quantum gravity. A possible example of this is the fuzzball program in string theory (See detail in Chapter 2). But more generally, what can non-perturbative approaches to quantum gravity tell us about BH echoes?

One of our greatest insights into the dynamics of quantum gravity has come from the Holographic Principle, that extending Bekenstein-Hawking area law for entropy of BHs [58], suggests the entire dynamics of a quantum gravitational system should be captured

on its boundary. The most concrete realization of this principle was proposed by Juan Maldacena [181], in the form a conjectured duality between quantum gravity in Anti-de Sitter (AdS) spacetime and a Conformal field theory (CFT), commonly known as AdS/CFT correspondence or conjecture. It proposes that CFT in spacetime of $d-1$ dimension, at the asymptotic boundary of an AdS spacetime is mathematically equivalent to string theory (or quantum gravity) within the bulk AdS in d dimension. This topic has been extremely fruitful over the past two decades, offering many synergies between seemingly disparate notions in geometry and quantum information. For example, the Ryu-Takayanagi conjecture [242] relates the entanglement entropy of boundary CFTs with the areas of extremal surfaces in the bulk AdS, generalizing the notion of Bekenstein-Hawking BH entropy to arbitrary geometries.

An intriguing connection between AdS/CFT and echoes is the appearance of echo times:

$$\Delta t_{\text{echo}} = t_{\text{scrambling}} = \frac{\ln(S_{\text{BH}})}{2\pi T_{\text{H}}}, \quad (7.1)$$

as “scrambling time”, in the AdS/CFT literature [253]. Here, S_{BH} and T_{H} are the entropy and temperature of the BH respectively. The scrambling time refers to the time it takes to destroy quantum entanglements in a chaotic system, while BHs (and their CFT duals) are conjectured to be fast scramblers, i.e. the most efficient in destroying entanglement (e.g., [179]). Interestingly, Saraswat and Afshordi [245] have recently shown that the scrambling time (computed using Ryu-Takayanagi conjecture in a dynamical setting) is identical to the Planckian echo times, for generic charged AdS BHs. Could this imply that echoes could be a generic property of (possibly a certain class of) quantum chaotic systems?

Another possible connection could come in the form of the fluid-gravity correspondence, e.g., in the context of membrane paradigm discussed in Sec. 1.2. For example, in [211], we have argued that Boltzmann reflectivity of GW echoes, implies that viscosity of the boundary fluid should vanish at small frequencies $\hbar\omega \ll kT$. One may also speculate that other holographic manifestations of BH echoes may appear in the Kerr/CFT conjecture [93], Braneworld BHs [110], or as Regge poles of the boundary plasma in AdS/CFT.

7.4 Einstein Telescope, Cosmic Explorer

The Einstein Telescope (ET) [236] and Cosmic Explorer (CE) [113] are the third-generation ground based GW detectors. The ET consists of three underground detectors with three arms 10 kilometers long and CE will be realized with two arms 40 kilometers long, which

are 10 times longer than Advanced LIGO's. These next-generation GW detectors might allow us to observe some Planckian signatures from quantum BHs such as GW echoes from merger events leading to a remnant BH. We plot the spectra of GW echoes and ringdown with the sensitivity curves of Advanced LIGO, ET, and CE in FIG. 7.1. The detection of GW echoes with the third generation GW observatories are discussed in [185, 261, 178], and it may be possible to distinguish ECOs with $|\mathcal{R}| \lesssim 0.3$ from BHs with at 2σ level when $\text{SNR} \sim 100$ in ringdown, which would be possible for the third-generation GW detectors. The relative error on the reflectivity of would-be horizon is also investigated in [185, 261, 178], and the relative error for measurement of reflectivity in ground-based detectors is approximately given by

$$\left| \frac{\Delta \mathcal{R}}{1 - \mathcal{R}} \right| \simeq 0.5 \times \left(\frac{8}{\rho_{\text{ringdown}}} \right), \quad (7.2)$$

where $M = 30M_{\odot}$, ρ_{ringdown} is the SNR in the ringdown phase, while the distance between the top of the angular momentum barrier and the would-be horizon is assumed to be longer than $50M$ in the tortoise coordinate. For comparison, we note that the loudest detected BBH event, GW150914, has $\rho_{\text{ringdown}} \simeq 8$.

The detectability of GW echoes from failed supernovae, leading to the formation of BHs, with the third-generation GW observatories is also discussed in [210]. Calculating the SNR of GW spectrum consisting of echo and ringdown, $\rho_{\text{ringdown+echo}}$, in the Boltzmann reflectivity model, the horizon distance D_{h} , defined as the distance where $\rho_{\text{ringdown+echo}} = 8$, is estimated.

For this analysis, [210] generalize Boltzmann reflectivity to:

$$\mathcal{R} = \exp \left[\frac{-\hbar\omega}{kT_{\text{QH}}} \right], \quad (7.3)$$

in terms of a *quantum horizon temperature* T_{QH} , which in general can be different from T_{H} .

Given the optimistic case in the Boltzmann reflectivity model, $T_{\text{H}}/T_{\text{QH}} = e^{15(\bar{a}-1)}$ (with marginal ergoregion stability), the horizon distance can be estimated as $D_{\text{h}} \sim 10$ Mpc for the Advanced LIGO at design sensitivity and $D_{\text{h}} \sim 100$ Mpc for the third-generation detectors such as ET and CE. Therefore, the authors in [210] argue that the searching for GW echoes, sourced by failed supernovae within our Galaxy and nearby galaxies, may be possible. However, in the case of $T_{\text{QH}} = T_{\text{H}}$, the horizon distance is less than or comparable with 10 Mpc and so the echo search with failed supernovae would be restricted to within the Local Group. For the comparison, the strain amplitude of GW echoes in $T_{\text{QH}}/T_{\text{H}} = 1$ and $T_{\text{QH}}/T_{\text{H}} = e^{15(\bar{a}-1)}$ are shown¹ in FIG. 7.2.

¹We here assume that the energy fraction of ringdown phase is $\epsilon_{\text{rd}} = 6 \times 10^{-7}$ although it highly depends

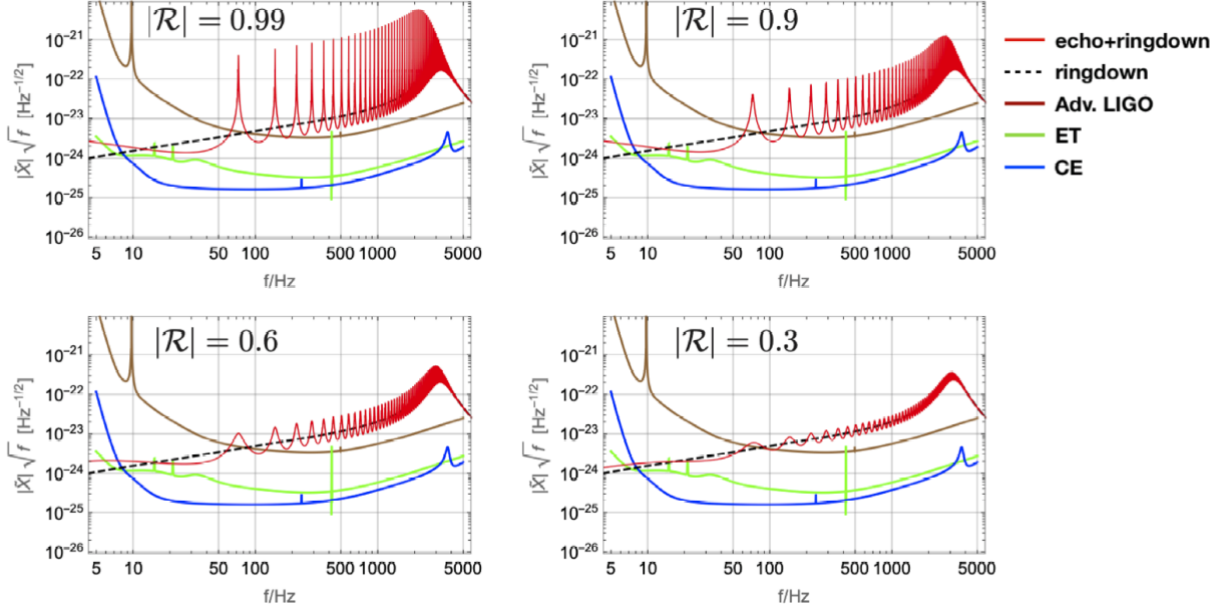


Figure 7.1: Spectra of ringdown and echo phases with the reflectivity of $|\mathcal{R}| = 0.99, 0.9, 0.6,$ and 0.3 . We set $D_o = 40$ Mpc, $\bar{a} = 0.1$, $\ell = m = 2$, $M = 4M_\odot$, $\theta = 20^\circ$, and $\epsilon_{\text{rd}} = 0.1\%$.

7.5 LISA

The Laser Interferometer Space Antenna (LISA) is planned to be the first GW observatory in space. It will have three satellites separated by millions of kilometers and their orbits maintain near-equilateral triangular formation. LISA might enable us to reach high-precision detection of ringdown in $\text{SNR} \sim \mathcal{O}(10^3)$, which puts stronger constraints on the reflectivity of BHs [261, 178].

Recently, a novel proposal to discriminate BH horizons based on the tidal heating was proposed in [107, 108]. One of the main targets of the LISA mission is precision measurements of extreme-mass-ratio inspirals (EMRIs), in which the tidal heating could be important. The (partial) absorption of ECOs or BHs plays the role of dissipation at the surface, by which tides back-react on the orbital trajectory. It is argued that this tidal heating is responsible for a large dephasing between the orbits of a BH and ECO. This dephasing accumulates over the timescale of months and the accumulation speed is faster

on the detail of nonlinear gravitational collapse.

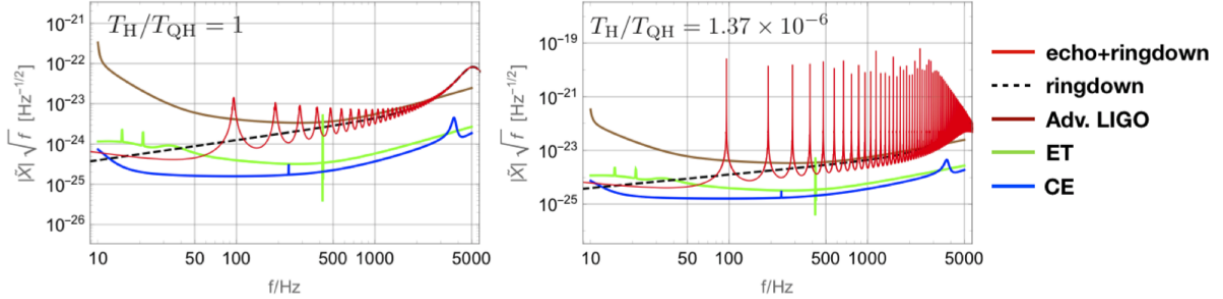


Figure 7.2: Spectra of ringdown and echo phases in the Boltzmann reflectivity model with $\bar{a} = 0.1$, $\epsilon_{\text{rd}} = 6 \times 10^{-7}$, $M = 2.4M_{\odot}$, $\theta = 90^{\circ}$, and $D_o = 1$ Mpc. Here we also assume $\gamma = 10^{-10}$, $T_{\text{H}}/T_{\text{QH}} = 1$ (left) and $T_{\text{H}}/T_{\text{QH}} = 1.37 \times 10^{-6}$ (right).

for a higher spin. The authors in [108] also found a proportionality relation between the dephasing $\delta\phi$ and energy reflectivity $|\mathcal{R}|^2$.

In order to make use of this scheme to put strong constraints on the reflectivity of ECOs, one has to obtain accurate EMRI waveforms by properly taking into account the tidal heating for orbiting objects, which may decrease systematic errors in data analysis.

Not only the tidal heating, but also the tidal deformability contributes to the GW Fourier phase and it can be characterized by the tidal Love number k . The Love number of ECO of mass M may scale as $1/|\log \delta|$, where $\delta \equiv r_0 - r_{\text{h}}$, with r_{h} is the BH horizon radius of mass M and r_0 is the radius of the ECO. So the $k - \delta$ relation is

$$\delta = r_{\text{h}} e^{-1/k}, \quad (7.4)$$

and assuming this relation, one can infer the near-horizon structure characterized by δ from the measurement of the Love number k . For instance, if the Love number of the order of $k \sim 10^{-2}$ is measured by LISA from a supermassive BH binary signal, leading to the formation of a BH of $M \sim 10^6 M_{\odot}$, it yields the resolution of $\delta \sim l_{\text{Pl}}$.

However, the authors in [32] point out that the statistical and quantum mechanical uncertainties in measurements of near-horizon lead to some difficulty to measure δ precisely. The former one comes from the fact that the statistical uncertainty in δ is proportional to $1/k$, and the inferred value of k , where the inferred value of δ is comparable with its statistical uncertainty, is around $k \sim 0.2$. Therefore, any inferred value of δ , derived from k that is smaller than ~ 0.2 , would be dominated by the statistical uncertainty. The latter one comes from the uncertainty principle in quantum mechanics. Once precisely measuring $\delta \sim l_{\text{Pl}}$, it may lead to the uncertainty in the mass of the ECO, which then leads to the

uncertainty in the binding energy. This results in the uncertainty in the orbital and GW frequencies, which means that one cannot measure δ precisely if it is much shorter than l_{Pl} .

7.6 Pulsar Timing Arrays

Following their first discovery in 1968 [146], over 2000 pulsars have now been detected by radio telescopes across the world. The pulsars' intrinsic properties, as well as propagation effects in the interstellar medium, can influence the arrival times of pulsar pulses. Therefore, pulsar timing arrays (PTA) can be used as a detection tool for BH binaries [147], and thus, might be used to detect signatures of echoes from quantum BHs. In particular, millisecond pulsars stand out for their unparalleled stability (comparable to atomic clocks!) without being subject to starquakes and accretion. To give an explicit example, we show the spectrum of GW echoes predicted by the Boltzmann reflectivity model [211, 281] with the sensitivity curve of International Pulsar Timing Array (IPTA) and Square Kilometre Array (SKA) (FIG. 7.3). The lower curve in Fig. [146] is for a $3 \times 10^9 M_{\odot}$ BH merger at $D_o = 1$ Gpc. Given that this mass is comparable to that of M87 supermassive BH, located at 16 Mpc, we expect $\sim 2 \times 10^5$ of such BHs at < 1 Gpc. Assuming that each BH merges once every Hubble time $\sim 10^{10}$ years, and that echoes last for 20 years (from simple mass scaling), the chances of detecting such a loud event with PTAs at any time is 0.1%. However, fainter events will be more prevalent as their number increases as $\text{SNR}^{-3/2}$ from volume scaling. Furthermore, increase in supermassive BH merger activity observed at high redshifts shall boost this statistics.

PTAs are anticipated to detect the low frequency GW signal from supermassive BBH within the next few years [147]. We expect that the first GW detection will be a stochastic background of supermassive BH binaries. With any luck, this shall lead to new insights into the nature of quantum BHs and gravity.

7.7 Final Word

In this thesis, we provided a comprehensive overview of the theoretical motivations for why quantum black holes in our universe may have different observable properties, in contrast to their classical counterparts in Einstein's theory of general relativity. The most prominent and potentially observable smoking gun for these quantum black holes comes in the form of gravitational wave echoes, which have been the subject of intense theoretical

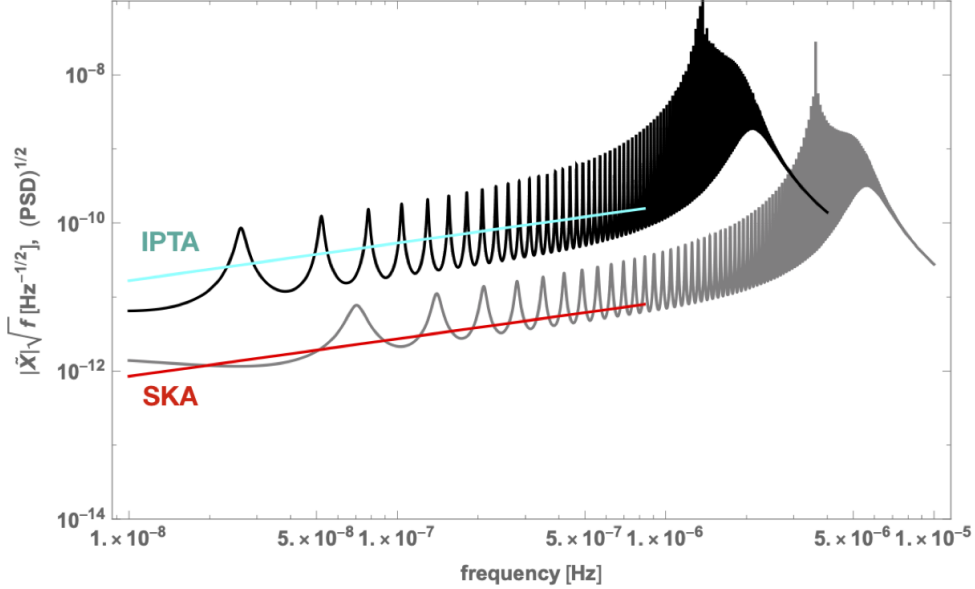


Figure 7.3: Spectra of GW echoes in the Boltzmann reflectivity model with $\bar{a} = 0.6$, $\ell = m = 2$, $D_o = 1$ Gpc, and $\gamma = 1$. The gray line shows the case of $M = 3 \times 10^9 M_\odot$, $\epsilon_{\text{rd}} = 0.005$, $T_{\text{H}}/T_{\text{QH}} = 0.1$ and the black line shows one for $M = 8 \times 10^9 M_\odot$, $\epsilon_{\text{rd}} = 0.01$, $T_{\text{H}}/T_{\text{QH}} = 0.05$. We also plot the PSD for the IPTA (blue) and SKA (red).

and observational scrutiny over the past few years. We provided a concise account of theoretical predictions. We closed the thesis by our vision of the future of “Quantum Black Holes in the Sky”, via a synergy of statistical methodology, quantum gravity, and numerical relativity, and in light of the next generation of gravitational wave observatories.

While this thesis focuses on the gravitational wave echoes, as arguably the most concrete and promising signature of quantum black holes, other possible observable signatures can be (and should be) explored. For example, interactions of photons or neutrinos with near-horizon quantum structure could lead to signatures in radio images in Event Horizon Telescope observations [241], or ultra high energy neutrinos in Ice Cube observatory [36], respectively. However, these signals will be suppressed if Boltzmann reflectivity is assumed, as they have $\hbar\omega \gg kT_{\text{H}}$. Another alternative to echoes may come through non-localities in non-violent unitarization, which would be observable far from the horizon (see Sec. 2.8). However, it is arguably difficult to pin down concrete predictions in this scenario.

To conclude, the world of Quantum Black Holes remains a wide open and largely uncharted territory, spanning from the dark corners of obscure mathematical structures

to the nitty-gritty details of gravitational wave detector noise. It also holds the promise to crack the century-old puzzle of quantum gravity, and yet be imminently testable in the next few years. Therefore, the study of “Quantum Black Holes in the Sky” remains extremely exciting, active, and confusing, and is bound to provide us with new surprises in the new decade, and beyond.

References

- [1] coherent waveburst. <https://gwburst.gitlab.io>.
- [2] Einstein toolkit. <https://einsteintoolkit.org>.
- [3] <https://www.gw-openscience.org>. <https://www.gw-openscience.org>.
- [4] LIGO Noise. <https://www.gw-openscience.org/events/GW150914/>.
- [5] Line of Best Fit (Least Square Method). https://www.varsitytutors.com/hotmath/hotmath_help/topics/line-of-best-fit.
- [6] Parameter estimation sample release for GWTC-1. <https://dcc.ligo.org/LIGO-P1800370/public>.
- [7] QNM spectrum of different black holes. <https://pages.jh.edu/~eberti2/ringdown/>.
- [8] Reconstructed Detector Responses for GW150914. https://www.atlas.aei.uni-hannover.de/work/salemi/reports/GWOSC_LH_GW150914_R1_org/ced/ced_1126258800_1200_GWOSC_LH_GW150914_R1_org_slag0_lag0_1_job1/L1H1_1126259462.125_1126259462.125/.
- [9] Reconstructed Detector Responses for GW151012. https://www.atlas.aei.uni-hannover.de/work/salemi/reports/GWOSC_LH_GW151012_R1_org/ced/ced_1128678000_1200_GWOSC_LH_GW151012_R1_org_slag0_lag0_1_job1/L1H1_1128678900.375_1128678900.375/.
- [10] Reconstructed Detector Responses for GW151226. https://www.atlas.aei.uni-hannover.de/work/salemi/reports/GWOSC_LH_GW151226_R1_org/ced/ced_1135136238_1200_GWOSC_LH_GW151226_R1_org_slag0_lag0_1_job1/L1H1_1135136350.312_1135136350.312/.

- [11] Superradiance. <https://centra.tecnico.ulisboa.pt/network/grit/files/ringdown/>.
- [12] B. P. Abbott et al. Binary Black Hole Mergers in the first Advanced LIGO Observing Run. *Phys. Rev.*, X6(4):041015, 2016.
- [13] B. P. Abbott et al. GW150914: The Advanced LIGO Detectors in the Era of First Discoveries. *Phys. Rev. Lett.*, 116(13):131103, 2016.
- [14] B. P. Abbott et al. GW151226: Observation of Gravitational Waves from a 22-Solar-Mass Binary Black Hole Coalescence. *Phys. Rev. Lett.*, 116(24):241103, 2016.
- [15] B. P. Abbott et al. Observation of Gravitational Waves from a Binary Black Hole Merger. *Phys. Rev. Lett.*, 116(6):061102, 2016.
- [16] B. P. Abbott et al. Tests of general relativity with GW150914. *Phys. Rev. Lett.*, 116(22):221101, 2016.
- [17] B. P. Abbott et al. GW170608: Observation of a 19-solar-mass Binary Black Hole Coalescence. *Astrophys. J.*, 851(2):L35, 2017.
- [18] B. P. Abbott et al. GW170814: A Three-Detector Observation of Gravitational Waves from a Binary Black Hole Coalescence. *Phys. Rev. Lett.*, 119(14):141101, 2017.
- [19] B. P. Abbott et al. GW170817: Observation of Gravitational Waves from a Binary Neutron Star Inspiral. *Phys. Rev. Lett.*, 119(16):161101, 2017.
- [20] B. P. Abbott et al. Search for Post-merger Gravitational Waves from the Remnant of the Binary Neutron Star Merger GW170817. *Astrophys. J.*, 851(1):L16, 2017.
- [21] Benjamin P. Abbott et al. GW170104: Observation of a 50-Solar-Mass Binary Black Hole Coalescence at Redshift 0.2. *Phys. Rev. Lett.*, 118(22):221101, 2017.
- [22] Jahed Abedi and Niayesh Afshordi. Echoes from the Abyss: A highly spinning black hole remnant for the binary neutron star merger GW170817. 2018.
- [23] Jahed Abedi and Niayesh Afshordi. Echoes from the Abyss: A Status Update. 2020.
- [24] Jahed Abedi, Niayesh Afshordi, Naritaka Oshita, and Qingwen Wang. Quantum Black Holes in the Sky. *Universe*, 6(3):43, 2020.

- [25] Jahed Abedi and Hessamaddin Arfaei. Fermionic greybody factors in dilaton black holes. *Class. Quant. Grav.*, 31(19):195005, 2014.
- [26] Jahed Abedi and Hessamaddin Arfaei. Obstruction of black hole singularity by quantum field theory effects. *JHEP*, 03:135, 2016.
- [27] Jahed Abedi, Hessamaddin Arfaei, Alek Bedroya, Aida Mehin-Rasuliani, Milad Noorikuhani, and Kamran Salehi-Vaziri. Anomaly induced quantum correction to charged black holes; geometry and thermodynamics. 2017.
- [28] Jahed Abedi, Hannah Dykaar, and Niayesh Afshordi. Echoes from the Abyss: Tentative evidence for Planck-scale structure at black hole horizons. *Phys. Rev. D*, 96(8):082004, 2017.
- [29] Jahed Abedi, Hannah Dykaar, and Niayesh Afshordi. Echoes from the Abyss: Tentative evidence for Planck-scale structure at black hole horizons. *Phys. Rev.*, D96(8):082004, 2017.
- [30] Jahed Abedi, Hannah Dykaar, and Niayesh Afshordi. Echoes from the Abyss: The Holiday Edition! 2017.
- [31] Jahed Abedi, Hannah Dykaar, and Niayesh Afshordi. Comment on: "Low significance of evidence for black hole echoes in gravitational wave data". 2018.
- [32] Andrea Addazi, Antonino Marciano, and Nicolas Yunes. Can we probe Planckian corrections at the horizon scale with gravitational waves? *Phys. Rev. Lett.*, 122(8):081301, 2019.
- [33] Ronald J. Adler, Pisin Chen, and David I. Santiago. The Generalized uncertainty principle and black hole remnants. *Gen. Rel. Grav.*, 33:2101–2108, 2001.
- [34] Niayesh Afshordi. Gravitational Aether and the thermodynamic solution to the cosmological constant problem. 2008.
- [35] Niayesh Afshordi and Joao Magueijo. The critical geometry of a thermal big bang. *Phys. Rev.*, D94(10):101301, 2016.
- [36] Niayesh Afshordi and Yasaman K. Yazdi. 'Firewall' phenomenology with astrophysical neutrinos. *Class. Quant. Grav.*, 33(23):235017, 2016.
- [37] Abhineet Agarwal and Niayesh Afshordi. Thermal Tachyacoustic Cosmology. *Phys. Rev.*, D90(4):043528, 2014.

- [38] Y. Aharonov, A. Casher, and S. Nussinov. The Unitarity Puzzle and Planck Mass Stable Particles. *Phys. Lett.*, B191:51, 1987.
- [39] Ahmed Almheiri, Donald Marolf, Joseph Polchinski, Douglas Stanford, and James Sully. An Apologia for Firewalls. *JHEP*, 09:018, 2013.
- [40] Ahmed Almheiri, Donald Marolf, Joseph Polchinski, and James Sully. Black Holes: Complementarity or Firewalls? *JHEP*, 02:062, 2013.
- [41] J. Ambjorn, J. Jurkiewicz, and R. Loll. Emergence of a 4-D world from causal quantum gravity. *Phys. Rev. Lett.*, 93:131301, 2004.
- [42] Damiano Anselmi. On the quantum field theory of the gravitational interactions. *JHEP*, 06:086, 2017.
- [43] Michael Appels, Ruth Gregory, and David Kubiznak. Black Hole Thermodynamics with Conical Defects. *JHEP*, 05:116, 2017.
- [44] Abhay Ashtekar and Jerzy Lewandowski. Background independent quantum gravity: A Status report. *Class. Quant. Grav.*, 21:R53, 2004.
- [45] Gregory Ashton, Ofek Birnholtz, Miriam Cabero, Collin Capano, Thomas Dent, Badri Krishnan, Grant David Meadors, Alex B. Nielsen, Alex Nitz, and Julian Westerweck. Comments on: "Echoes from the abyss: Evidence for Planck-scale structure at black hole horizons". 2016.
- [46] Siavash Aslanbeigi, Georg Robbers, Brendan Z. Foster, Kazunori Kohri, and Niyesh Afshordi. Phenomenology of Gravitational Aether as a solution to the Old Cosmological Constant Problem. *Phys. Rev.*, D84:103522, 2011.
- [47] I. G. Avramidi and A. O. Barvinsky. ASYMPTOTIC FREEDOM IN HIGHER DERIVATIVE QUANTUM GRAVITY. *Phys. Lett.*, 159B:269–274, 1985.
- [48] Tom Banks, M. O’Loughlin, and Andrew Strominger. Black hole remnants and the information puzzle. *Phys. Rev.*, D47:4476–4482, 1993.
- [49] Enrico Barausse, Richard Brito, Vitor Cardoso, Irina Dvorkin, and Paolo Pani. The stochastic gravitational-wave background in the absence of horizons. *Class. Quant. Grav.*, 35(20):20LT01, 2018.
- [50] Enrico Barausse, Ted Jacobson, and Thomas P. Sotiriou. Black holes in Einstein-aether and Horava-Lifshitz gravity. *Phys. Rev.*, D83:124043, 2011.

- [51] Carlos Barceló, Raúl Carballo-Rubio, and Luis J. Garay. Where does the physics of extreme gravitational collapse reside? *Universe*, 2(2):7, 2016.
- [52] James M. Bardeen. Interpreting the semi-classical stress-energy tensor in a Schwarzschild background, implications for the information paradox. 2018.
- [53] James M. Bardeen. Models for the nonsingular transition of an evaporating black hole into a white hole. 2018.
- [54] James M. Bardeen, B. Carter, and S. W. Hawking. The Four laws of black hole mechanics. *Commun. Math. Phys.*, 31:161–170, 1973.
- [55] C. Barrabes, Valeri P. Frolov, and R. Parentani. Stochastically fluctuating black hole geometry, Hawking radiation and the transPlanckian problem. *Phys. Rev.*, D62:044020, 2000.
- [56] J. D. Bekenstein. Black holes and the second law. *Lett. Nuovo Cim.*, 4:737–740, 1972.
- [57] J. D. Bekenstein. The quantum mass spectrum of the Kerr black hole. *Lett. Nuovo Cim.*, 11:467, 1974.
- [58] Jacob D. Bekenstein. Black holes and entropy. *Phys. Rev.*, D7:2333–2346, 1973.
- [59] Jacob D. Bekenstein. Generalized second law of thermodynamics in black hole physics. *Phys. Rev.*, D9:3292–3300, 1974.
- [60] Jacob D. Bekenstein and Viatcheslav F. Mukhanov. Spectroscopy of the quantum black hole. *Phys. Lett.*, B360:7–12, 1995.
- [61] Emanuele Berti, Vitor Cardoso, and Marc Casals. Eigenvalues and eigenfunctions of spin-weighted spheroidal harmonics in four and higher dimensions. *Phys. Rev.*, D73:024013, 2006. [Erratum: *Phys. Rev.* D73,109902(2006)].
- [62] Emanuele Berti, Vitor Cardoso, and Andrei O. Starinets. Quasinormal modes of black holes and black branes. *Class. Quant. Grav.*, 26:163001, 2009.
- [63] Emanuele Berti, Vitor Cardoso, and Clifford M. Will. On gravitational-wave spectroscopy of massive black holes with the space interferometer LISA. *Phys. Rev.*, D73:064030, 2006.

- [64] Swetha Bhagwat, Xisco Jimenez Forteza, Paolo Pani, and Valeria Ferrari. Ringdown overtones, black hole spectroscopy and, no-hair theorem tests. 2019.
- [65] G. D. Birkhoff. *Relativity and Modern Physics*. Cambridge, Massachusetts: Harvard University Press. LCCN 23008297.
- [66] D. Blas and S. Sibiriyakov. Horava gravity versus thermodynamics: The Black hole case. *Phys. Rev.*, D84:124043, 2011.
- [67] Diego Blas, Oriol Pujolas, and Sergey Sibiriyakov. Models of non-relativistic quantum gravity: The Good, the bad and the healthy. *JHEP*, 04:018, 2011.
- [68] Luca Bombelli, Jooan Lee, David Meyer, and Rafael Sorkin. Space-Time as a Causal Set. *Phys. Rev. Lett.*, 59:521–524, 1987.
- [69] Raphael Bousso. Complementarity Is Not Enough. *Phys. Rev.*, D87(12):124023, 2013.
- [70] Samuel L. Braunstein, Stefano Pirandola, and Karol Zyczkowski. Better Late than Never: Information Retrieval from Black Holes. *Phys. Rev. Lett.*, 110(10):101301, 2013.
- [71] Richard Brito, Vitor Cardoso, and Paolo Pani. Superradiance. *Lect. Notes Phys.*, 906:pp.1–237, 2015.
- [72] Avery E. Broderick, Abraham Loeb, and Ramesh Narayan. The Event Horizon of Sagittarius A*. *Astrophys. J.*, 701:1357–1366, 2009.
- [73] Avery E. Broderick, Ramesh Narayan, John Kormendy, Eric S. Perlman, Marcia J. Rieke, and Sheperd S. Doeleman. The Event Horizon of M87. *Astrophys. J.*, 805(2):179, 2015.
- [74] R. Brout, C. Gabriel, M. Lubo, and P. Spindel. Minimal length uncertainty principle and the transPlanckian problem of black hole physics. *Phys. Rev.*, D59:044005, 1999.
- [75] Ram Brustein and Merav Hadad. Wave function of the quantum black hole. *Phys. Lett.*, B718:653–656, 2012.
- [76] Pablo Bueno, Pablo A. Cano, Frederik Goelen, Thomas Hertog, and Bert Vercoocke. Echoes of Kerr-like wormholes. *Phys. Rev.*, D97(2):024040, 2018.

- [77] A. Buonanno and T. Damour. Effective one-body approach to general relativistic two-body dynamics. *Phys. Rev.*, D59:084006, 1999.
- [78] C. P. Burgess, Ryan Plestid, and Markus Rummel. Effective Field Theory of Black Hole Echoes. *JHEP*, 09:113, 2018.
- [79] Raúl Carballo-Rubio. Stellar equilibrium in semiclassical gravity. *Phys. Rev. Lett.*, 120(6):061102, 2018.
- [80] Vitor Cardoso, Valentino F. Foit, and Matthew Kleban. Gravitational wave echoes from black hole area quantization. 2019.
- [81] Vitor Cardoso, Edgardo Franzin, and Paolo Pani. Is the gravitational-wave ringdown a probe of the event horizon? *Phys. Rev. Lett.*, 116(17):171101, 2016. [Erratum: *Phys. Rev. Lett.* 117, no. 8, 089902 (2016)].
- [82] Vitor Cardoso, Seth Hopper, Caio F. B. Macedo, Carlos Palenzuela, and Paolo Pani. Gravitational-wave signatures of exotic compact objects and of quantum corrections at the horizon scale. *Phys. Rev.*, D94(8):084031, 2016.
- [83] Vitor Cardoso and Paolo Pani. Tests for the existence of horizons through gravitational wave echoes. *Nat. Astron.*, 1:586–591, 2017.
- [84] Vitor Cardoso and Paolo Pani. The observational evidence for horizons: from echoes to precision gravitational-wave physics. 2017.
- [85] Vitor Cardoso and Paolo Pani. Testing the nature of dark compact objects: a status report. *Living Rev. Rel.*, 22(1):4, 2019.
- [86] Vitor Cardoso, Paolo Pani, Mariano Cadoni, and Marco Cavaglia. Ergoregion instability of ultracompact astrophysical objects. *Phys. Rev.*, D77:124044, 2008.
- [87] Steven Carlip and Claudio Teitelboim. The Off-shell black hole. *Class. Quant. Grav.*, 12:1699–1704, 1995.
- [88] B. Carter. Axisymmetric Black Hole Has Only Two Degrees of Freedom. *Phys. Rev. Lett.*, 26(6):331–333, Feb 1971.
- [89] Roberto Casadio and Roldao da Rocha. Stability of the graviton Bose–Einstein condensate in the brane-world. *Phys. Lett.*, B763:434–438, 2016.

- [90] Roberto Casadio, Piero Nicolini, and Roldao da Rocha. Generalised uncertainty principle Hawking fermions from minimally geometric deformed black holes. *Class. Quant. Grav.*, 35(18):185001, 2018.
- [91] Marc Casals and Luís F. Longo Micchi. Spectroscopy of extremal and near-extremal Kerr black holes. *Phys. Rev.*, D99(8):084047, 2019.
- [92] Marc Casals and Peter Zimmerman. Perturbations of Extremal Kerr Spacetime: Analytic Framework and Late-time Tails. 2018.
- [93] Alejandra Castro, Alexander Maloney, and Andrew Strominger. Hidden Conformal Symmetry of the Kerr Black Hole. *Phys. Rev.*, D82:024008, 2010.
- [94] S. Chandrasekhar and Steven L. Detweiler. The quasi-normal modes of the Schwarzschild black hole. *Proc. Roy. Soc. Lond.*, A344:441–452, 1975.
- [95] S. Chandrasekhar and Steven L. Detweiler. Equations governing gravitational perturbations of the Kerr black-hole. *Proc. Roy. Soc. Lond.*, A350:165–174, 1976.
- [96] Borun D. Chowdhury and Andrea Puhm. Is Alice burning or fuzzing? *Phys. Rev. D*, 88:063509, 2013.
- [97] Andrew Coates, Sebastian H. Völkel, and Kostas D. Kokkotas. Spectral Lines of Quantized, Spinning Black Holes and their Astrophysical Relevance. *Phys. Rev. Lett.*, 123(17):171104, 2019.
- [98] Randy S. Conklin and Bob Holdom. Gravitational Wave "Echo" Spectra. 2019.
- [99] Randy S. Conklin, Bob Holdom, and Jing Ren. Gravitational wave echoes through new windows. 2017.
- [100] Miguel R. Correia and Vitor Cardoso. Characterization of echoes: a Dyson-series representation of individual pulses. 2018.
- [101] Bethan Cropp, Stefano Liberati, Arif Mohd, and Matt Visser. Ray tracing Einstein-Æther black holes: Universal versus Killing horizons. *Phys. Rev.*, D89(6):064061, 2014.
- [102] Pedro V. P. Cunha, Emanuele Berti, and Carlos A. R. Herdeiro. Light-Ring Stability for Ultracompact Objects. *Phys. Rev. Lett.*, 119(25):251102, 2017.

- [103] Roldao da Rocha and Carlos H. Coimbra-Araujo. Extra dimensions in LHC via mini-black holes: Effective Kerr-Newman brane-world effects. *Phys. Rev.*, D74:055006, 2006.
- [104] Thibault Damour. Introductory lectures on the Effective One Body formalism. *Int. J. Mod. Phys.*, A23:1130–1148, 2008.
- [105] Thibault Damour and Sergey N. Solodukhin. Wormholes as black hole foils. *Phys. Rev.*, D76:024016, 2007.
- [106] Thibaut Damour. Black-hole eddy currents. *Phys. Rev. D*, 18:3598–3604, Nov 1978.
- [107] Sayak Datta and Sukanta Bose. Probing the nature of central objects in extreme-mass-ratio inspirals with gravitational waves. *Phys. Rev.*, D99(8):084001, 2019.
- [108] Sayak Datta, Richard Brito, Sukanta Bose, Paolo Pani, and Scott A. Hughes. Tidal heating as a discriminator for horizons in extreme mass ratio inspirals. 2019.
- [109] Steven L. Detweiler. Resonant oscillations of a rapidly rotating black hole. *Proc. Roy. Soc. Lond.*, A352:381–395, 1977.
- [110] Ramit Dey, Sumanta Chakraborty, and Niayesh Afshordi. Echoes from the braneworld black holes. 2020.
- [111] John F. Donoghue. General relativity as an effective field theory: The leading quantum corrections. *Phys. Rev.*, D50:3874–3888, 1994.
- [112] J. Droste. The field of a single centre in Einstein’s theory of gravitation, and the motion of a particle in that field. *Proceedings of the Royal Netherlands Academy of Arts and Science.*, 19 (1): 197–215. Bibcode:1917KNAB...19..197D., 1917.
- [113] Sheila Dwyer, Daniel Sigg, Stefan W. Ballmer, Lisa Barsotti, Nergis Mavalvala, and Matthew Evans. Gravitational wave detector with cosmological reach. *Phys. Rev. D*, 91:082001, Apr 2015.
- [114] A. Einstein. Zur Quantentheorie der Strahlung. *Physikalische Zeitschrift*, 18, 1917.
- [115] Christopher Eling, Brendan Z. Foster, Ted Jacobson, and Aron C. Wall. Lorentz violation and perpetual motion. *Phys. Rev.*, D75:101502, 2007.
- [116] T Elster. Vacuum polarization near a black hole creating particles. *Physics Letters A*, 94(5):205–209, 1983.

- [117] A. Fabbri and J. Navarro-Salas. *Modeling black hole evaporation*. 2005.
- [118] V. Ferrari and K. D. Kokkotas. Scattering of particles by neutron stars: Time evolutions for axial perturbations. *Phys. Rev. D*, 62:107504, Oct 2000.
- [119] Valeria Ferrari and Bahram Mashhoon. New approach to the quasinormal modes of a black hole. *Phys. Rev.*, D30:295–304, 1984.
- [120] L. H. Ford and N. F. Svaiter. Cosmological and black hole horizon fluctuations. *Phys. Rev.*, D56:2226–2235, 1997.
- [121] E. S. Fradkin and Arkady A. Tseytlin. Renormalizable asymptotically free quantum theory of gravity. *Nucl. Phys.*, B201:469–491, 1982.
- [122] J. L. Friedman. Ergosphere instability. *Communications in Mathematical Physics*, 63:243–255, October 1978.
- [123] Andrei V. Frolov and Valeri P. Frolov. Rigidly rotating zero-angular-momentum observer surfaces in the Kerr spacetime. *Phys. Rev.*, D90(12):124010, 2014.
- [124] G. W. Gibbons and S. W. Hawking. Action Integrals and Partition Functions in Quantum Gravity. *Phys. Rev.*, D15:2752–2756, 1977.
- [125] Steven B. Giddings. Quantum mechanics of black holes. In *Proceedings, Summer School in High-energy physics and cosmology: Trieste, Italy, June 13-July 29, 1994*, pages 0530–574, 1994.
- [126] Steven B. Giddings. Black hole information, unitarity, and nonlocality. *Phys. Rev. D*, 74:106005, 2006.
- [127] Steven B. Giddings. Gravitational wave tests of quantum modifications to black hole structure – with post-GW150914 update. *Class. Quant. Grav.*, 33(23):235010, 2016.
- [128] Steven B. Giddings. Nonviolent unitarization: basic postulates to soft quantum structure of black holes. *JHEP*, 12:047, 2017.
- [129] Steven B. Giddings. Black holes in the quantum universe. *Phil. Trans. Roy. Soc. Lond.*, A377(2161):20190029, 2019.
- [130] Ramandeep Gill, Antonios Nathanail, and Luciano Rezzolla. When Did the Remnant of GW170817 Collapse to a Black Hole? *Astrophys. J.*, 876(2):139, 2019.

- [131] Florian Girelli, Franz Hinterleitner, and Seth Major. Loop Quantum Gravity Phenomenology: Linking Loops to Observational Physics. *SIGMA*, 8:098, 2012.
- [132] Stefano Giusto, Ashish Saxena, and Simon F Ross. Non-supersymmetric microstates of the d1-d5-kk system. *Journal of High Energy Physics*, 2007(12):065, 2007.
- [133] Steven N. Goodman. Of P-Values and Bayes: A Modest Proposal.
- [134] Michel Goossens, Frank Mittelbach, and Alexander Samarin. *The L^AT_EX Companion*. Addison-Wesley, Reading, Massachusetts, 1994.
- [135] Ruth Gregory, Ian G. Moss, and Benjamin Withers. Black holes as bubble nucleation sites. *JHEP*, 03:081, 2014.
- [136] Bin Guo, Shaun Hampton, and Samir D. Mathur. Can we observe fuzzballs or firewalls? 2017.
- [137] Anshu Gupta, Badri Krishnan, Alex Nielsen, and Erik Schnetter. Dynamics of marginally trapped surfaces in a binary black hole merger: Growth and approach to equilibrium. 2018.
- [138] Daniel Harlow. Jerusalem Lectures on Black Holes and Quantum Information. *Rev. Mod. Phys.*, 88:15002, 2016. [Rev. Mod. Phys.88,15002(2016)].
- [139] Daniel Harlow and Patrick Hayden. Quantum Computation vs. Firewalls. *JHEP*, 06:085, 2013.
- [140] J. B. Hartle and S. W. Hawking. Path-integral derivation of black-hole radiance. *Phys. Rev. D*, 13:2188–2203, Apr 1976.
- [141] S. W. Hawking. Black hole explosions. *Nature*, 248:30–31, 1974.
- [142] S. W. Hawking. Particle Creation by Black Holes. *Commun. Math. Phys.*, 43:199–220, 1975. [,167(1975)].
- [143] S. W. Hawking. Breakdown of Predictability in Gravitational Collapse. *Phys. Rev.*, D14:2460–2473, 1976.
- [144] S. W. Hawking. Quantum Gravity and Path Integrals. *Phys. Rev.*, D18:1747–1753, 1978.
- [145] Patrick Hayden and John Preskill. Black holes as mirrors: Quantum information in random subsystems. *JHEP*, 09:120, 2007.

- [146] A. Hewish, S. J. Bell, J. D. H Pilkington, P. F. Scott, and R. A. Collins. Observation of a rapidly pulsating radio source. *Nature*, 217:709–713, 1968.
- [147] G. Hobbs et al. The international pulsar timing array project: using pulsars as a gravitational wave detector. *Class. Quant. Grav.*, 27:084013, 2010.
- [148] Shahar Hod. Onset of superradiant instabilities in the composed Kerr-black-hole-mirror bomb. *Phys. Lett.*, B736:398–402, 2014.
- [149] Bob Holdom. A ghost and a naked singularity; facing our demons. In *Scale invariance in particle physics and cosmology Geneva (CERN), Switzerland, January 28-February 1, 2019*, 2019.
- [150] Bob Holdom. Not quite black holes at LIGO. 2019.
- [151] Bob Holdom and Jing Ren. QCD analogy for quantum gravity. *Phys. Rev.*, D93(12):124030, 2016.
- [152] Bob Holdom and Jing Ren. Not quite a black hole. *Phys. Rev.*, D95(8):084034, 2017.
- [153] Petr Horava. Quantum Gravity at a Lifshitz Point. *Phys. Rev.*, D79:084008, 2009.
- [154] Maximiliano Isi, Matthew Giesler, Will M. Farr, Mark A. Scheel, and Saul A. Teukolsky. Testing the no-hair theorem with GW150914. *Phys. Rev. Lett.*, 123(11):111102, 2019.
- [155] Werner Israel. Event horizons in static electrovac space-times. *Communications in Mathematical Physics*, 8(3):245–260, Sep 1968.
- [156] Ted Jacobson, Arif Mohd, and Sudipta Sarkar. Membrane paradigm for Einstein-Gauss-Bonnet gravity. *Phys. Rev.*, D95(6):064036, 2017.
- [157] Ioannis Kamaretsos, Mark Hannam, Sascha Husa, and B. S. Sathyaprakash. Black-hole hair loss: Learning about binary progenitors from ringdown signals. *Phys. Rev. D*, 85:024018, Jan 2012.
- [158] Hikaru Kawai and Yuki Yokokura. Interior of Black Holes and Information Recovery. *Phys. Rev.*, D93(4):044011, 2016.
- [159] Hikaru Kawai and Yuki Yokokura. A Model of Black Hole Evaporation and 4D Weyl Anomaly. *Universe*, 3(2):51, 2017.

- [160] Roy P. Kerr. Gravitational field of a spinning mass as an example of algebraically special metrics. *Phys. Rev. Lett.*, 11:237–238, Sep 1963.
- [161] Elias B. Kiritsis and Georgios Kofinas. On Horava-Lifshitz ‘Black Holes’. *JHEP*, 01:122, 2010.
- [162] Donald Knuth. *The T_EXbook*. Addison-Wesley, Reading, Massachusetts, 1986.
- [163] K. D. Kokkotas. Pulsating relativistic stars. In *Relativistic gravitation and gravitational radiation. Proceedings, School of Physics, Les Houches, France, September 26-October 6, 1995*, pages 89–102, 1995.
- [164] Kostas D. Kokkotas and Bernd G. Schmidt. Quasinormal modes of stars and black holes. *Living Rev. Rel.*, 2:2, 1999.
- [165] R. A. Konoplya, Z. Stuchlík, and A. Zhidenko. Echoes of compact objects: new physics near the surface and matter at a distance. *Phys. Rev.*, D99(2):024007, 2019.
- [166] R. Kubo. The fluctuation-dissipation theorem. *Reports on Progress in Physics*, 29:255–284, January 1966.
- [167] Claus Lämmerzahl and Patricia Rademaker. Higher order equations of motion and gravity. *Phys. Rev. D*, 86:124017, Dec 2012.
- [168] Leslie Lamport. *L^AT_EX — A Document Preparation System*. Addison-Wesley, Reading, Massachusetts, second edition, 1994.
- [169] L. D. Landau and E. M. Lifshitz. *Fluid mechanics*. 1959.
- [170] Stefano Liberati and Luca Maccione. Astrophysical constraints on Planck scale dissipative phenomena. *Phys. Rev. Lett.*, 112:151301, 2014.
- [171] R. K. L. Lo, T. G. F. Li, and A. J. Weinstein. Template-based Gravitational-Wave Echoes Search Using Bayesian Model Selection. *Phys. Rev.*, D99(8):084052, 2019.
- [172] Lionel London, Deirdre Shoemaker, and James Healy. Modeling ringdown: Beyond the fundamental quasinormal modes. *Phys. Rev. D*, 90:124032, Dec 2014.
- [173] Jorma Louko and Donald Marolf. Inextendible Schwarzschild black hole with a single exterior: How thermal is the Hawking radiation? *Phys. Rev. D*, 58:024007, 1998.
- [174] Oleg Lunin and Samir D. Mathur. AdS / CFT duality and the black hole information paradox. *Nucl. Phys.*, B623:342–394, 2002.

- [175] Oleg Lunin and Samir D. Mathur. Statistical interpretation of Bekenstein entropy for systems with a stretched horizon. *Phys. Rev. Lett.*, 88:211303, 2002.
- [176] Elisa Maggio, Vitor Cardoso, Sam R. Dolan, and Paolo Pani. Ergoregion instability of exotic compact objects: electromagnetic and gravitational perturbations and the role of absorption. 2018.
- [177] Elisa Maggio, Paolo Pani, and Valeria Ferrari. Exotic Compact Objects and How to Quench their Ergoregion Instability. 2017.
- [178] Elisa Maggio, Adriano Testa, Swetha Bhagwat, and Paolo Pani. Analytical model for gravitational-wave echoes from spinning remnants. *Phys. Rev.*, D100(6):064056, 2019.
- [179] Juan Maldacena, Stephen H. Shenker, and Douglas Stanford. A bound on chaos. *JHEP*, 08:106, 2016.
- [180] Juan Maldacena and Leonard Susskind. Cool horizons for entangled black holes. *Fortsch. Phys.*, 61:781–811, 2013.
- [181] Juan Martin Maldacena. The Large N limit of superconformal field theories and supergravity. *Int. J. Theor. Phys.*, 38:1113–1133, 1999. [Adv. Theor. Math. Phys.2,231(1998)].
- [182] Shuhei Mano, Hisao Suzuki, and Eiichi Takasugi. Analytic solutions of the Regge-Wheeler equation and the postMinkowskian expansion. *Prog. Theor. Phys.*, 96:549–566, 1996.
- [183] Zachary Mark, Aaron Zimmerman, Song Ming Du, and Yanbei Chen. A recipe for echoes from exotic compact objects. *Phys. Rev.*, D96(8):084002, 2017.
- [184] Andrea Maselli, Paolo Pani, Vitor Cardoso, Tiziano Abdelsalhin, Leonardo Gualtieri, and Valeria Ferrari. Probing Planckian corrections at the horizon scale with LISA binaries. *Phys. Rev. Lett.*, 120(8):081101, 2018.
- [185] Andrea Maselli, Sebastian H. Völkel, and Kostas D. Kokkotas. Parameter estimation of gravitational wave echoes from exotic compact objects. *Phys. Rev.*, D96(6):064045, 2017.
- [186] Samir D. Mathur. Emission rates, the correspondence principle and the information paradox. *Nucl. Phys.*, B529:295–320, 1998.

- [187] Samir D. Mathur. The Fuzzball proposal for black holes: An Elementary review. *Fortsch. Phys.*, 53:793–827, 2005.
- [188] Samir D. Mathur. Fuzzballs and the information paradox: A Summary and conjectures. 10 2008.
- [189] Samir D Mathur. Fuzzballs and the information paradox: a summary and conjectures. *Advanced Science Letters*, 2(2):133–150, 2009.
- [190] Samir D. Mathur. The Information paradox: A Pedagogical introduction. *Class. Quant. Grav.*, 26:224001, 2009.
- [191] Samir D. Mathur. What Exactly is the Information Paradox? *Lect. Notes Phys.*, 769:3–48, 2009.
- [192] Samir D. Mathur. Tunneling into fuzzball states. *Gen. Rel. Grav.*, 42:113–118, 2010.
- [193] Samir D. Mathur and David Turton. Comments on black holes I: The possibility of complementarity. *JHEP*, 01:034, 2014.
- [194] Pawel O. Mazur and Emil Mottola. Gravitational condensate stars: An alternative to black holes. 2001.
- [195] Pawel O. Mazur and Emil Mottola. Gravitational vacuum condensate stars. *Proc. Nat. Acad. Sci.*, 101:9545–9550, 2004.
- [196] Emil Mottola. New Horizons in Gravity: Dark Energy and Condensate Stars. *J. Phys. Conf. Ser.*, 314:012010, 2011.
- [197] Hiroyuki Nakano, Norichika Sago, Hideyuki Tagoshi, and Takahiro Tanaka. Black hole ringdown echoes and howls. *PTEP*, 2017(7):071E01, 2017.
- [198] Ramesh Narayan and Jeffrey E. McClintock. Observational Evidence for Black Holes. 2013.
- [199] Keith K. Ng, Robert B. Mann, and Eduardo Martin-Martinez. Over the horizon: distinguishing the Schwarzschild spacetime and the \mathbb{RP}^3 spacetime using an Unruh-DeWitt detector. *Phys. Rev. D*, 96(8):085004, 2017.
- [200] David A. Nichols and Yanbei Chen. A hybrid method for understanding black-hole mergers: head-on case. *Phys. Rev. D*, 82:104020, 2010.

- [201] David A. Nichols and Yanbei Chen. Hybrid method for understanding black-hole mergers: Inspiralling case. *Phys. Rev. D*, 85:044035, 2012.
- [202] Max Niedermaier and Martin Reuter. The Asymptotic Safety Scenario in Quantum Gravity. *Living Rev. Rel.*, 9:5–173, 2006.
- [203] Alex B. Nielsen, Collin D. Capano, Ofek Birnholtz, and Julian Westerweck. Parameter estimation and statistical significance of echoes following black hole signals in the first Advanced LIGO observing run. *Phys. Rev.*, D99(10):104012, 2019.
- [204] Hans-Peter Nollert. TOPICAL REVIEW: Quasinormal modes: the characteristic ‘sound’ of black holes and neutron stars. *Class. Quant. Grav.*, 16:R159–R216, 1999.
- [205] M. Nouri-Zonoz and T. Padmanabhan. The Classical essence of black hole radiation. 12 1998.
- [206] Maria Okounkova, Leo C. Stein, Jordan Moxon, Mark A. Scheel, and Saul A. Teukolsky. Numerical relativity simulation of GW150914 beyond general relativity. 2019.
- [207] Maria Okounkova, Leo C. Stein, Mark A. Scheel, and Saul A. Teukolsky. Numerical binary black hole collisions in dynamical Chern-Simons gravity. *Phys. Rev.*, D100(10):104026, 2019.
- [208] Naritaka Oshita. Resolution to the firewall paradox: The black hole information paradox and highly squeezed interior quantum fluctuations. *Class. Quant. Grav.*, 34(19):195002, 2017.
- [209] Naritaka Oshita and Niayesh Afshordi. Probing microstructure of black hole spacetimes with gravitational wave echoes. *Phys. Rev.*, D99(4):044002, 2019.
- [210] Naritaka Oshita, Daichi Tsuna, and Niayesh Afshordi. Quantum Black Hole Seismology I: Echoes, Ergospheres, and Spectra. 2020.
- [211] Naritaka Oshita, Qingwen Wang, and Niayesh Afshordi. On Reflectivity of Quantum Black Hole Horizons. *JCAP*, 04:016, 2020.
- [212] J. Ovalle, R. Casadio, R. da Rocha, and A. Sotomayor. Anisotropic solutions by gravitational decoupling. *Eur. Phys. J.*, C78(2):122, 2018.
- [213] J. Ovalle, R. Casadio, R. da Rocha, A. Sotomayor, and Z. Stuchlik. Black holes by gravitational decoupling. *Eur. Phys. J.*, C78(11):960, 2018.

- [214] T. Padmanabhan. Quantum structure of space-time and black hole entropy. *Phys. Rev. Lett.*, 81:4297–4300, 1998.
- [215] T. Padmanabhan. Event horizon: Magnifying glass for Planck length physics. *Phys. Rev.*, D59:124012, 1999.
- [216] T. Padmanabhan. Thermality of the Rindler horizon: A simple derivation from the structure of the inertial propagator. *Phys. Rev.*, D100(4):045024, 2019.
- [217] Don N Page. Thermal stress tensors in static einstein spaces. *Physical Review D*, 25(6):1499, 1982.
- [218] Don N. Page. Average entropy of a subsystem. *Phys. Rev. Lett.*, 71:1291–1294, 1993.
- [219] Don N. Page. Information in black hole radiation. *Phys. Rev. Lett.*, 71:3743–3746, 1993.
- [220] Don N. Page. Time Dependence of Hawking Radiation Entropy. *JCAP*, 1309:028, 2013.
- [221] Paolo Pani, Emanuele Berti, Vitor Cardoso, Yanbei Chen, and Richard Norte. Gravitational wave signatures of the absence of an event horizon. I. Nonradial oscillations of a thin-shell gravastar. *Phys. Rev.*, D80:124047, 2009.
- [222] Kyriakos Papadodimas and Suvrat Raju. An Infalling Observer in AdS/CFT. *JHEP*, 10:212, 2013.
- [223] R. Parentani. Quantum metric fluctuations and Hawking radiation. *Phys. Rev.*, D63:041503, 2001.
- [224] Leonard Parker and David Toms. *Quantum field theory in curved spacetime: quantized fields and gravity*. Cambridge University Press, 2009.
- [225] DD Pawar, VR Patil, and SN Bayaskar. Spherically symmetric fluid cosmological model with anisotropic stress tensor in general relativity. *ISRN Mathematical Physics*, 2012, 2012.
- [226] Ue-Li Pen and Avery E. Broderick. Possible Astrophysical Observables of Quantum Gravity Effects near Black Holes. *Mon. Not. Roy. Astron. Soc.*, 445(4):3370–3373, 2014.

- [227] Roger Penrose. Gravitational Collapse and Space-Time Singularities. *Phys. Rev. Lett.*, 14(3):57–59, Jan 1965.
- [228] Eric Poisson. *A Relativist’s Toolkit: The Mathematics of Black-Hole Mechanics*. Cambridge University Press, 2009.
- [229] Eric Poisson and W. Israel. Inner-horizon instability and mass inflation in black holes. *Phys. Rev. Lett.*, 63:1663–1666, 1989.
- [230] J. Polchinski. *String theory. Vol. 1: An introduction to the bosonic string*. Cambridge Monographs on Mathematical Physics. Cambridge University Press, 2007.
- [231] G. Poschl and E. Teller. Bemerkungen zur Quantenmechanik des anharmonischen Oszillators. *Z. Phys.*, 83:143–151, 1933.
- [232] Chanda Prescod-Weinstein, Niayesh Afshordi, and Michael L. Balogh. Stellar Black Holes and the Origin of Cosmic Acceleration. *Phys. Rev.*, D80:043513, 2009.
- [233] Chanda Prescod-Weinstein, Niayesh Afshordi, and Michael L Balogh. Stellar black holes and the origin of cosmic acceleration. *Physical Review D*, 80(4):043513, 2009.
- [234] W. H. Press and S. A. Teukolsky. Floating Orbits, Superradiant Scattering and the Black-hole Bomb. , 238:211–212, July 1972.
- [235] Richard H. Price and Gaurav Khanna. Gravitational wave sources: reflections and echoes. *Class. Quant. Grav.*, 34(22):225005, 2017.
- [236] M. Punturo et al. The Einstein Telescope: A third-generation gravitational wave observatory. *Class. Quant. Grav.*, 27:194002, 2010.
- [237] Tullio Regge and John A. Wheeler. Stability of a Schwarzschild singularity. *Phys. Rev.*, 108:1063–1069, 1957.
- [238] Jing Ren. Anatomy of a Burning 2-2-hole. 2019.
- [239] Oscar Reula and Olivier Sarbach. The Initial-Boundary Value Problem in General Relativity. *Int. J. Mod. Phys.*, D20:767–783, 2011.
- [240] Carlo Rovelli. Black hole entropy from loop quantum gravity. *Phys. Rev. Lett.*, 77:3288–3291, 1996.
- [241] Markus Rummel and C. P. Burgess. Constraining Fundamental Physics with the Event Horizon Telescope. 2019.

- [242] Shinsei Ryu and Tadashi Takayanagi. Aspects of Holographic Entanglement Entropy. *JHEP*, 08:045, 2006.
- [243] Nobuyuki Sakai, Hiromi Saida, and Takashi Tamaki. Gravastar Shadows. *Phys. Rev.*, D90(10):104013, 2014.
- [244] F. Salemi, E. Milotti, G. A. Prodi, G. Vedovato, C. Lazzaro, S. Tiwari, S. Vinciguerra, M. Drago, and S. Klimenko. A wider look at the gravitational-wave transients from GWTC-1 using an unmodeled reconstruction method. 2019.
- [245] Krishan Saraswat and Niayesh Afshordi. Quantum Nature of Black Holes: Fast Scrambling versus Echoes. 2019.
- [246] Mehdi Saravani, Niayesh Afshordi, and Robert B. Mann. Dynamical Emergence of Universal Horizons during the formation of Black Holes. *Phys. Rev.*, D89(8):084029, 2014.
- [247] Mehdi Saravani, Niayesh Afshordi, and Robert B Mann. Empty black holes, firewalls, and the origin of bekenstein–hawking entropy. *International Journal of Modern Physics D*, 23(13):1443007, 2014.
- [248] Mehdi Saravani, Niayesh Afshordi, and Robert B. Mann. Empty black holes, firewalls, and the origin of Bekensteinentropy. *Int. J. Mod. Phys. D*, 23(13):1443007, 2015.
- [249] Misao Sasaki and Takashi Nakamura. Gravitational Radiation From a Kerr Black Hole. 1. Formulation and a Method for Numerical Analysis. *Prog. Theor. Phys.*, 67:1788, 1982.
- [250] Misao Sasaki and Hideyuki Tagoshi. Analytic black hole perturbation approach to gravitational radiation. *Living Rev. Rel.*, 6:6, 2003.
- [251] Bernard F. Schutz and Clifford M. Will. BLACK HOLE NORMAL MODES: A SEMIANALYTIC APPROACH. *Astrophys. J.*, 291:L33–L36, 1985.
- [252] K. Schwarzschild. Über das Gravitationsfeld eines Massenpunktes nach der Einsteinschen Theorie. *Sitzungsberichte der Königlich Preussischen Akademie der Wissenschaften.*, 7: 189–196., 1916.
- [253] Yasuhiro Sekino and Leonard Susskind. Fast Scramblers. *JHEP*, 10:065, 2008.

- [254] Masaru Shibata, Misao Sasaki, Hideyuki Tagoshi, and Takahiro Tanaka. Gravitational waves from a particle orbiting around a rotating black hole: PostNewtonian expansion. *Phys. Rev.*, D51:1646–1663, 1995.
- [255] K. Srinivasan and T. Padmanabhan. Particle production and complex path analysis. *Phys. Rev.*, D60:024007, 1999.
- [256] A. A. Starobinskiĭ. Amplification of waves during reflection from a rotating “black hole”. *Soviet Journal of Experimental and Theoretical Physics*, 37:28, July 1973.
- [257] K. S. Stelle. Renormalization of Higher Derivative Quantum Gravity. *Phys. Rev.*, D16:953–969, 1977.
- [258] Leonard Susskind. *New Concepts for Old Black Holes*. 2013.
- [259] Leonard Susskind and Larus Thorlacius. Gedanken experiments involving black holes. *Phys. Rev.*, D49:966–974, 1994.
- [260] Leonard Susskind, Larus Thorlacius, and John Uglum. The Stretched horizon and black hole complementarity. *Phys. Rev.*, D48:3743–3761, 1993.
- [261] Adriano Testa and Paolo Pani. Analytical template for gravitational-wave echoes: signal characterization and prospects of detection with current and future interferometers. *Phys. Rev.*, D98(4):044018, 2018.
- [262] Saul A Teukolsky. Perturbations of a rotating black hole. i. fundamental equations for gravitational, electromagnetic, and neutrino-field perturbations. *The Astrophysical Journal*, 185:635–648, 1973.
- [263] R. T. Thompson and L. H. Ford. Enhanced Black Hole Horizon Fluctuations. *Phys. Rev.*, D78:024014, 2008.
- [264] Kip S. Thorne, R. H. Price, and D. A. Macdonald, editors. *BLACK HOLES: THE MEMBRANE PARADIGM*. 1986.
- [265] Kazuhiro Tomimaga, Motoyuki Saijo, and Kei-ichi Maeda. Gravitational waves from a test particle scattered by a neutron star: Axial mode case. *Phys. Rev.*, D60:024004, 1999.
- [266] Ka Wa Tsang, Archisman Ghosh, Anuradha Samajdar, Katerina Chatziioannou, Simone Mastrogiovanni, Michalis Agathos, and Chris Van Den Broeck. A morphology-independent search for gravitational wave echoes in data from the first and second observing runs of Advanced LIGO and Advanced Virgo. 2019.

- [267] Ka Wa Tsang, Michiel Rollier, Archisman Ghosh, Anuradha Samajdar, Michalis Agathos, Katerina Chatziioannou, Vitor Cardoso, Gaurav Khanna, and Chris Van Den Broeck. A morphology-independent data analysis method for detecting and characterizing gravitational wave echoes. *Phys. Rev.*, D98(2):024023, 2018.
- [268] Nami Uchikata, Hiroyuki Nakano, Tatsuya Narikawa, Norichika Sago, Hideyuki Tagoshi, and Takahiro Tanaka. Searching for black hole echoes from the LIGO-Virgo Catalog GWTC-1. 2019.
- [269] William G. Unruh and Robert M. Wald. Information Loss. *Rept. Prog. Phys.*, 80(9):092002, 2017.
- [270] Sergiu I. Vacaru. Modified Dispersion Relations in Horava-Lifshitz Gravity and Finsler Brane Models. *Gen. Rel. Grav.*, 44:1015–1042, 2012.
- [271] L. Vanzo, G. Acquaviva, and R. Di Criscienzo. Tunnelling Methods and Hawking’s radiation: achievements and prospects. *Class. Quant. Grav.*, 28:183001, 2011.
- [272] Rodrigo Vicente, Vitor Cardoso, and Jorge C. Lopes. Penrose process, superradiance, and ergoregion instabilities. *Phys. Rev.*, D97(8):084032, 2018.
- [273] A. Vilenkin. Exponential Amplification of Waves in the Gravitational Field of Ultrarelativistic Rotating Body. *Phys. Lett.*, 78B:301–303, 1978.
- [274] Matt Visser. *Lorentzian wormholes: From Einstein to Hawking*. 1995.
- [275] B. L. Voronov. *Yad.Fiz.(Sov.J.Nucl.Phys.)*, 39:998, 1984.
- [276] Sebastian H. Völkel and Kostas D. Kokkotas. Ultra Compact Stars: Reconstructing the Perturbation Potential. *Class. Quant. Grav.*, 34(17):175015, 2017.
- [277] Sebastian H. Völkel and Kostas D. Kokkotas. Wormhole Potentials and Throats from Quasi-Normal Modes. *Class. Quant. Grav.*, 35(10):105018, 2018.
- [278] Robert M. Wald. Black hole entropy is the Noether charge. *Phys. Rev.*, D48(8):R3427–R3431, 1993.
- [279] Qingwen Wang and Niayesh Afshordi. Physical Structure of “Horizons” in (Mock) Fuzzballs. 2016.
- [280] Qingwen Wang and Niayesh Afshordi. Black hole echology: The observer’s manual. *Phys. Rev.*, D97(12):124044, 2018.

- [281] Qingwen Wang, Naritaka Oshita, and Niayesh Afshordi. Echoes from Quantum Black Holes. 2019.
- [282] Julian Westerweck, Alex Nielsen, Ofek Fischer-Birnholtz, Miriam Cabero, Collin Capano, Thomas Dent, Badri Krishnan, Grant Meadors, and Alexander H. Nitz. Low significance of evidence for black hole echoes in gravitational wave data. 2017.
- [283] Jeffrey Winicour. Boundary Conditions for the Gravitational Field. *Class. Quant. Grav.*, 29:113001, 2012.
- [284] Huan Yang, Aaron Zimmerman, Anil Zenginoğlu, Fan Zhang, Emanuele Berti, and Yanbei Chen. Quasinormal modes of nearly extremal Kerr spacetimes: spectrum bifurcation and power-law ringdown. *Phys. Rev.*, D88(4):044047, 2013. [Phys. Rev.D88,044047(2013)].
- [285] James W. York. Dynamical origin of black-hole radiance. *Phys. Rev. D*, 28:2929–2945, Dec 1983.
- [286] Beni Yoshida. Firewalls vs. Scrambling. *JHEP*, 10:132, 2019.
- [287] Anil Zenginoglu. A Geometric framework for black hole perturbations. *Phys. Rev.*, D83:127502, 2011.
- [288] F.J. Zerilli. Gravitational field of a particle falling in a schwarzschild geometry analyzed in tensor harmonics. *Phys. Rev. D*, 2:2141–2160, 1970.

APPENDICES

Appendix A

Derivation of $e^{-|\tilde{\omega}|/T}$ from the modified dispersion relation

Here we show the details of the derivation of $e^{-|\tilde{\omega}|/T}$ in the Kerr spacetime by starting with the analytic solution of the modified SN equation. The absolute value of the frequency is very important since the ergoregion instability can be induced if the reflectivity was given by $e^{-\tilde{\omega}/T}$. Let us start with the modified SN equation:

$$\left(\frac{-i\gamma|\tilde{\omega}|}{\tilde{F}\sqrt{\delta(r)}E_{\text{Pl}}} \frac{d^2}{dx^2} + \frac{d^2}{dx^2} - \mathcal{F} \frac{d}{dx} - \mathcal{U} \right) \psi_{\tilde{\omega}} = 0, \quad (\text{A.1})$$

in tortoise coordinate:

$$\begin{aligned} x &\equiv \int dr \frac{r^2 + a^2}{r^2 \delta(r)} \\ &= r + \frac{r_g r_+}{r_+ - r_-} \ln \frac{r - r_+}{r_g} - \frac{r_g r_-}{r_+ - r_-} \ln \frac{r - r_-}{r_g}, \end{aligned} \quad (\text{A.2})$$

where $a \equiv GM\bar{a}$ is the spin parameter, $r_{\pm} \equiv GM \pm \sqrt{(GM)^2 - a^2}$, the forms of \mathcal{F} and \mathcal{U} can be found in [249], and $\tilde{F}\sqrt{\delta(r)}$ is the blue shift factor of Kerr spacetime derived in

[205]

$$\tilde{F} \equiv \sqrt{\frac{r^2(r^2 + a^2 \cos^2 \theta)}{(r^2 + a^2)(r^2 + a^2 \cos^2 \theta) + a^2 r_g r \sin^2 \theta}}, \quad (\text{A.3})$$

$$\times \frac{a^2(r^2 + a^2) \cos^2 \theta + r^2(r^2 + a^2 + r_g a^2 \sin^2 \theta/r)}{(r^2 + a^2)(r^2 + a^2 \cos^2 \theta)},$$

$$\delta^{1/2} \equiv \sqrt{1 - r_g/r + a^2/r^2}, \quad (\text{A.4})$$

For spinning BHs, with the Hawking temperature is

$$T \equiv \frac{\kappa_+}{2\pi} = \frac{1}{2\pi r_g} \left(\frac{\sqrt{1 - \bar{a}^2}}{1 + \sqrt{1 - \bar{a}^2}} \right), \quad (\text{A.5})$$

where κ_+ is the surface gravity at the outer horizon $r = r_+$, while the horizon-frame frequency $\tilde{\omega}$ is related to the frequency seen by the distant observer ω via

$$\tilde{\omega} = \omega - m\Omega_{\text{H}}, \quad \Omega_{\text{H}} = \frac{\bar{a}}{(1 + \sqrt{1 - \bar{a}^2})r_g}. \quad (\text{A.6})$$

Here, Ω_{H} is the angular velocity of the horizon, and m is the azimuthal angular momentum number (=2 for dominant mode of BH ringdown perturbations).

In the near horizon limit ($x \rightarrow -\infty$), the blue-shift factor reduces to

$$\lim_{x \rightarrow -\infty} \tilde{F}(r, \theta) \sqrt{\delta} = \tilde{F}(r = r_+, \theta) C e^{\kappa_+ x}, \quad (\text{A.7})$$

where C has the form of

$$C \equiv \exp \left[\frac{1}{2} \frac{\sqrt{1 - \bar{a}^2}}{r_+^2/r_g^2 + \bar{a}^2/4} \left(-r_+/r_g + \frac{r_-^2/r_g^2 + \bar{a}^2/4}{2\sqrt{1 - \bar{a}^2}} \log(1 - \bar{a}^2) \right) + \frac{1}{2} \log \sqrt{1 - \bar{a}^2} - \log(r_+/r_g) \right], \quad (\text{A.8})$$

and the SN equation reduces to the following form:

$$\left(-i \frac{\gamma |\tilde{\omega}|}{C \tilde{F} E_{\text{Pl}}} e^{-\kappa_+ x} \frac{d^2}{dx^2} + \frac{d^2}{dx^2} - \tilde{\omega}^2 \right) \psi_{\tilde{\omega}} = 0. \quad (\text{A.9})$$

The solution of (A.9) which satisfies the aforementioned boundary condition is

$$\lim_{x \rightarrow -\infty} \psi_{\tilde{\omega}} = {}_2F_1 \left[-i \frac{\tilde{\omega}}{\kappa_+}, i \frac{\tilde{\omega}}{\kappa_+}, 1, -i \frac{C \tilde{F} E_{\text{Pl}} e^{\kappa_+ x}}{\gamma |\tilde{\omega}|} \right], \quad (\text{A.10})$$

and one can read that in the intermediate region, $-\kappa_+^{-1} \log [C\tilde{F}E_{\text{Pl}}/(\gamma|\tilde{\omega}|)] \ll x \ll -r_g$, $\psi_{\tilde{\omega}}$ can be expressed as the superposition of outgoing and ingoing modes

$$\psi_{\tilde{\omega}} = \begin{cases} e^{\pi\tilde{\omega}/(2\kappa_+)} A_+ e^{-i\tilde{\omega}x} + e^{-\pi\tilde{\omega}/(2\kappa_+)} A_+^* e^{i\tilde{\omega}x} & \text{for } \tilde{\omega} > 0, \\ e^{-\pi\tilde{\omega}/(2\kappa_+)} A_- e^{-i\tilde{\omega}x} + e^{\pi\tilde{\omega}/(2\kappa_+)} A_-^* e^{i\tilde{\omega}x} & \text{for } \tilde{\omega} < 0, \end{cases} \quad (\text{A.11})$$

where A_{\pm} has the form of

$$A_{\pm} \equiv \frac{\Gamma(-2i\tilde{\omega}/\kappa_+)}{\Gamma(-i\tilde{\omega}/\kappa_+)\Gamma(1-i\tilde{\omega}/\kappa_+)} e^{i\tilde{\omega}x_{\text{echo}}}, \quad (\text{A.12})$$

$$\text{with } x_{\text{echo}} = \frac{1}{\kappa_+} \log \left[\frac{\gamma|\tilde{\omega}|}{C\tilde{F}(\theta)E_{\text{Pl}}} \right]. \quad (\text{A.13})$$

Therefore, the energy reflectivity is given by

$$R = \begin{cases} \left| \frac{e^{-\pi\tilde{\omega}/(2\kappa_+)} A_+^*}{e^{\pi\tilde{\omega}/(2\kappa_+)} A_+} \right|^2 = e^{-2\pi\tilde{\omega}/\kappa_+} & \text{for } \tilde{\omega} > 0, \\ \left| \frac{e^{\pi\tilde{\omega}/(2\kappa_+)} A_-^*}{e^{-\pi\tilde{\omega}/(2\kappa_+)} A_-} \right|^2 = e^{2\pi\tilde{\omega}/\kappa_+} & \text{for } \tilde{\omega} < 0, \end{cases} \quad (\text{A.14})$$

where we used $|A_{\pm}^*/A_{\pm}| = 1$, and finally we obtain $R = e^{-|\tilde{\omega}|/T}$.

Let us note that, in deriving Equation (A.9) from (A.1) in the near-horizon limit, we have ignored the angular momentum barrier terms $\mathcal{F} \frac{d}{dx} - \mathcal{U}$, which are exponentially suppressed near horizon and are negligible as long as $|x_{\text{echo}}| \sim \kappa_+^{-1} \ln [E_{\text{Pl}}/(\gamma|\tilde{\omega}|)] \ll \kappa_+^{-1}$. Given that Astrophysical gravitational wave frequencies are $\sim 10^2$ Hz, while Planck frequency/energy is 10^{43} Hz, this means that our derivation of Boltzmann reflectivity is independent of the exact value of γ , as long as $\gamma \ll 10^{41}$. Furthermore, the trans-Planckian frequency is involved at $x = x_{\text{echo}}$ when $\gamma \lesssim 1$, in which the semi-classical treatment might break down and so the range of γ would be restricted to $\gamma \gtrsim 1$ to avoid this. Therefore, our calculation may only be valid for

$$1 \lesssim \gamma \ll 10^{41}. \quad (\text{A.15})$$

We should also remark on the θ -dependence of the blue-shift factor \tilde{F} . The θ -dependence implies that the separability of the Teukolsky equation with our modification term breaks down. However, as is shown in FIG. A.1, \tilde{F} only has a small angular variation and appears inside the log in x_{echo} (see Eq. A.13). The effect on Δt_{echo} is $< 0.1\%$, and thus can be safely ignored. We note, however, that the full problem of the separability of the modified wave equation may be more complicated and our argument is only approximately valid in the specific case.

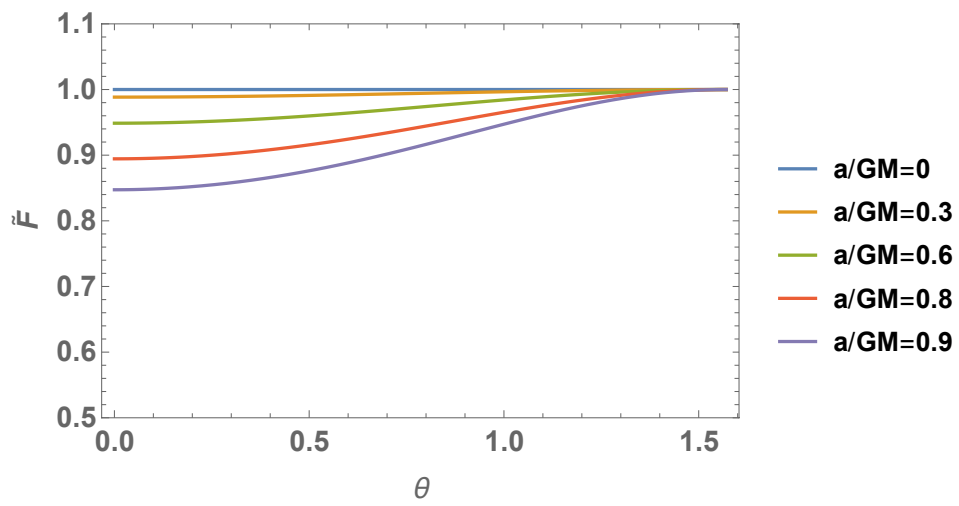


Figure A.1: Plot of $\tilde{F}(r = r_+, \theta)$ for various values of spin.